R-05-11

Variable-density groundwater flow simulations and particle tracking – numerical modelling using DarcyTools

Preliminary site description Simpevarp subarea – version 1.2

Sven Follin, SF GeoLogic AB

Martin Stigsson, Svensk Kärnbränslehantering AB

Urban Svensson, Computer-aided Fluid Engineering AB

December 2005

Svensk Kärnbränslehantering AB
Swedish Nuclear Fuel
and Waste Management Co
Box 5864
SE-102 40 Stockholm Sweden
Tel 08-459 84 00
+46 8 459 84 00
Fax 08-661 57 19
+46 8 661 57 19

ISSN 1402-3091
SKB Rapport R-05-11

Variable-density groundwater flow simulations and particle tracking – numerical modelling using DarcyTools

Preliminary site description Simpevarp subarea – version 1.2

Sven Follin, SF GeoLogic AB

Martin Stigsson, Svensk Kärnbränslehantering AB

Urban Svensson, Computer-aided Fluid Engineering AB

December 2005

Symbols, notations and abbreviations

a_w	Flow wetted surface area per unit volume of flowing water
b_{hyd}	Hydraulic thickness of the flowing fracture
c	Coefficient in $T = c\ r^{\,d}$
d	Exponent in $T = c\ r^{\,d}$
e_f	Total thickness of the empty space in the flowing fracture
e_t	Fracture transport aperture
F	F-factor
FWS_f	Flow wetted surface area of fracture f
$G[r' > r]$	Complementary cumulative density function (= 1–P[$r' \leq r$])
k	Shape parameter
k_r	(k–2)
k_{FWS}	Proportionality constant
L	Side length of a square-shaped fracture; $L = \pi\ \sqrt{r}$
L_w	Length of flow path from the release point to the discharge point
m_r	Value of r at G[$r' > r$] = 1
N_{CAL}	No. of Open and Partly open fractures
N_{CON}	No. of connected Open and Partly open fractures
N_{PFL}	No. of flowing Open and Partly open fractures with $T > (1–2)\cdot10^{-9}$ m^2/s
P_{10}	Observed frequency of flowing Open and Partly open fractures
$P_{10,corr}$	Terzaghi corrected fracture frequency
$P_{32}[r > r_{min}]$	Total fracture surface are per unit volume of rock of all fractures $r > r_{min}$
r	Fracture radius
r_0	Location parameter
r_0^*	The smallest fracture radius treated in SKB's site investigations with regard to the fracture statistics acquired in cored boreholes
r_w	Borehole radius of core drilled boreholes in SKB's site investigations
t	Outcrop fracture trace length
t_w	Advective travel time
T	Fracture transmissivity
T_g	Geometric mean fracture transmissivity
α	Fracture intensity
α_i	Mass transfer coefficient i
β_G	Capacity ratio
ε	Kinematic porosity of a grid cell

ε_f	Kinematic porosity of a fracture
ε_{PFL}	Kinematic porosity of PFL-f flow anomalies with $T > (1–2)\cdot10^{-9}$ m^2/s
κ	Fisher concentration
λ	Inverse of the expected value for an exponentially distributed size model

Executive summary

Overview

SKB is conducting site investigations for a high-level nuclear waste repository in fractured crystalline rocks at two candidate areas in Sweden, Forsmark and Simpevarp. The investigations started in 2002 and have been planned since the late 1990's. The site characterisation work is divided into two phases, an initial site investigation phase (ISI) and a complete site investigation phase (CSI). The results of the ISI phase are used as a basis for deciding on the subsequent CSI phase. On the basis of the CSI investigations a decision is made as to whether detailed characterisation will be performed (including sinking of a shaft).

An integrated component in the site characterisation work is the development of site descriptive models. These comprise basic models in three dimensions with an accompanying text description. Central in the modelling work is the geological model which provides the geometrical context in terms of a model of deformation zones and the rock mass between the zones. Using the geological and geometrical description models as a basis, descriptive models for other disciplines (surface ecosystems, hydrogeology, hydrogeochemistry, rock mechanics, thermal properties and transport properties) will be developed. Great care is taken to arrive at a general consistency in the description of the various models and assessment of uncertainty and possible needs of alternative models.

The 1.1 hydrogeological modelling conducted in the Simpevarp regional model area was fairly uncertain since there was no geological DFN model and no hydraulic test data to take into account, cf /SKB 2004/. Many of the parameter values chosen were based on data from Äspö HRL, TRUE Block Scale and/or the 1.1 site investigations in Forsmark. The main objectives of this study are:

- to develop a hydrogeological DFN model based on the 1.2 geological DFN modelling conducted by /La Pointe and Hermanson 2005/ and the high resolution fracture flow data acquired with the Posiva Flow Log measurements /Rouhiainen and Pöllänen 2003ab/ in deep, core drilled boreholes, and
- to conduct variable density flow simulations on a regional scale with DarcyTools based on an equivalent porous media representation of the hydrogeological DFN model.

Another objective of this study is to assess the assumptions in the geological DFN modelling. The methodology used by /La Pointe and Hermanson 2005/ is based on experiences gained from modelling projects conducted at Äspö HRL primarily, the conditions of which may not be fully compatible with those studied in the Simpevarp and Forsmark areas. An improved understanding of the uncertainties involved is necessary in order to gain credibility for the Site Description in general and the hydrogeological description in particular. The latter will serve as a basis for describing the present-day hydrogeological conditions as well as predictions of future hydrogeological conditions.

As a means to address the third objective we compare the results reported from the geological DFN modelling conducted by /La Pointe and Hermanson 2005/ with those reported from the alternative geological DFN modelling conducted by /Darcel et al. 2004/.

Analysis of structural and hydraulic data

The body of the geological DFN modelling reported for the 1.2 modelling stage focuses on investigating the scaling properties of steeply dipping fractures in four cleared outcrops in three different rock domains (denoted by A, B and C in the report). Structural and hydraulic data are available for modelling from four deep, core drilled boreholes KSH01A, KSH02, KSH03 and KAV01. The three KSH-holes are all located in the Simpevarp peninsula, which have been assigned a tentative repository layout for the sake of the 1.2 modelling stage.

The work reported here uses a new methodology developed by the DarcyTools modelling team. A cornerstone in this methodology is the high resolution difference fracture flow method (PFL-f; 5 m/0.1 m). The KSH01A and KSH02 boreholes, which penetrate the B and C rock domains, are the only boreholes that are investigated with this method in the Simpevarp peninsula.

From DFN to block scale properties

The analysis of borehole data and the process by which the DFN properties are transformed to grid cell (block scale) hydraulic properties, e.g. a hydraulic conductivity tensor, is called upscaling. The block scale properties are computed for two purposes:

- to analyse the magnitude of the hydraulic conductivity on a 20 m and a 100 m scale, in particular with regard to hydraulic anisotropy in different rock domains, and
- to model variable density flow on a regional scale (hundreds of square kilometres). Particle tracking from two release areas, Simpevarp and Laxemar, are used to test the sensitivity to different hydrogeological uncertainties and the need for far-field realism.

The first purpose is requested by Repository Engineering, whereas the second purpose addresses issues of importance to Safety Assessment. The upscaling results reported here indicate a fairly homogeneous and isotropic hydraulic conductivity tensor on both scales of interest (20 m and 100 m). The main reasons for this result are the high frequency of Open fractures in all orientations and the flow anomalies reported for the rock mass outside the interpreted deformation zones in the analysed boreholes.

Regional variable density flow simulations

Many of the assumptions made in the 1.1 modelling stage were made without data support from the site investigations. The work reported here demonstrates that there is considerable overlap between the 1.1 and 1.2 modelling stages in terms of input parameter values. That is, the 1.1 modelling stages have been vindicated by data gathered during the 1.2 stage. Hence, the regional variable density flow modelling presented here become on a whole a refinement of the sensitivity study carried out in the 1.1 stage. This inevitable limits the novelty of the work reported here since the overall tasks for the two modelling stages are the same.

Five sensitivity cases are treated in the work reported here:

A. Higher fracture intensity.

B. Larger and smaller size of the model domain.

C. Depth dependence in the transmissivity field.

D. Later start of the Littorina Sea period.

E. Different values of the capacity ratio.

Cases A–D are known to be important for the advective flow, whereas case E controls the effectiveness of rock matrix diffusion as implemented in DarcyTools.

Sensitivity Case A

Sensitivity Case A shows that the inferred magnitude of the hydrogeological DFN intensity is crucial for the simulation results. An upscaling of borehole intensity data creates grid cell hydraulic properties on a 100 m scale that resemble a fairly conductive porous medium. An alternative approach, intensity downscaling, is suggested in the work reported here. The intensity downscaling approach honours the number of large deformation zones. Intensity downscaling renders in this study a DFN intensity on a 100 m scale that is 1/3 of the intensity inferred from the intensity upscaling approach. The effects of this difference are considerable for the simulation of variable density flow.

Figure S-1 illustrates the concept of intensity upscaling and downscaling, respectively. The top row images in Figure S-2 illustrate the difference in DFN intensity on a 100 m scale using intensity upscaling and downscaling, respectively. The bottom row images demonstrate the hydrogeological/hydrogeochemical effects. The profiles show the simulated remaining concentrations of initial groundwater of glacial origin for the two approaches of intensity scaling.

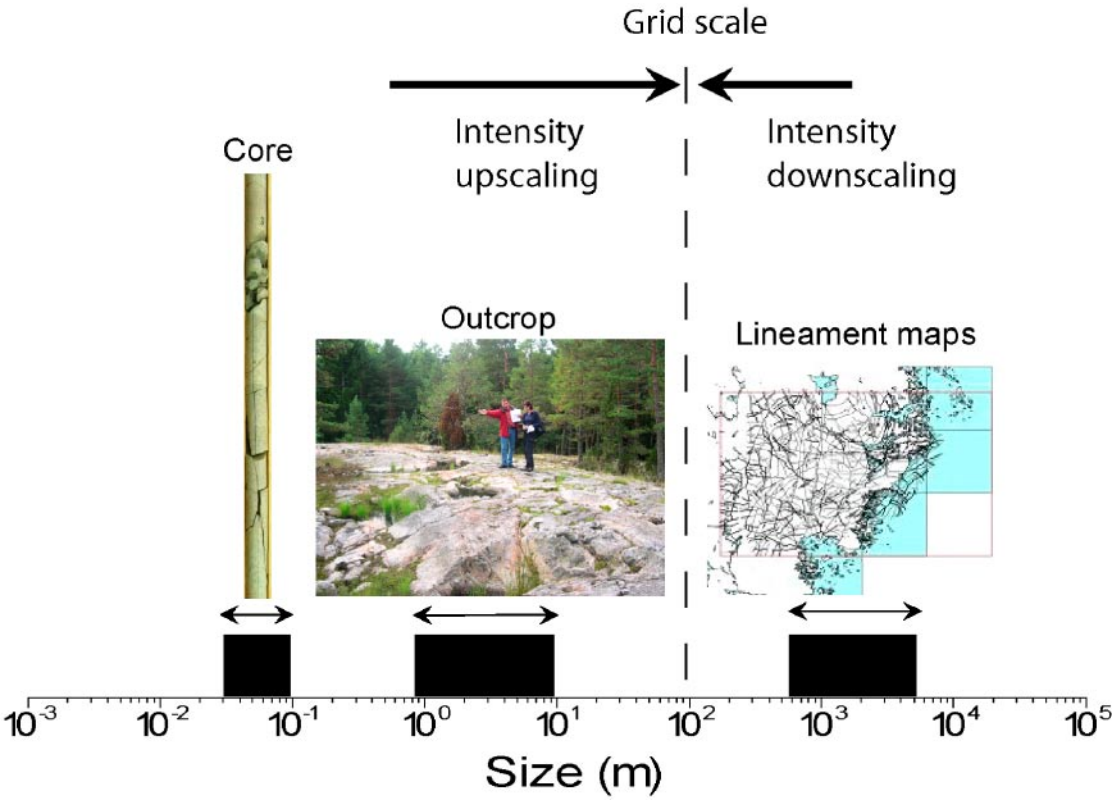

Figure S-1. *Numerical simulations of groundwater flow in fractured rock are often made with a continuum formulation. The choice of grid scale (resolution) is an important decision as it affects the representation of fracture flow heterogeneity and anisotropy. Usually the size of the smallest fractures in the stochastic fracture network realisations underpinning the computation of grid cell hydraulic properties are on the same order as the chosen grid resolution. The intensity of conductive fractures of different sizes is a vital characteristic of the stochastic network realisations. Simulations based on intensity upscaling (left) and intensity downscaling (right) may lead to quite different results, see Figure S-2.*

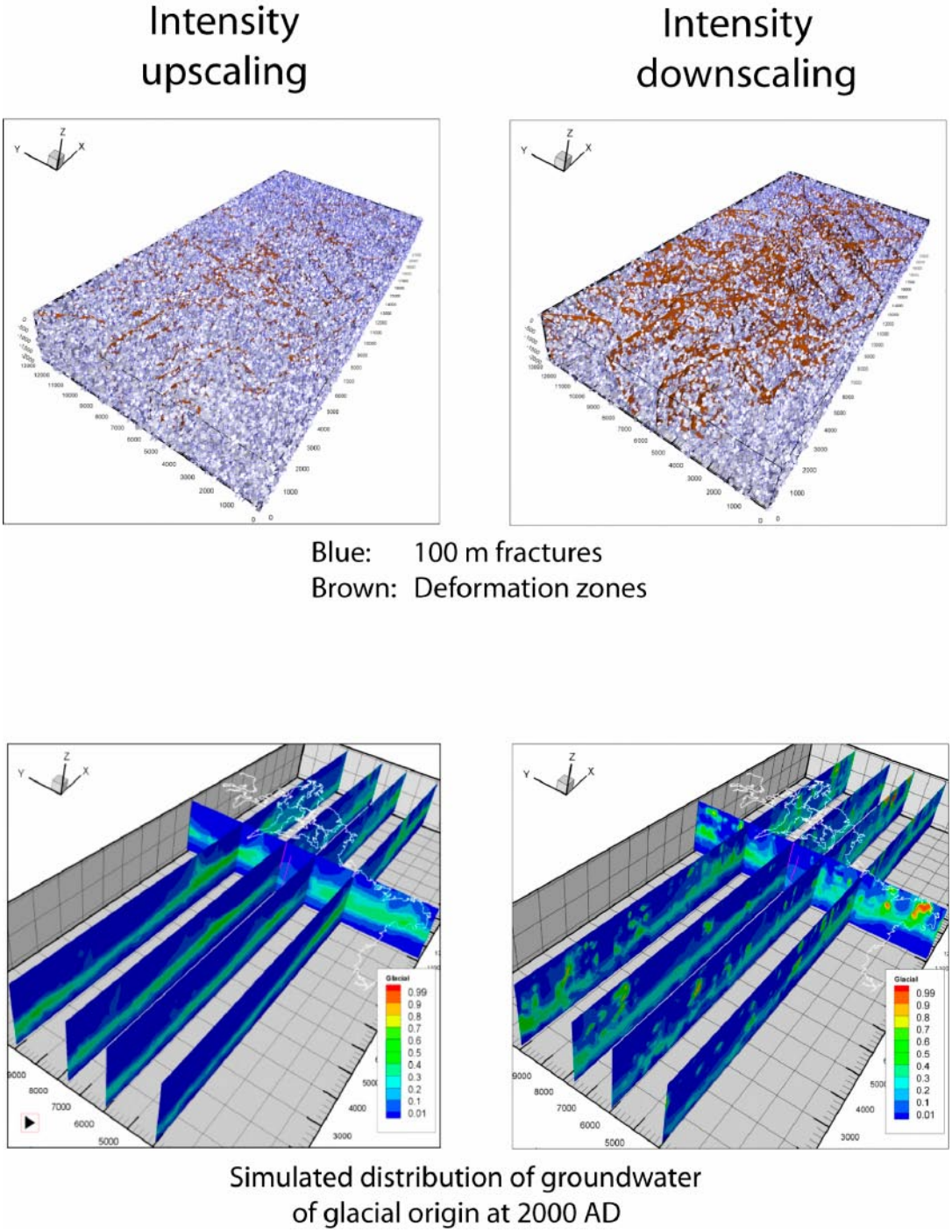

Figure S-2. *Upscaling of borehole intensity data creates grid cell hydraulic properties on a 100 m scale that resemble a fairly conductive porous medium. An alternative approach, intensity downscaling, is suggested in the work reported here. Intensity downscaling honours the number of large deformation zones. Intensity downscaling renders in this study a DFN intensity on a 100 m grid scale that is c 1/3 of the intensity inferred from the intensity upscaling approach. The effects of this difference are considerable for the simulation of variable density flow. The top row images illustrate the difference in DFN intensity on a 100 m scale using intensity upscaling and downscaling, respectively. The bottom row images demonstrate the hydrogeological/hydrogeochemical effects. The profiles show the simulated remaining concentrations of initial groundwater of glacial origin for the two scaling approaches.*

Sensitivity Case B

Sensitivity Case B shows that the size of the model domain is not a major issue for the Simpevarp subarea because of its proximity to the Baltic Sea. For the Laxemar subarea more data from this part of the model domain are required. The work presented here assumes that the conditions in Laxemar are the same as in the Simpevarp subarea.

Sensitivity Case C

Sensitivity Case C shows that a depth trend in the hydraulic properties have a fairly large impact on the simulations results. In fact, the match against measured salinities and calculated M3 mixing proportions improve. We note that a decreasing trend is supported by the hydrogeological DFN analysis carried out in Chapter 5.

Sensitivity Case D

Sensitivity Case D suggests that a delay of the start of the Littorina Sea period by 750 years does not alter the simulated present-day concentrations along the KLX02 borehole. The interpretation of this result is not straightforward, however, because the elevation of the Laxemar area may already be above or very close to the highest elevation of the Littorina Sea at the time of interest for the Littorina Sea intrusion.

Sensitivity Case E

The capacity ratio is a key parameter of the multi-rate diffusion model, which is the diffusion model implemented in DarcyTools. A series of capacity boxes with different mass transfer coefficients are used in the multi-rate model to model the diffusive exchange of matter between the mobile and immobile pore volumes. The classic diffusion model assumes a single-rate.

The capacity ratio is the ratio between immobile and mobile pore volumes. The pore volume in the rock matrix accessible for diffusion is expected to be 10–100 times greater than the pore volume in the water-conducting fractures. The current working hypothesis used in DarcyTools is that the capacity ratio ought to be of the same order of magnitude.

Sensitivity Case E shows that the magnitude of the capacity ratio alters the grid cell fluxes at depth, which in turn affect the penetration depths of the Littorina Sea water type and the subsequent flushing of the Meteoric water type. The sensitivities observed are complex, however, and demonstrate that the multi rate diffusion model must be subjected to more modelling experiments as a means to better understand how its parameters shall be handled in the site descriptive modelling. The values used in the work reported here are based on the results reported by /Svensson and Follin 2005/.

Contents

1 Introduction

1.1 Background

SKB is conducting site investigations for a high-level nuclear waste repository in fractured crystalline rocks at two coastal areas in Sweden. The two candidate areas are named Forsmark and Simpevarp. The investigations started in 2002 and have been planned since the late 1990's. The site characterisation work is divided into two phases, an initial site investigation phase (ISI) and a complete site investigation phase (CSI). The results of the ISI phase are used as a basis for deciding on the subsequent CSI phase. On the basis of the CSI investigations a decision is made as to whether detailed characterisation will be performed.

An integrated component in the site characterisation work is the development of site descriptive models. These comprise basic models in three dimensions with an accompanying text description. Central in the modelling work is the geological model which provides the geometrical context in terms of a model of deformation zones and the less fractured rock mass between the zones. Using the geological and geometrical description models as a basis, descriptive models for other disciplines (surface ecosystems, hydrogeology, hydrogeochemistry, rock mechanics, thermal properties and transport properties) will be developed. Great care is taken to arrive at a general consistency in the description of the various models and assessment of uncertainty and possible needs of alternative models.

1.2 Scope and objectives

The 1.1 hydrogeological modelling conducted in the Simpevarp regional model area was fairly uncertain since there was no geological DFN model and no hydraulic test data to take into account, cf /SKB 2004/. Many of the parameter values chosen were based on data from Äspö HRL and/or the 1.1 site investigations in Forsmark (cf /Rhén et al. 1997, SKB 2004/). Hence, the main objectives of this study are:

- to develop a hydrogeological DFN model based on the 1.2 geological DFN modelling conducted by /La Pointe and Hermanson 2005/ and the high resolution fracture flow data acquired with the Posiva Flow Log measurements /Rouhiainen and Pöllänen 2003ab/, and
- to conduct variable density flow simulations on a regional scale with DarcyTools /Svensson et al. 2004, Svensson and Ferry 2004, Svensson 2004a/.

Another objective of this study is to assess the methodology in the 1.2 geological DFN modelling. The methodology used by /La Pointe and Hermanson 2005/ is based on experiences gained from modelling projects conducted at Äspö HRL primarily, the conditions of which may not be fully compatible with those studied in the Simpevarp subarea, Laxemar subarea or Forsmark area. An improved understanding is necessary in order to gain credibility for the Site Description in general and the hydrogeological description in particular. The latter will serve as a basis for describing the present-day hydrogeological conditions as well as predictions of future hydrogeological conditions.

As a means to address the third objective we compare the results reported from the geological DFN conducted by /La Pointe and Hermanson 2005/ with those reported from the alternative geological DFN modelling conducted by /Darcel et al. 2004/.

1.3 Setting, assumptions and limitations

There are seven rock domains, A–G, in the 1.2 modelling stage, see Figure 1-1.

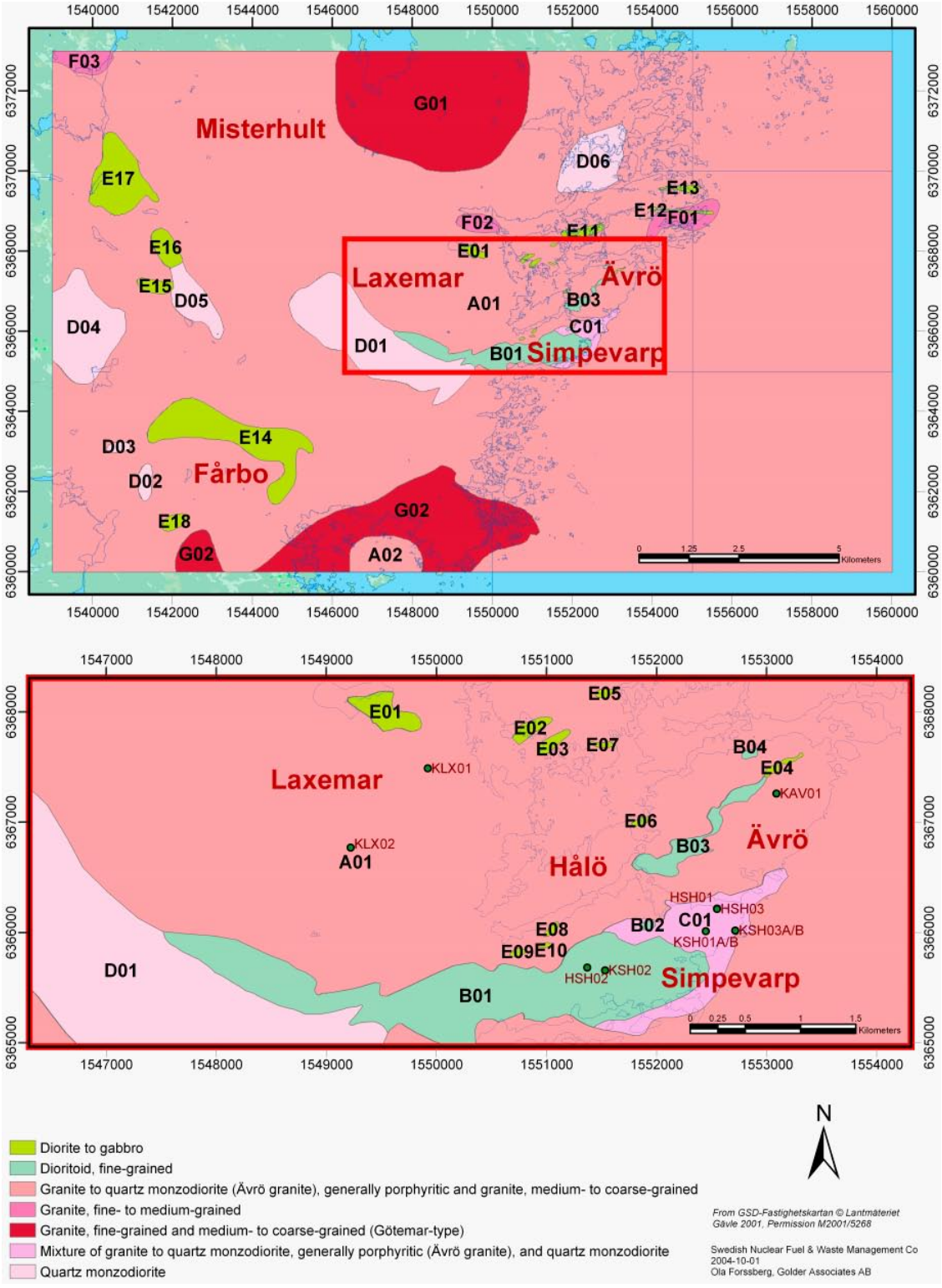

Figure 1-1. *Rock domains identified in the 1.2 modelling stage /SKB 2005/. The available boreholes for structural analyses in the vertical direction are indicated. The names of the core drilled boreholes begin with the letter K and the names of the percussion drilled boreholes begin with the letter H.*

Lineaments in the regional model area have been identified on the basis of a joint integrated interpretation of different sets of lineaments, each of which has been identified separately from the following data sets /Rönning et al. 2003, Triumf et al. 2003, Wiklund 2002, Elhammer and Sandkvist 2005/:

- Helicopter-borne geophysical survey data, i.e. data on the total magnetic field, electromagnetic (EM) multifrequency data and very low frequency electromagnetic (VLF) data.
- Fixed-wing airborne, very low frequency electromagnetic (VLF) data.
- Detailed topographic data (terrain model).
- Terrain model of the sea bottom and bedrock surface in the sea area outside Simpevarp.

The linked lineaments identified in the 1.2 Simpevarp regional model area are presented in Figure 1-2, where their assigned trace length class (regional > 10 km and local major 1–10 km) are identified. The latter is an expert judgement that relates to the degree of clarity in surface expression of the lineaments where 1 = low, 2 = medium and 3 = high uncertainty. A weighted average is calculated according to the length of each segment in the linked lineament. For a more detailed explanation, see /Triumf 2004/. It is vital to note that the map of linked lineaments covers a smaller area than the regional scale model area, cf Figure 1-2. For modelling purposes, lineaments from earlier work /SKB 2002a/ have been evaluated and combined with the linked lineaments in areas with no detailed coverage.

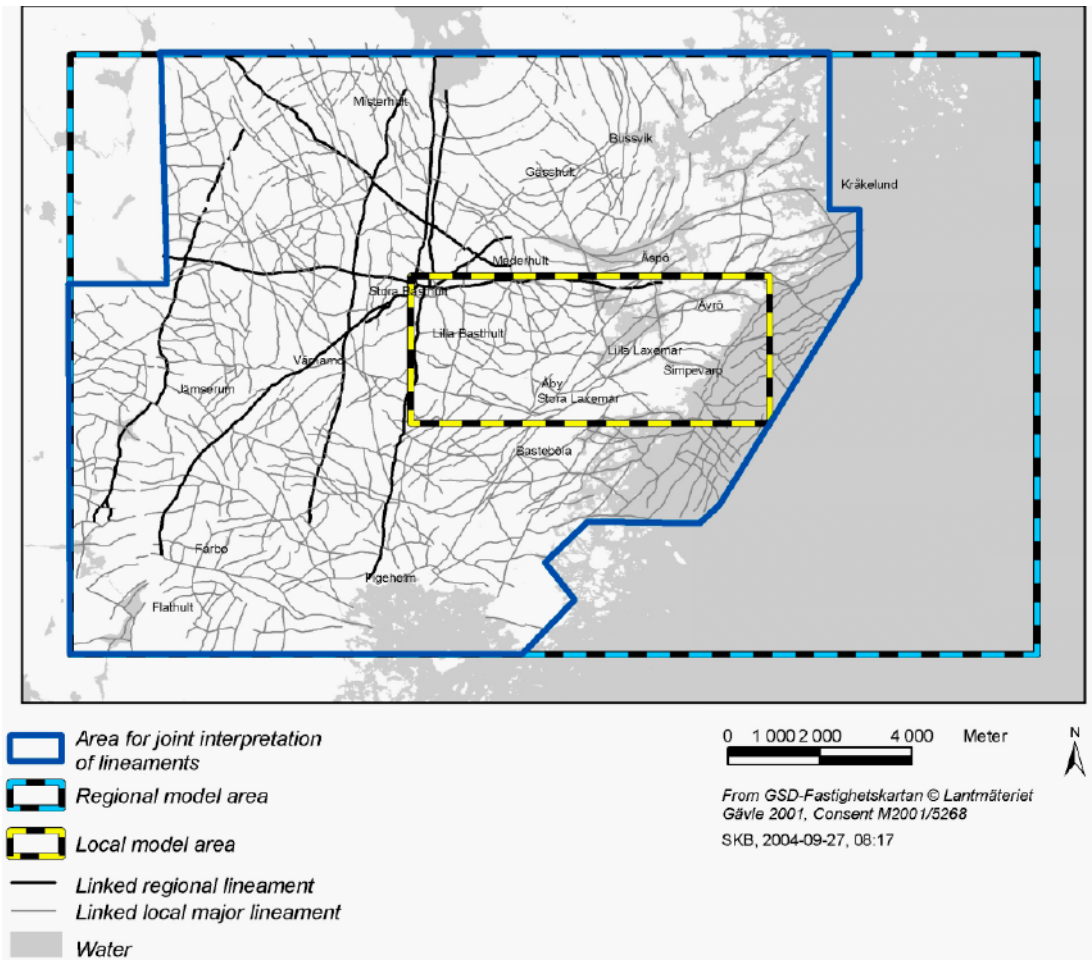

Figure 1-2. *Interpreted linked lineaments in the 1.2 modelling stage /SKB 2005/.*

The construction of the 1.2 deformation zone model is made on the basis of linked lineaments (see /SKB 2005/ for an explanation). In short, there are 188 deterministically modelled deformation zones within the regional model domain. All zones are modelled to be more or less steeply dipping and have trace lengths greater than 1,000 m, see Figure 1-3. The deformation zones have different levels of geological confidence, and possibly the number of true deformations zones is less than 188. For instance, 22 deformation zones only have a high confidence in the 1.2 modelling stage. Each one of the high confidence deformation zones is observed both indirectly, through lineament or geophysical data, and directly through borehole or tunnel observations. The exception to this is the Mederhult zone (ZSMEW002A), see Figure 1-4, which has not been observed in boreholes or tunnels.

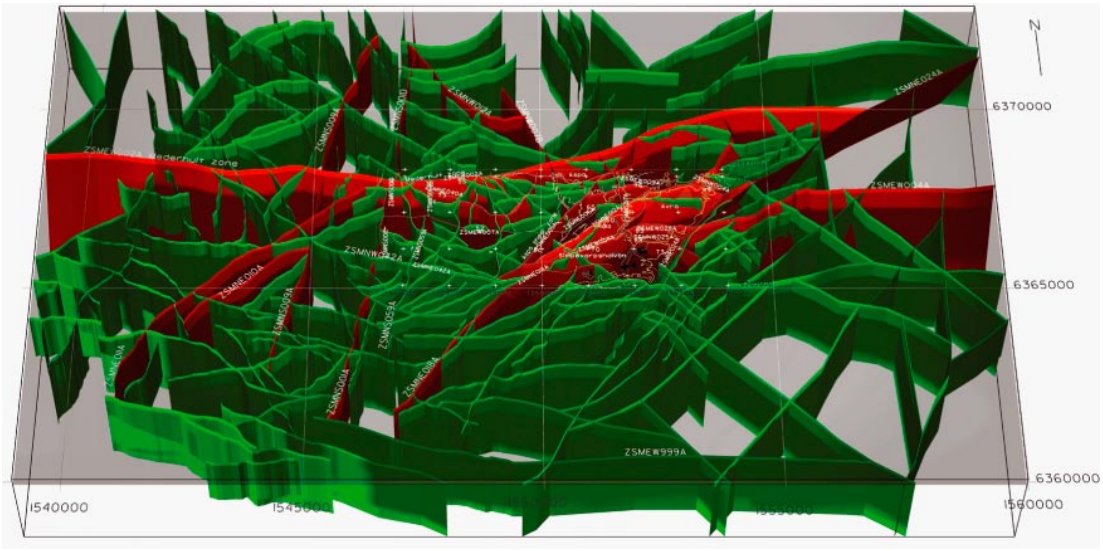

Figure 1-3. *High confidence deformation zones (red) and low confidence deformation zones (green) within the 1.2 Simpevarp regional model domain /SKB 2005/.*

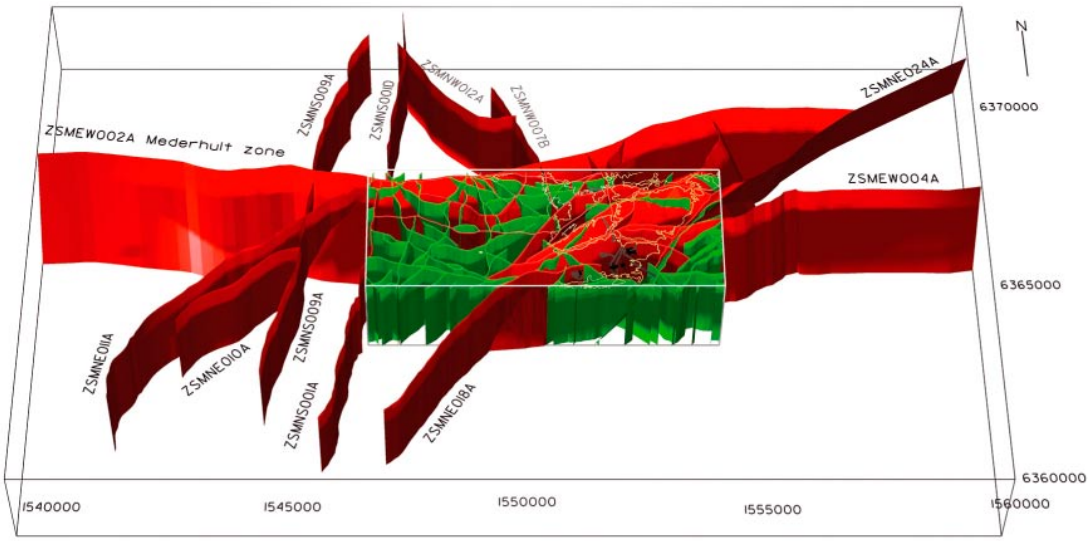

Figure 1-4. *High confidence deformation zones (red) in the 1.2 Simpevarp regional model domain and truncated low confidence zones (green) within the 1.2 Simpevarp local model domain /SKB 2005/.*

Detailed fracture mapping has been carried out in four cleared outcrops in the Simpevarp subarea. The sites were chosen on both a geographical and lithological basis, i.e. the sites were distributed between different parts of, and between the various dominant rock types in, the Simpevarp subarea, see Figure 1-5. The cleared outcrops are c 20 times 20 square metres in size.

Fracture trace maps that show fracture trace geometry, were produced for each outcrop during the detailed fracture mapping, see Figure 1-6. The assembled data include the three dimensional geometry of fracture traces and their associated geological parameters, including mineralogy, undulation, trace length and characteristics of termination. The truncation (minimum) mapped trace length was 50 cm and the maximum trace length was limited to the size of the cleared outcrop (about $(20\ m)^2$). The number of fractures mapped in each outcrop varied between 876 and 1,175. Scan line measurements were also completed at each site along NS and EW directions, employing a mapped truncation length of 20 cm.

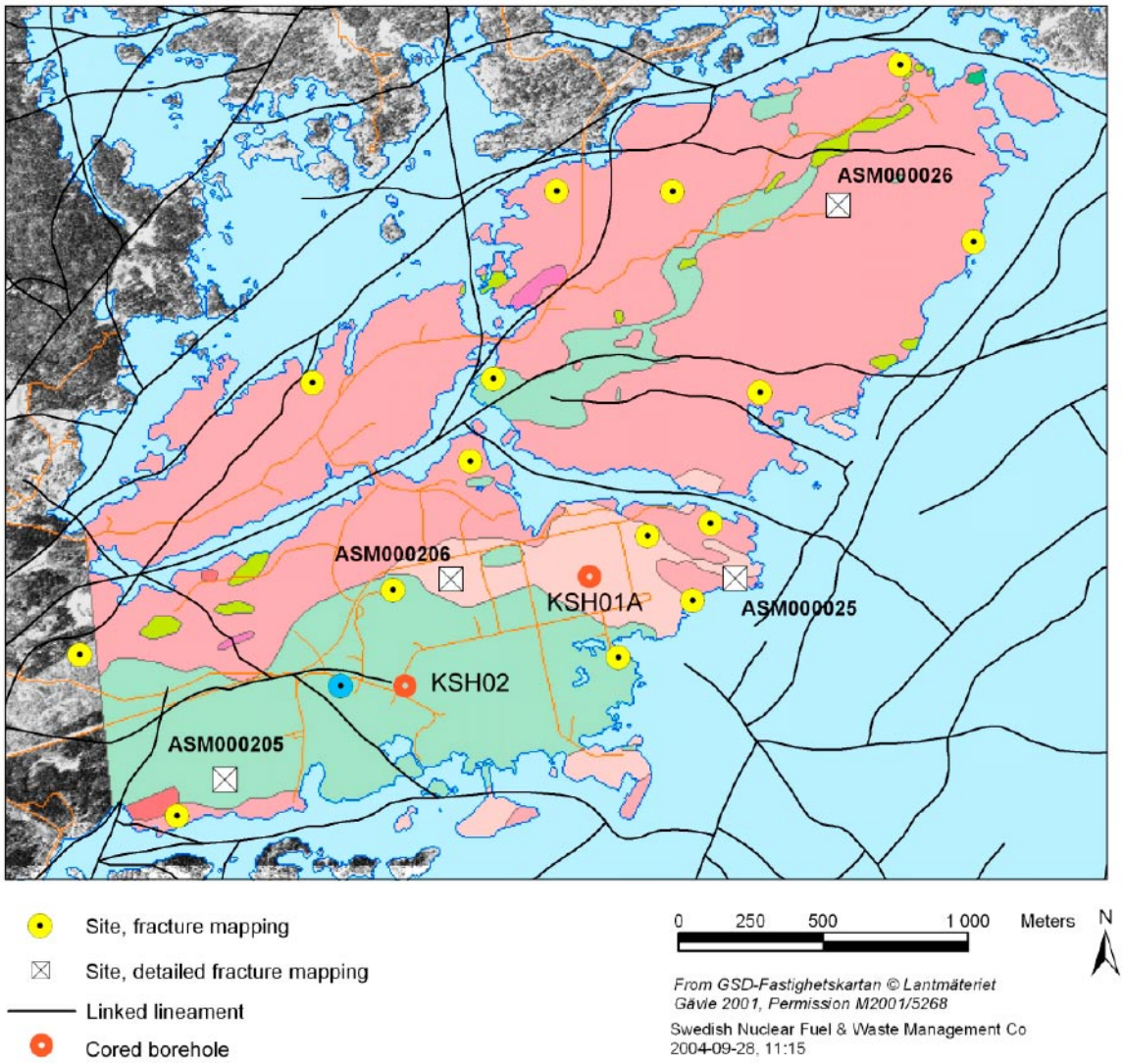

Figure 1-5. *Sites where detailed and scan line mapping of fractures have been carried out. For an explanation of the bedrock legend (coloured areas), see Figure 1-1. White squares with a cross show the locations of the cleared outcrops /SKB 2005/.*

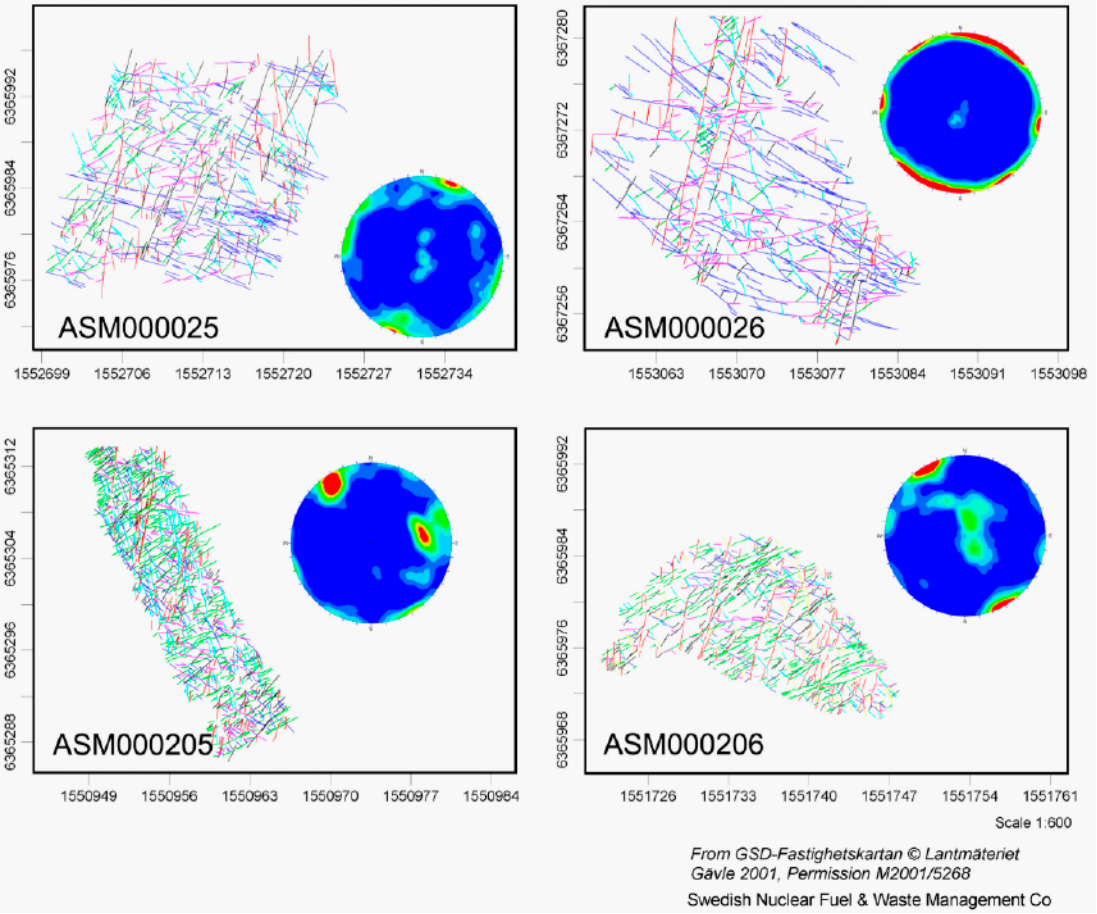

Figure 1-6. *Fracture trace maps and fracture lower hemisphere contour plots of fracture poles from the four cleared outcrops (ASM000025, ASM000026, ASM000205 and ASM000206) where detailed fracture mapping was carried out, cf Figure 1-5 for geographical reference. The Coloured traces represent different fracture sets. There are six in each outcrop except in the ASM000206 outcrop where there are seven steeply dipping fracture sets and one gently dipping /La Pointe and Hermanson 2005/.*

The body of the geological DFN modelling reported for the 1.2 modelling stage focuses on investigating the scaling properties of steeply dipping fractures in four cleared outcrops in three different rock domains (A, B and C) in the Simpevarp subarea. Structural data at repository depth are available from four deep boreholes drilled in the Simpevarp subarea, KSH01A, KSH02, KSH03 and KAV01. The three KSH-holes are all located in the Simpevarp peninsula, which have been assigned a hypothetical repository layout during the 1.2 modelling stage, see Figure 1-7.

The work reported here uses a new methodology developed by the DarcyTools modelling team. A cornerstone in this methodology is the high resolution difference fracture flow method (PFL-f; 5 m/0.1 m). Simultaneous high resolution structural and hydraulic data available for detailed geological and hydrogeological DFN modelling are acquired in the KSH01A and KSH02 boreholes. The two boreholes penetrate the B and C rock domains, see Figure 1-8. /La Pointe and Hermanson 2005/ state that the C rock domain is quite similar to the more abundant A rock domain from a structural point of view (cf Figure 1-1). We cannot comment this notion because the KSH01A and KSH02 boreholes do not penetrate the A rock domain.

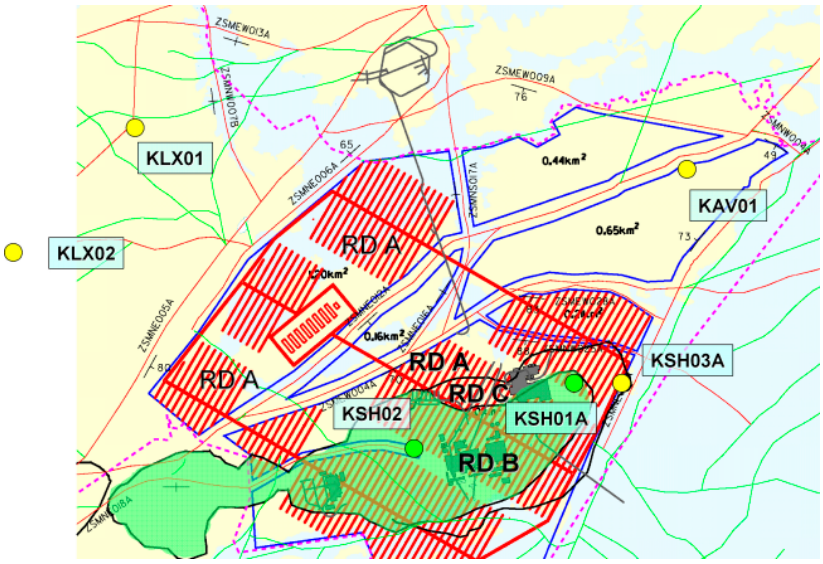

Figure 1-7. *Hypothetical repository layout in the Simpevarp peninsula used for planning purposes during the 1.2 modelling stage. Simultaneous structural and hydraulic data at repository depth available for detailed geological and hydrogeological DFN modelling are acquired in the KSH01A and KSH02 boreholes only. The two boreholes penetrate the B and C rock domains. The C rock domain is quite similar to the abundant A rock domain from a structural point of view, however /La Pointe and Hermanson 2005/.*

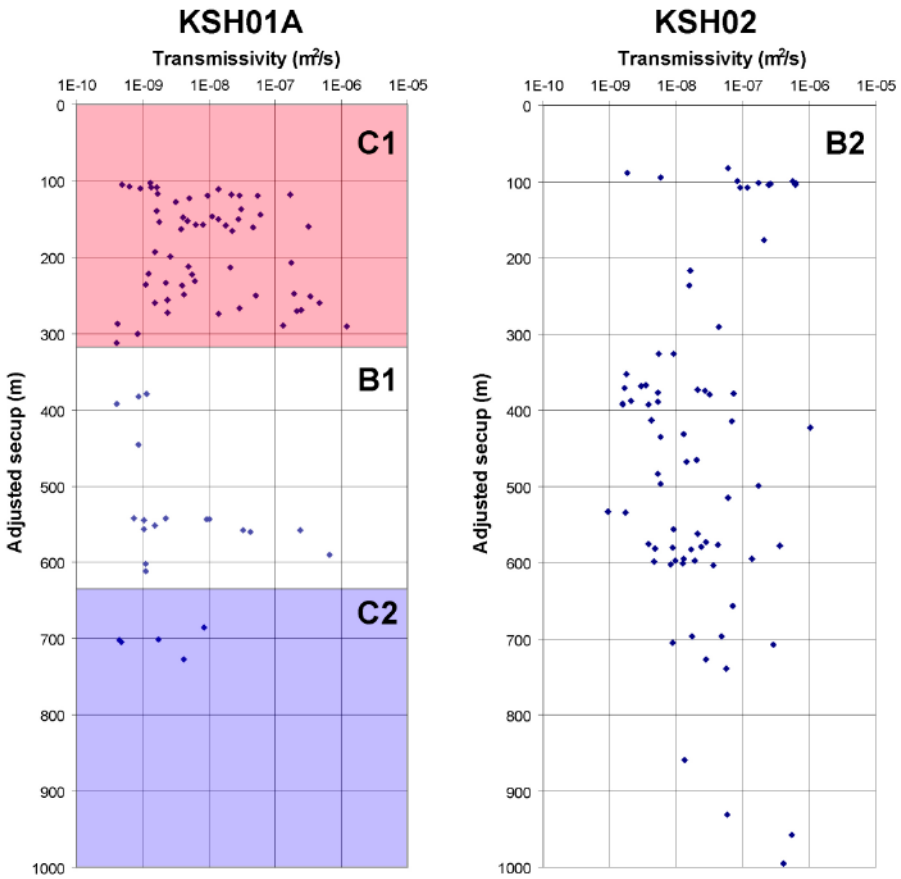

Figure 1-8. *PFL-f transmissivities acquired in the KSH01A and KSH02 boreholes together with the inferred rock domain intervals C1, B1, C2 and B2.*

The motive for keeping the B and C rock domains apart in this study is based on the geological division solely. The refined division into sub rock domains C1, B1 and C2 (KSH01A) and B2 (KSH02) explained below is based on the hydraulic data analysed, however. /La Pointe and Hermanson 2005/ do not make this distinction.

1.4 This report

The work presented in this report was conducted by the DarcyTools Team involving hydrogeologists from SF GeoLogic, Swedish Nuclear Fuel and Waste Management Company and Computer-aided Fluid Engineering. A complementary study to the work presented here is provided by /Hartley et al. 2005/. Hence, the scope of work is addressed by two modelling team working in parallel.

The DarcyTools code is developed and maintained by Computer-aided Fluid Engineering /Svensson et al. 2004, Svensson and Ferry 2004, Svensson 2004a/. The structure of the report is as follows:

- Chapter 2 presents SKB's systems approach to hydrogeological modelling and the concepts, methods and equations implemented in the DarcyTools code.
- Chapter 3 presents the bedrock hydraulic test data available for a detailed structural-hydraulic DFN modelling.
- Chapter 4 treats the hydraulic properties of the Hydraulic Conductor Domains (HCD).
- Chapter 5 treats the hydraulic properties of the Hydraulic Rock Domains (HRD). More specifically, a methodology for hydrogeological DFN modelling suggested by the DarcyTools Team is presented and applied to the detailed structural and high resolution difference fracture flow data acquired in the KSH01A and KSH02 boreholes. We also compare the results from the geological DFN conducted by /La Pointe and Hermanson 2005/ with the results reported from the alternative geological DFN modelling conducted by /Darcel et al. 2004/.
- Chapter 6 treats the hydraulic properties of the Hydraulic Soils Domains (HSD).
- Chapter 7 compares the properties inferred in the work reported here with the properties postulated in the 1.1 modelling stage. Secondly, we present the regional variable density flow modelling carried out.
- Chapter 8 presents a discussion of the results and the conclusions drawn.

2 Model set-up and specifications

2.1 Systems approach and modelling methodology

The systems approach presented in /Rhén et al. 2003/ describes how different modelling concepts, field investigations, and interpretation techniques come into play depending on the nature of the geological and hydraulic domains considered. Regional groundwater flow models are constructed from the following three hydraulic domains:

HCD Hydraulic Conductor Domains – deterministically treated deformation zones (of high to low confidence).

HRD Hydraulic Rock Domains – the sparsely fractured rock mass between the deterministically treated deformation zones. (The HRDs generally coincide with the lithological rock domains defined by geology.) Several lithological rock domains may be merged into one HRD or one lithological rock domain may be divided into several HRDs depending on the structural and hydrogeological complexities.)

HSD Hydraulic Soil Domains – the overburden (Quaternary deposits mainly) on top of the bedrock.

The regional scale variable density flow modelling presented in this report is based on a single geological model for the deterministically treated deformation zones, see Figure 1-3.

The Simpevarp regional model domain consists predominantly of seven rock domains, A–G, see Figure 1-1. Chapter 4 presents an assessment of hydraulic properties of the HCDs, Chapter 5 the hydraulic properties of the HRDs and Chapter 6 the properties of the HSDs as used in the regional modelling.

The uncertainties in the hydraulic properties of the HRDs are of key importance and may be modelled with alternative approaches depending on, among other things, the fracture intensity. The “simplest” case, at least from a geometrical point of view, is perhaps that of a uniform (or multicomponent) Continuous Porous Medium (CPM), where fractures are either absent or of very low transmissivity. Such a system also has a very low porosity. The “most complex” case is presumably a very heterogeneously fractured rock mass, where groundwater flow occurs in a Channel Network (CN), the geometric and hydraulic properties of which are not readily characterised by measurements and simulated by means of simple statistical distributions in space. Between these two “bounding” cases we may invoke different more or less “moderately complex” notions. Figure 2-1 illustrates schematically the different modelling approaches found in the literature and the kind of flow fields these may treat, the Discrete Fracture Network (DFN), the Equivalent Porous Medium (EPM) and the Stochastic Continuum (SC). It is noteworthy that the approaches shown in Figure 2-1 are all based on the same constitutive parameters time, pressure and flow rate. Hence, they are not true alternative model approaches, but rather alternative (model approach) variants. The premises for one or the other ‘model approach’ are essential to the overall hydrogeological uncertainty assessment. ‘Model approaches’ may or may not be used in parallel dependent on the objectives and the scale of the flow problem treated.

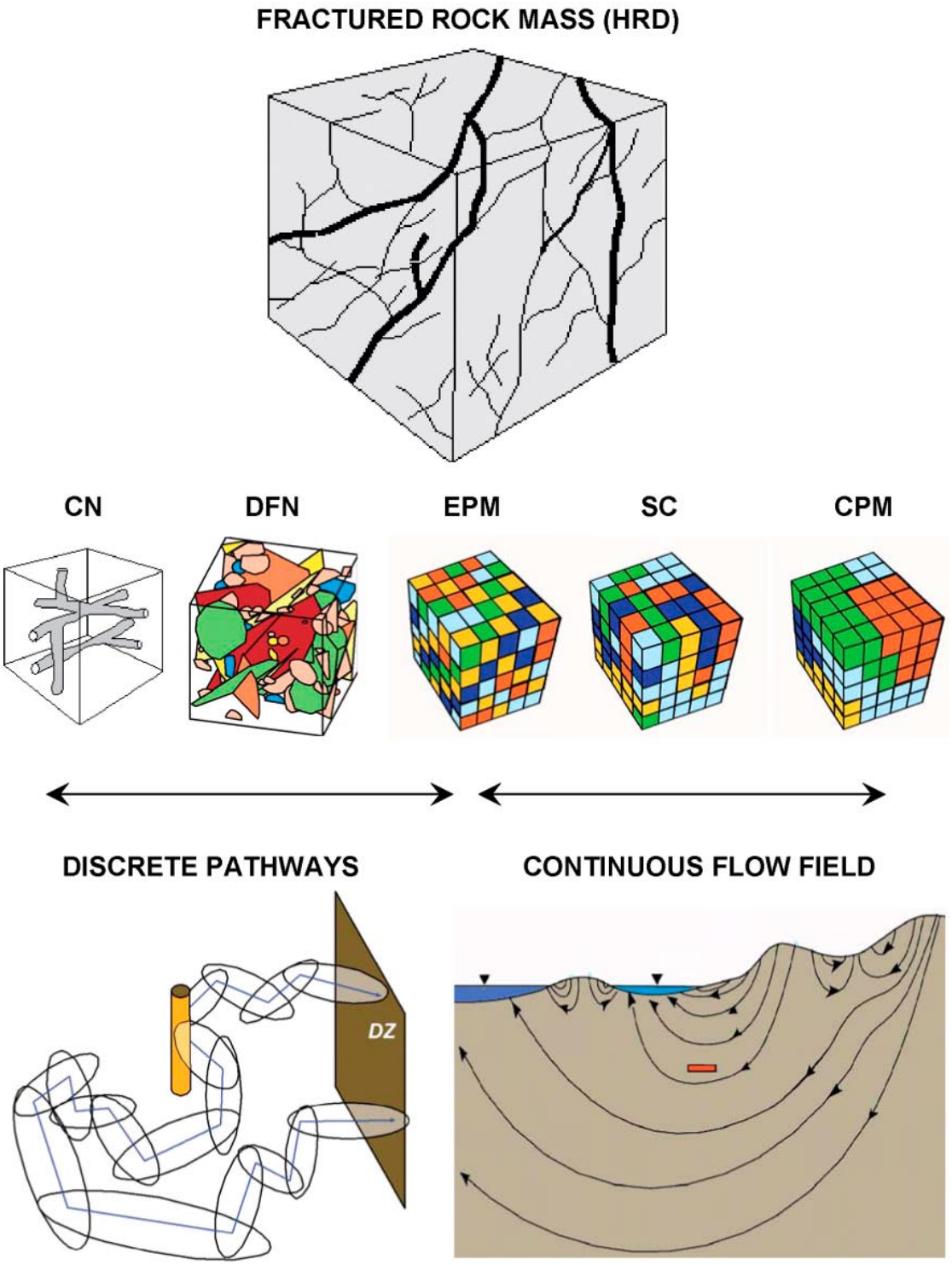

Figure 2-1. *Different modelling approaches to groundwater flow in crystalline rock and the kind of flow fields these may address. It is noteworthy that all approaches shown are based on the same constitutive parameters time, pressure and flow rate. Hence, they are not true alternative model approaches, but rather alternative (model approach) variants. CN = Channel Network, DFN = Discrete Fracture Network, EPM = Equivalent Porous Medium, SC = Stochastic Continuum, CPM = Continuous Porous Media (single-component or multi-component), DZ = Deformation Zone.*

Figure 2-2 illustrates the work flow of hydrogeological modelling envisaged for the modelling stage. The details of the work flow may be described as follows:

- A hydrogeological DFN (HydroDFN) analysis is carried out based on core mapping data, PFL and PSS test data. The hydrogeological DFN modelling is underpinned by the geological DFN modelling. Uncertainties in the geological DFN modelling, e.g. the intensity in the power law size distribution, need to be scrutinised in detail in the hydrogeological DFN modelling.
- The output parameters (connected fracture intensity and fracture transmissivity) are applied to a structural DFN model (characterised by fracture orientation, size, geological intensity and spatial distribution) to estimate equivalent porous media (EPM) block size properties and to analyse possibilities for anisotropy in flow.
- The EPM block size calculations are requested by Repository Engineering, but are useful also for the inclusion of the hydrogeological DFN findings into a regional scale groundwater flow model. The computation of EPM grid block tensors from a regional hydrogeological DFN simulation (upscaling) is a vital step in the flow modelling and the hydraulic properties derived are sensitive to the properties of the DFN model and to the chosen resolution of the grid blocks.
- The EPM model is combined with the models defined for the HCDs and HSDs and calibrated against hydraulic test data and hydrogeochemical data, e.g. chemical composition (salinity), water types, and/or natural isotopes.
- The calibrated EPM regional model is used for sensitivity analyses of ground water flow paths and transport of solutes.

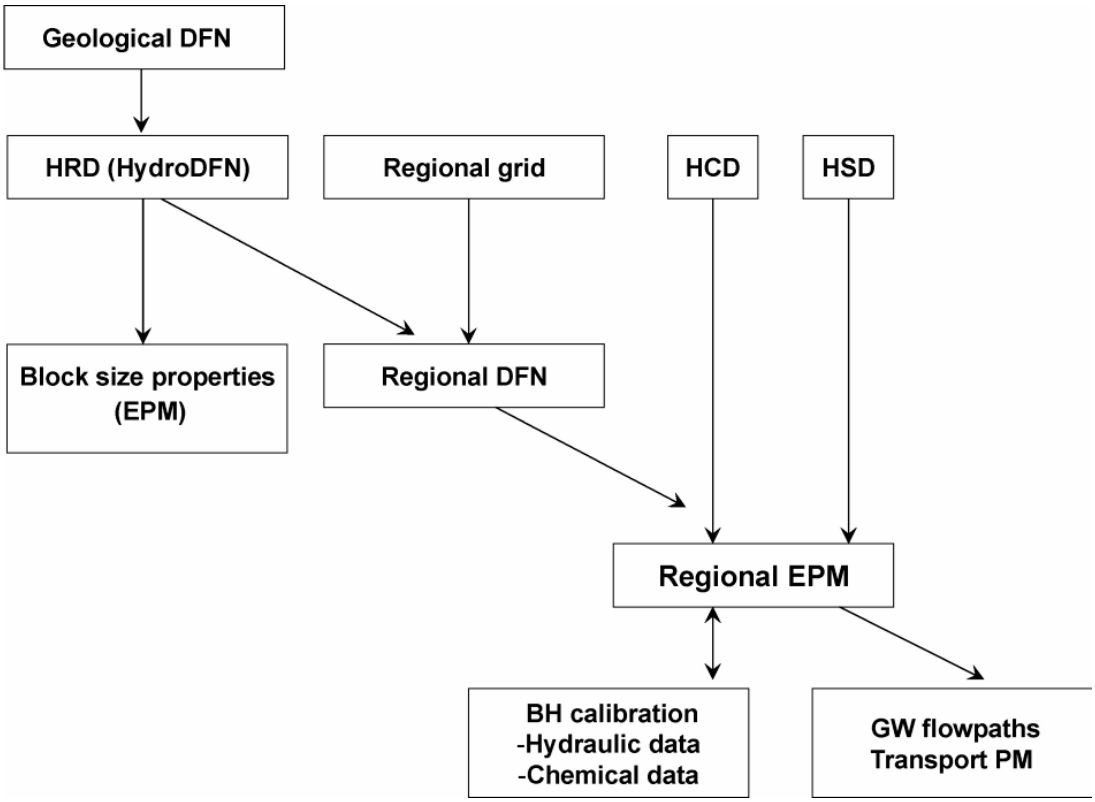

Figure 2-2. *Work flow of hydrogeological modelling in the 1.2 modelling stage. PM = performance measures. BH = borehole. The other acronyms are explained in the text.*

2.2 Modelling with DarcyTools

DarcyTools is a porous media variable-density flow code specifically designed to treat flow and salt transport in sparsely fractured crystalline rock intersected by transmissive fractures. It comprises, among other things, a fracture network generator, upscaling algorithms for the computation of finite-volume (block-size) properties and a multi-rate diffusion model. The work flow of modelling with DarcyTools essentially follows that shown in Figure 2-2 with one important exception. The approach taken in DarcyTools is to discard stochastic features smaller than the grid size and treat the processes on scales smaller than the grid resolution analytically, cf /Svenson et al. 2004a/.

2.3 Discrete Fracture Network (DFN) representation

The built-in discrete fracture network (DFN) generator of DarcyTools is a simple model of reality and based on the following key geometric assumptions/limitations:

- Univariate Fisher distributed fracture orientations.
- Power law distributed fracture sizes.
- Poisson distributed fracture centres.

These basic assumptions are used to define geometry of the stochastically modelled fracturing. The hydraulic properties are either specified or sampled from probability distribution functions (PDFs) specified for each fracture set. The properties may be sampled independently or correlated. In model version 1.2 the site-specific fracture data available for modelling consist of fracture transmissivities T [m^2/s], whereas general formulae are used for assigning equivalent parameter values of the storativity S [–] and the transport aperture e_t [m]:

$$S = 7 \cdot 10^{-4}\, T^{0.5} \tag{2-1}$$

$$e_t = 0.5 T^{0.5} \tag{2-2}$$

These formulae are taken from /Rhén et al. 1997, Rhén and Forsmark 2001, Andersson et al. 1998b, 2000, Dershowitz et al. 2003/. It is noted that the storativity and the transport aperture are both modelled as power law functions of the fracture transmissivity. Chapter 5 presents motives for assuming that fracture transmissivity is correlated to fracture size, which, in turn, is postulated to be power law distributed.

The key parameters of a power law size population providing the number of fractures of different sizes are the shape parameter k and the location parameter r_0, where $k > 0$ and $r_0 > 0$ m. SKB recommends using the following notation representing the power law probability density function /Munier 2004/:

$$f(r) = \frac{k\, r_0^k}{r^{k+1}},\ r_0 \le r < \infty \tag{2-3}$$

Equation (2-3) treats fractures as circular discs. In DarcyTools, however, fractures are modelled as squares. The equivalent radius r of a square of size L is simply:

$$r = L/\sqrt{\pi} \tag{2-4}$$

The location parameter r_0 is defined as the smallest value in the power law size distribution, i.e.:

$$G[r > r] = (1 - P[r' \le r]) = \left(\frac{r_0}{r}\right)^{k_r} \tag{2-5}$$

We assume that the data set available for modelling is a representative sample of the population parameters, i.e. $k \approx k^*$ and $r_0 \approx r_0^*$, where k^* and r_0^* designate sample parameters the values of which are determined from field observations. Furthermore, we assume that r_0^* is the smallest fracture radius treated in the site investigation with regard to the fracture statistics acquired in cored boreholes. That is, we assume that $r_0^* \approx r_w$, where r_w is the radius of a cored borehole used in SKB's site investigations, 0.038 m.

If $P_{32}[r > r_0]$ denote the fracture surface area of all fractures greater than the location parameter we can write:

$$P_{32}[r > r_1] = P_{32}[r > r_0] \left(\frac{r_0}{r_1} \right)^{(k-2)} \tag{2-6}$$

where $P_{32}[r > r_1]$ is the fracture surface area of all fractures r greater than the size r_1. Consequently, in accordance with the assumptions state above, we may write that $P_{32}[r > r_0] \approx P_{32}[r > r_w]$.

From a modelling point of view it is necessary to decide the size range r_{min}, r_{max} that will be used in the numerical simulations. For $r_{min} \geq r_0$ and $r_{max} \geq r_1$ Equation (2-6) implies that log $P_{32}[r > r_{min}]$ vs log r plots as a straight line with a slope of (k–2), see Figure 2-3.

In conclusion, the fracture intensity of a DFN model with fractures in the size interval $[r_{min}, r_{max}]$ may be written as:

$$P_{32}[r_{min}, r_{max}] \approx P_{32}[r > r_w] \left(\frac{(r_{min})^{(2-k)} - (r_{max})^{(2-k)}}{(r_w)^{(2-k)}} \right) \tag{2-7}$$

The fracture intensity term in DarcyTools is denoted by α. Its relation to P_{32}, r, and (k–2) may be written as:

$$\alpha = \frac{(k-2)}{\pi} \left(P_{32}[r > r_{min}] \, r_{min}^{(k-2)} \right) \tag{2-8}$$

Equation (2-6) implies that the product $P_{32}[r > r_{min}] \, r_{min}^{(k-2)} = \text{const}$. Hence, the intensity value α in Equation (2-8) is also constant, cf Figure 2-3. Figure 2-4 shows the dependence of P_{32} on r_{min}, k and α.

The vital geometric/geological parameters/assumptions in this study are the shape parameter k, the fracture intensity α, the assumptions for the location parameter r_0 and the inter-connected fracture intensity available for flow $P_{32CON}[r > r_0]$ (explained in Chapter 5). The vital hydraulic assumption in DarcyTools concerns the foundation and derivation of a power law correlation between fracture transmissivity and fracture size:

$$T = c \, r^d \tag{2-9}$$

The motives for this assumption are discussed in Chapter 5.

We conclude this section by noting that the notation used in the geological DFN modelling by /La Pointe and Hermanson 2005/ uses k and $P_{32}[r > r_0]$, whereas the notation used in the alternative geological DFN modelling by /Darcel et al. 2004/ uses a and α. The relationship between α and $P_{32}[r > r_0]$ is shown in Equation (2-8) and the relationship between a and k is simply:

$$a = k + 1 \tag{2-10}$$

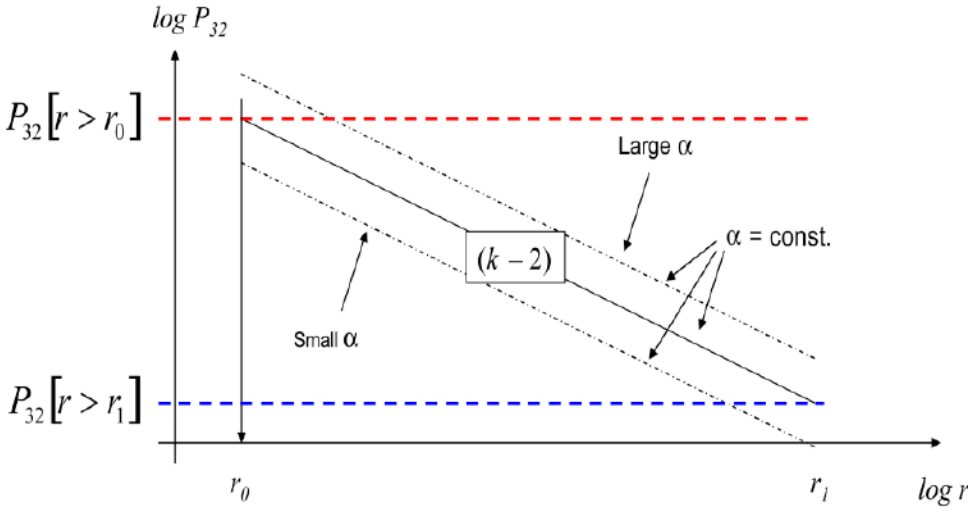

Figure 2-3. *Graph showing the relationship between P_{32} and r in Equation (2-6). α denotes the intensity parameter used in DarcyTools. Its relation to P_{32}, r, and (k–2) is explained in the text.*

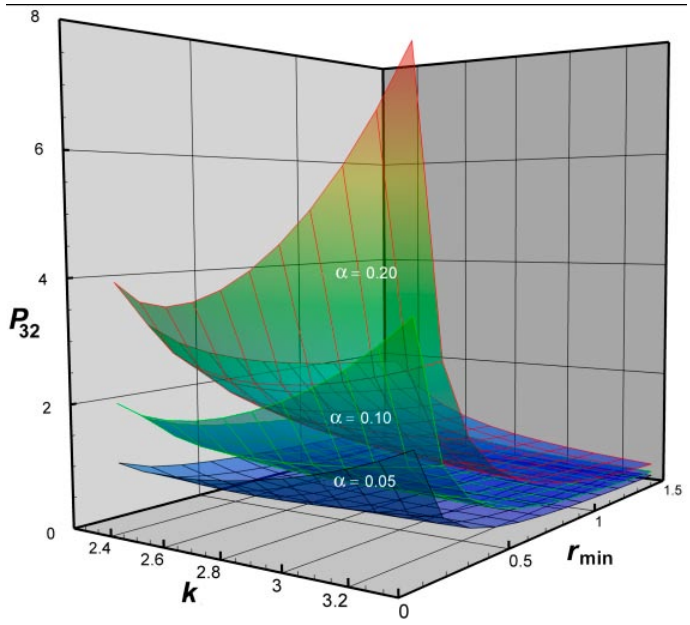

Figure 2-4. *Illustration of the dependence of P_{32} on r_{min}, k and α.*

2.4 Conversion from fracture properties to grid cell properties

In order to assess the implications of the inferred DFN model on flow and transport on the regional-scale, it is necessary for practical reasons to convert the DFN model to an EPM model with appropriate properties. The resulting parameters are a directional hydraulic conductivity tensor, fracture kinematic porosity and other transport properties (such as the fracture surface area per unit volume).

DarcyTools uses a staggered computational grid of cells, which means that scalar entities such as pressure, flow porosity and salinity use a cell-centred mesh, whereas directional entities such as hydraulic conductivity, hydrodynamic diffusivity, mass flux and Darcy velocity use a mesh centred at the cell walls. This grid arrangement was first introduced by /Harlow and Welch 1965/ and is described in textbooks, see e.g. /Patankar 1980/. Each variable is assumed to be representative for a certain control volume, which is the volume the discretised equations are formulated for. In DarcyTools a technique called the GEHYCO-method is used for the conversion from fracture properties to grid cell properties:

A fracture contributes to the grid value of a variable by an amount which is equal to the intersecting fracture volume times the value of the variable in question. Contributions from all elements that intersect the control volume are added and the sum is divided by the volume of the cell.

The GEHYCO-method is obviously very simple but still general enough to handle even complex fracture networks. A few properties of the method are noted:

- All cell wall hydraulic conductivities will be different in the general case. In result, an anisotropic hydraulic conductivity field is obtained.
- A fracture smaller than the cell size can not generally contribute to the anisotropy or the correlation of the hydraulic conductivity field.

A connectivity analysis is conducted prior to the conversion from fracture properties to grid cell properties is applied. Hence, it is only the inter-connected fractures that are retained and contribute in the conversion from fracture properties to grid cell properties. A notion often used in flow modelling with DarcyTools is that the size of smallest fracture considered determines the grid cell size. That is, contributions to flow from fractures smaller that the grid cell size are assumed to be relatively insignificant. This hypothesis is strongly coupled to the invoked power law correlation between fracture transmissivity and fracture size in Equation (2-9). The contribution to the "background" flow from sub-grid scale fractures can easily be tested by using finer grids /Svensson 2001ab, Svensson et al. 2004/ provide calculations that illustrate the GEHYCO method and the accuracy that can be expected.

It should be noted that no extra component for matrix conductivity or micro-fracturing is added in DarcyTools in the general case. However, the stochastic DFN is necessarily truncated in some way, i.e. $[r_{min}, r_{max}]$, which means that some cells may not include a connected network of fractures or may only be connected in some directions. To avoid this just being a result of the choice of truncation limit and chance, a minimum grid cell conductivity and porosity assigned for each cell that has nil hydraulic diffusivity.

The exchange of matter with the flowing water through molecular diffusion is modelled by means of the multi-rate diffusion approach in DarcyTools /Haggerty and Gorelick 1995/. The exchange of matter is governed by mass transfer coefficients and capacity boxes (storage volumes), see Section 2.5.

2.5 Variable density groundwater flow and salt transport

DarcyTools computes fracture network flows using a continuum model in which the mass conservation equation for groundwater is associated to several mass fraction transport equations for the salinity and/or particle mass concentrations, and to a heat transport equation. The mass conservation for groundwater in DarcyTools is written as:

$$\frac{\partial(\rho\varepsilon)}{\partial t}+\frac{\partial}{\partial x}(\rho u)+\frac{\partial}{\partial y}(\rho v)+\frac{\partial}{\partial z}(\rho w)=Q \qquad (2\text{-}11)$$

The mass conservation equation is turned into a pressure equation by means of the Darcy assumption:

$$\begin{aligned}\rho u &= -\frac{K_x}{g}\frac{\partial p}{\partial x}\\ \rho v &= -\frac{K_y}{g}\frac{\partial p}{\partial y}\\ \rho w &= -\frac{K_z}{g}\frac{\partial p}{\partial z}-K_z(\rho-\rho_0)\end{aligned} \qquad (2\text{-}12)$$

Salt transport is treated by means of two processes in DarcyTools:

- advection-diffusion within the mobile pore volume in the computational grid, and
- diffusive exchange between the immobile and mobile pore volumes on a sub-grid scale (multi-rate diffusion).

The mass fraction transport equation (the advection-dispersion equation) for the salinity in DarcyTools is written as /Svensson et al. 2004/:

$$\begin{aligned}&\frac{\partial(\rho\varepsilon)}{\partial t}+\frac{\partial}{\partial x}\left(\rho u C-\rho\gamma D_x\frac{\partial C}{\partial x}\right)\\ &\quad+\frac{\partial}{\partial y}\left(\rho v C-\rho\gamma D_y\frac{\partial C}{\partial y}\right)\\ &\quad+\frac{\partial}{\partial z}\left(\rho w C-\rho\gamma D_z\frac{\partial C}{\partial z}\right)=Q C+Q_c\end{aligned} \qquad (2\text{-}13)$$

In Equations (2-11) through (2-13) ρ is the fluid density, ε the grid cell kinematic porosity, (u, v, w) the Darcy fluxes, (K_x, K_y, K_z) the grid cell wall (inter-node) hydraulic conductivities, g the acceleration of gravity, ρ_0 a reference fluid density, p the dynamic fluid pressure relative to the reference hydrostatic pressure, C the transported mass fraction of salt and (D_x, D_y, D_z) the hydrodynamic dispersion. Q and Q_c are source/sink terms per unit volume of fluid mass, where Q_c represents the diffusive exchange of salt between the mobile and immobile pore volumes. The concept of diffusion into immobile volumes in DarcyTools ranges from the short time (fast) diffusion into the easily reached stagnant pools of water nearby a flowing fracture to the long time (slow) diffusion into the less porous rock "far" away from the flowing fracture, the depth of which depends on the modelled time scale and the matrix properties. Figure 2-5 shows a conceptual model of the transition zone between flow and immobile pore volumes.

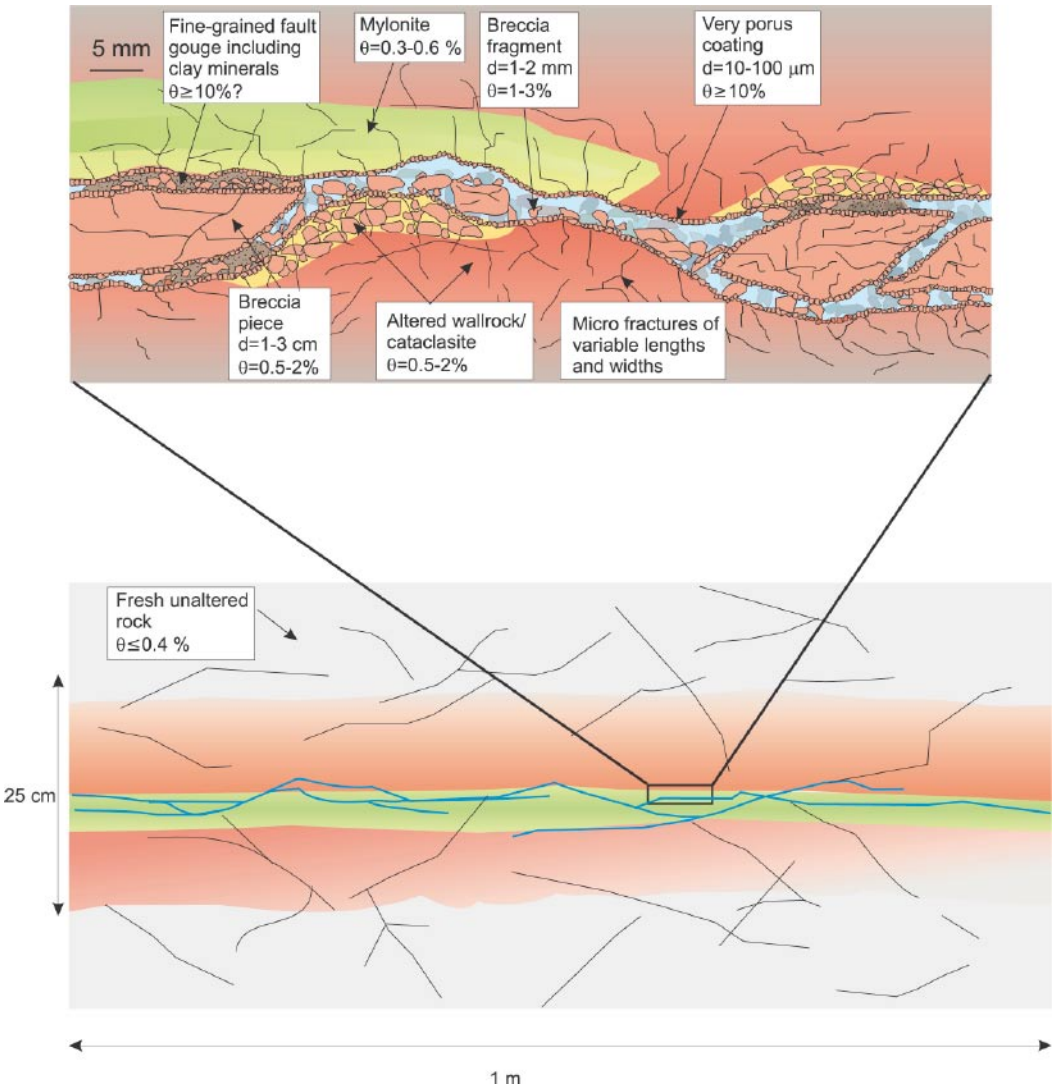

Figure 2-5. *Generalised conceptual model of a typical conductive structure /Winberg et al. 2002/.*

The diffusive exchange of salt between the immobile and mobile pore volumes Q_c is modelled by a multi-rate diffusion process in DarcyTools. The implementation of the multi-rate diffusion process is based on the one-dimensional multi-rate diffusion model by /Haggerty and Gorelick 1995/. One of the key parameters of the multi-rate diffusion model is the capacity ratio between the immobile and mobile pore volumes. The pore volume in the rock matrix accessible for diffusion V_p is expected to be 10–100 times greater than the pore volume in the water-conducting fractures, V_f /Neretnieks 2004/. The current working hypothesis used in DarcyTools is that the capacity ratio ought to be of the same order of magnitude. The capacity ratio as used in DarcyTools is defined in Equation (2-14).

The multi-rate diffusion parameter values used in the work reported here are presented in Chapter 7. The values used are adopted from the experiences gained in Task 6 /Svensson and Follin 2005, Svensson 2004b/. No particular adaptation is made to the fracture size statistics derived in the DFN analysis presented in Chapter 5. Since a power law size relationship is assumed, also fractures in the immobile volume are related to the DFN statistics. Below follows a brief summary of how the multi-rate diffusion method is implemented in DarcyTools version 2.1.

The grid cell capacity ratio β_c in DarcyTools may be written as:

$$\beta_c = \frac{V_{im,c}}{V_{m,c}} \tag{2-14}$$

where $V_{im,c}$ and $V_{m,c}$ are the grid cell values of the immobile and mobile pore volumes, respectively. By the same token, the total, or global, capacity ratio of the entire model domain β_G may be written as:

$$\beta_G = \frac{\sum_c V_{im,c}}{\sum_c V_{m,c}} \tag{2-15}$$

In DarcyTools it is assumed that the spatial distribution of the immobile pore volume is directly proportional to the spatial distribution of the accumulated flow wetted surface area. If FWS_f denotes the contribution to the flow wetted surface area of a grid cell from fracture f and FWS_c the accumulated flow wetted surface area of all connected fractures that intersect the cell, the assumption made in DarcyTools may be written as:

$$FWS_c = \left(\sum_f FWS_f \right)_c \tag{2-16}$$

$$V_{im,c} = k_{FWS}\ FWS_c \tag{2-17}$$

$$\sum_c V_{im,c} = k_{FWS} \sum_c FWS_c \tag{2-18}$$

The ratio between the immobile pore volume in a grid cell and the total immobile pore volume may be written as:

$$\frac{V_{im,c}}{\sum_c V_{im,c}} = \frac{FWS_c}{\sum_c FWS_c} \tag{2-19}$$

If the value of the total capacity ratio of the bedrock is given, or assumed to be known, the spatial distribution of the capacity ratio on the scale of a computational grid cell can be estimated by combining the definitions in Equations (2-14) and (2-15) with the assumption behind Equation (2-18):

$$\beta_c = \beta_G \left(\frac{FWS_c}{\sum_c FWS_c} \right) \left(\frac{\sum_c V_{m,c}}{V_{m,c}} \right) \tag{2-20}$$

As a consequence, the value of the proportionality constant k_{FWS} in Equations (2-17) and (2-18) may be written as:

$$k_{FWS} = \frac{\beta_G}{\left(\frac{\sum_c FWS_c}{\sum_c V_{m,c}} \right)} \tag{2-21}$$

A series of capacity boxes with different mass transfer coefficients α_i are used in the multi-rate model to model the diffusive exchange of matter between the mobile and immobile pore volumes /Haggerty and Gorelick 1995, Svensson et al. 2004/. α_i has the unit $[s^{-1}]$, thus $(\alpha_i)^{-1}$ may be interpreted as the residence time for the diffusive exchange of matter to enter and exit capacity box *i*.

The exchange of matter by diffusion with the rock mass exposed by the flow wetted surface area can be expected to be related to two parameters; the flow wetted surface area per unit volume of flowing water a_w and the advective travel time t_w. The exchange will increase with both these parameters and a new variable, the *F*-factor) /Andersson et al. 1998a/ has been introduced for this product:

$$F = a_w t_w \tag{2-22}$$

The discretised form of Equation (2-22) for a flow path through a grid cell may be written as:

$$F_c = \left(\frac{FWS}{V_m} \right)_c \left(t_{exit} - t_{entrance} \right)_w \tag{2-23}$$

Integration along the entire flow path yields:

$$F = \sum_c F_c \tag{2-24}$$

The mobile pore volume of a grid cell *c* in DarcyTools may be written as:

$$V_{m,c} = \sum \left(\varepsilon_f \, V_f \right)_c \tag{2-25}$$

where ε_f is the kinematic porosity of an intersecting water-conducting fracture and V_f the volume of the fracture in the grid cell. The grid cell kinematic porosity ε becomes:

$$\varepsilon = \frac{V_{m,c}}{V_c} \tag{2-26}$$

The kinematic porosity of a fracture may be written as:

$$\varepsilon_f = \frac{e_f}{b_{hyd}} \tag{2-27}$$

where e_f is the total thickness of the empty space in the flowing fracture and b_{hyd} the hydraulic thickness of the flowing fracture. If there is no fracture fill then $b_{hyd} = e_f$ and

$$\varepsilon = \frac{\sum \left(V_f \right)_c}{V_c} \tag{2-28}$$

e_f may be thought of as the transport aperture e_t for which there exists several expressions, among which the cubic law probably is the most well known. Equation (2-2) shows a power law expression used in the TRUE project at the Äspö HRL. It is noted that Equation (2-2) is derived from tracer experiments in single fractures over short distances and that there are few if any tracer experiments conducted in fractured rocks over longer distances, e.g. 100 m or more. There is also limited experience of using Equation (2-2) in regional flow studies such as the work reported here.

The transmissivities and spacing of connected fractures above the lower measurement limit of the Posiva Flow Log (high resolution difference fracture flow logging (PFL-f); $(1–2)\cdot10^{-9}$ m^2/s) may be used to estimate the mean bedrock kinematic porosity for fractures above this measurement limit. Thus, for scooping calculations we may define ε_{PFL} as:

$$\varepsilon_{PFL} = \frac{\sum(e_t)}{\left(\frac{L_{PFL}}{N_{PFL}}\right)} \qquad (2\text{-}29)$$

where L_{PFL} denotes the length along the borehole that corresponds to the number of PFL flow anomalies observed L_{PFL}.

The practical use of the equations listed above for a computational grid cell can best be illustrated by an example:

A grid cell of size (100 m)^3 is intersected by a large horizontal deformation zone, which has a hydraulic thickness of 10 m and a transmissivity of $2\cdot10^{-5}$ m^2/s. Equation (2-2) renders that the transport aperture of the zone is $2.24\cdot10^{-3}$ m and Equation (2-27) that its kinematic porosity is $2.24\cdot10^{-4}$. Its contribution to the grid cell's total mobile pore volume is 22.4 m^3 according to Equation (2-25) and if no other fractures are intersecting the grid cell, the kinematic porosity of the grid cell becomes $2.24\cdot10^{-5}$.

2.6 Water types

Two primary concepts used in the regional-scale palaeo-hydrogeological groundwater flow modelling with DarcyTools are:

- The current hydrogeological and hydrogeochemical situation in Simpevarp is the result of natural transient processes (infiltration of glacial water, land-rise, marine transgressions and regressions, dilution/mixing of sea water) that have evolved during the Holocene period. These processes are associated with the ongoing shoreline displacement. Since 14,000 BC the Simpevarp area has raised c115 m and during the 10,000 years to come the area is expected to rise another 15 m /Follin et al. 1996/.
- The integration with hydrogeochemistry is evaluated by assuming appropriate initial and boundary condition with regard to the aforementioned processes during Holocene. In DarcyTools four different types of inert water are released according to the past hydrogeological and hydrogeochemical situation in the Simpevarp area. The four types of water correspond, ideally, to the four reference waters treated by hydrogeochemistry – Rain 1960, Marine, Glacial and Brine – see /Laaksoharju et al. 1999, 2004/. If the concentrations of the reference waters modelled by hydrogeochemistry are similar to the simulated water type concentrations this suggests that mixing may be an important process for the hydrogeochemical understanding.

In the work reported here we did not try to subject the water types to matrix diffusion, but it is noted that the multi-rate diffusion model used for modelling diffusion of salt can be used also for modelling diffusion of water types. Five water types are treated in the DarcyTools simulations. These are named in a fashion that resembles the names of the reference waters treated by hydrogeochemistry, Brine, Glacial, Littorina, Meteoric (precipitation before 1960), and Rain 1960 (precipitation after 1960). The boundary and initial conditions associated with the usage of five water types are explained in Section 2.7.

2.7 Flow-related transport performance measures

One objective of the site descriptive modelling is to understand groundwater flow paths from a local-scale area to the surface. The approach taken is to track particles moving with the advective flow velocity from a range of release points until they reach the top surface. Although it would be possible in DarcyTools to track particles as they move through a velocity field that evolves in time, it is preferred here to only use the velocity field from the present day. This is mainly because particle tracks released in a transient velocity field would be sensitive to the release time and the kinematic porosity, making it more difficult to interpret the results due to the added uncertainties.

There are three performance measures suggested for the site descriptive hydrogeological modelling:

- the advective travel time t_w from the release point to the discharge point:

$$t_w = \sum \left(\frac{\varepsilon \, \delta}{q} \right) \tag{2-30}$$

  where ε is the grid cell kinematic porosity, δ an increment in distance along the flow path and q the Darcy velocity

- the length L_w of the flow path from the release point to the discharge point:

$$L_w = \sum (\delta) \tag{2-31}$$

- the Darcy velocity at the release point (canister flux) q_0
- the F-factor of the flow path from the release point to the discharge point:

$$F = \sum \left(\frac{2 \, P_{32CON}[r > r_0] \, \delta}{q} \right) \tag{2-32}$$

  where $P_{32CON}[r > r_0]$ is the interconnected fracture surface area per unit volume of rock mass (cf Chapter 5), δ an increment in distance along the flow path and q the Darcy velocity. (Equations (2-32) and (2-22) are equivalent since $a_w = 2 \, P_{32CON}[r > r_0]/\varepsilon$ and $t_w = \delta/(q/\varepsilon)$.)

The approach to calculating the performance measures is to release a large number of particles distributed evenly (fixed spacing) over a postulated release area and use these to produce ensemble statistics for the performance measures, as well as locating the discharge areas. No attempt is made to avoid starting particles in either deterministic fracture zones or high transmissivity stochastic fractures. In reality such fractures are likely to be avoided during repository construction, and hence the model may tend to see particles start in a wider range of possible fracture transmissivities than might be encountered in reality.

3 Hydraulic test data available for a detailed geological-hydrogeological DFN modelling

3.1 Introduction

A number of hydraulic test methods are used in a more or less standardised fashion for the hydraulic characterisation of the bedrock penetrated by the boreholes drilled during the site investigations. The hydraulic characterisation of the uppermost part of the bedrock down to c 200 m depth is conducted mainly by means of single hole hydraulic tests (HTHB tests) in 140 mm diameter percussion drilled boreholes (H-holes). The hydraulic characterisation of the interval 100–1,000 m depth is conducted by means of single hole hydraulic tests (PFL-s (5 m) tests, PFL-f (5 m/0.1 m) tests and PSS 100 m, PSS 20 m and PSS 5 m tests) in 76 mm diameter cored drilled boreholes (K-holes).

The locations of the core drilled KSH01A, KSH02, KSH03A, KAV01, KLX01 and KLX02 boreholes available for modelling at the time of 1.2 data freeze in the Simpevarp subarea are shown in Figure 3-1.

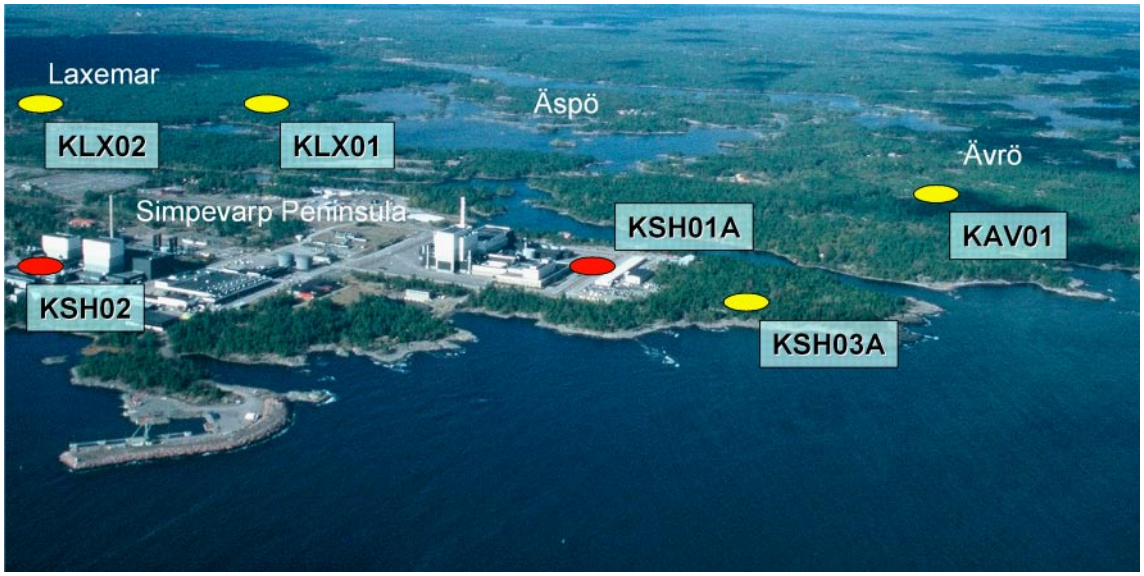

Figure 3-1. *Locations of the core drilled KSH01A, KSH02, KSH03A, KAV01, KLX01 and KLX02 boreholes available for modelling at the time of 1.2 data freeze in the Simpevarp subarea.*

3.2 High resolution difference fracture flow data (PFL-f)

A detailed structural-hydraulic analysis (hydrogeological DFN modelling) requires high resolution fracture flow measurements. The measurements of interest for the methodology suggested in the work reported here are the high resolution fracture transmissivity tests (PFL-f). Such test are conducted in the KSH01A and KSH02 boreholes only /Rouhiainen and Pöllänen 2003ab/. The hydrogeological DFN modelling conducted in the work reported here is presented in Chapter 5. Figure 3-2 shows a BIPS image of a flowing fracture detected by the PFL-f tests in the KSH01A borehole.

The practical lower measurement limit for transmissivity of PFL-f data is typically c $(1–2)\cdot10^{-9}$ m^2/s. Sometimes values below this "threshold" are interpreted. For instance, there are 82 PFL-f anomalies in the KSH01A borehole with a minimum transmissivity value of $3.9\cdot10^{-10}$ m^2/s and there are 80 PFL-f anomalies in the KSH02 borehole with a minimum transmissivity value of $9.4\cdot10^{-10}$ m^2/s. 41 of the 82 PFL-f anomalies in the KSH01A borehole are found in the rock mass outside the 13 (!) length intervals interpreted to have deformation zone type properties. In comparison, there are 70 PFL-f anomalies in the rock mass in the KSH02 borehole. There are 4 length intervals in the KSH02 borehole interpreted to have deformation zone type properties. The structural and hydraulic information in the KSH01A and KSH02 boreholes is the basis for the hydrogeological DFN modelling presented in Chapter 5.

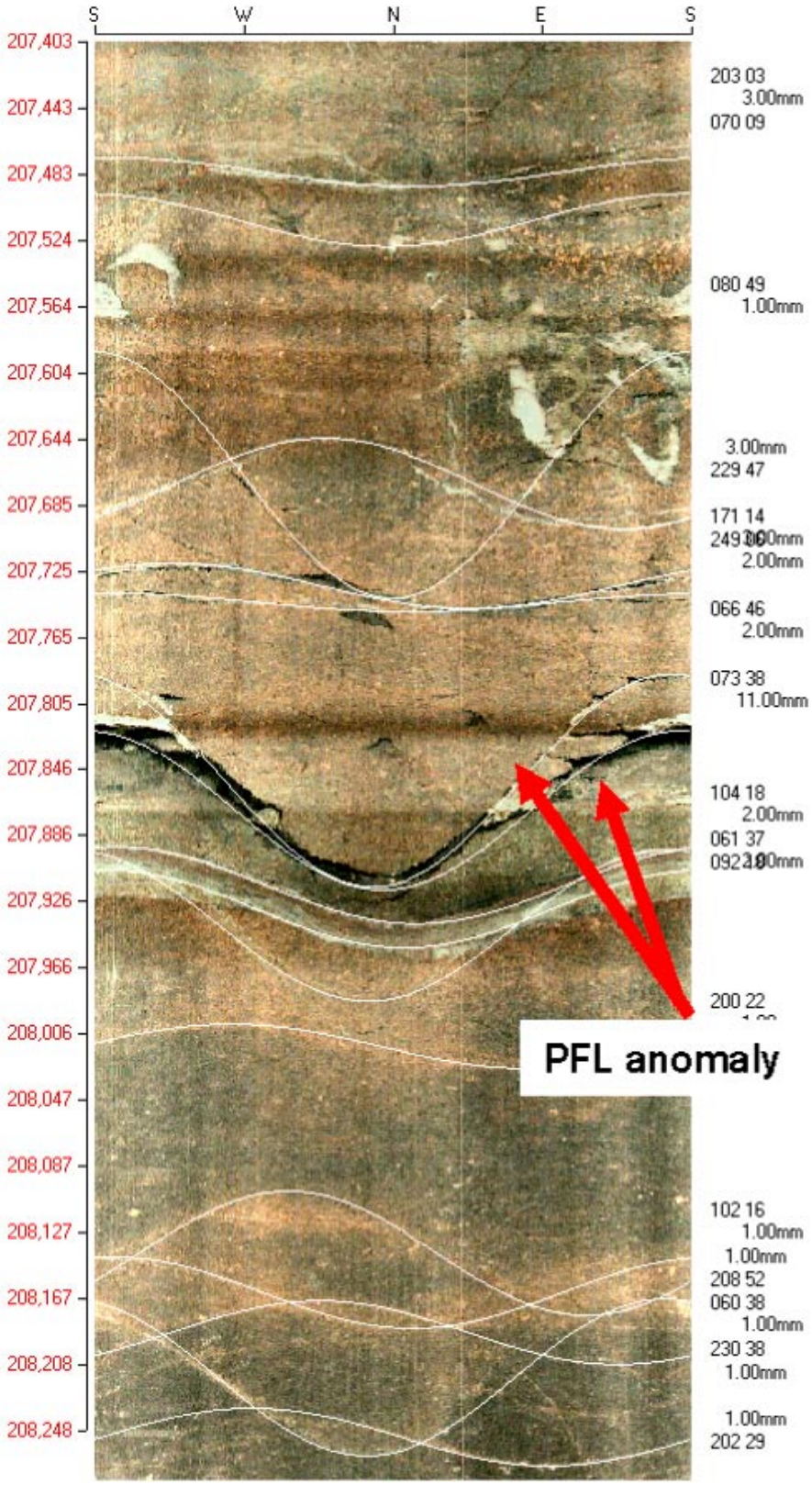

Figure 3-2. *BIPS image of a c 88 cm long borehole section in the KSH01A borehole. White lines represent different mapped objects as Open and Sealed fractures, rock contacts etc. The transmissivity of the marked object is $1.7 \cdot 10^{-7}$ m^2/s. Generally Open fractures cannot be seen in BIPS as in the example above. /Forssman et al. 2005/.*

3.3 Preparations for a joint structural and hydraulic single hole interpretation

In the core mapping, each fracture is classified as Sealed, Open or Partly open and with a judgement of how certain the geologist is of this classification – expressed as Certain, Probable and Possible. Partly open fractures refers to all fractures that do not cut the core entirely but have (1) altered or weathered fracture planes or are (2) associated with a measurable aperture in the borehole wall using BIPS to indicate an edge of a fracture. The number of Partly open fractures is generally small. However, they demonstrate that one reason the division of fractures into Open and Sealed is not a clear cut, nor is the definition of fracture frequency. The identification of a flow anomaly with the Posiva Flow Log is classified as Certain or Uncertain. Both the core mapped data and the flow anomalies are rigorously length corrected (i.e. spatially located along the borehole). It is expected that the positions of objects along the boreholes normally can be correlated to within 0.2–0.3 m.

/Forssman et al. 2005/ merged different data sets and made a quality control analysis in preparation for the joint structural and hydraulic single hole interpretation conducted by the DarcyTools Team. The quality control encompassed a screening of the positions of the identified PFL-f anomalies with regard to the fracture data from the core mapping and the single-hole geological interpretations of rock domains and deformation zones. Figure 3-3 and Figure 3-4 summarise the results provided by /Forssman et al. 2005/.

The classification of "flow indication Open fractures", or the PFL-f confidence, is defined as the distance between the PFL-f anomaly and the interpreted fracture. That is, if the anomaly has a flow indication in Class 1, the interpreted fracture is within 1 dm from the anomaly. In the same way, the anomaly has the flow indication Class 2, if the interpreted fracture is within 2 dm from the anomaly. Four classes have been defined: Class 1: 0–1 dm; Class 2: 1–2 dm; Class 3: 2–3 dm; and Class 4: 3–4 dm.

As a first assumption all Open and Partly open fractures as well as Crush Zones are assumed to be potential flowing fractures. In most cases, one or several Open fractures were identified within 0.2 m from a given flow anomaly. Only in a few cases could no Open fractures, Partly open fractures or Crush Zones be linked to within 0.5 m of a flow anomaly, probably indicating that a fracture mapped as Sealed should have been classified as Open. In such cases one could generally find Sealed fractures classified as Probable or Possible and mapped as broken near the flow anomaly.

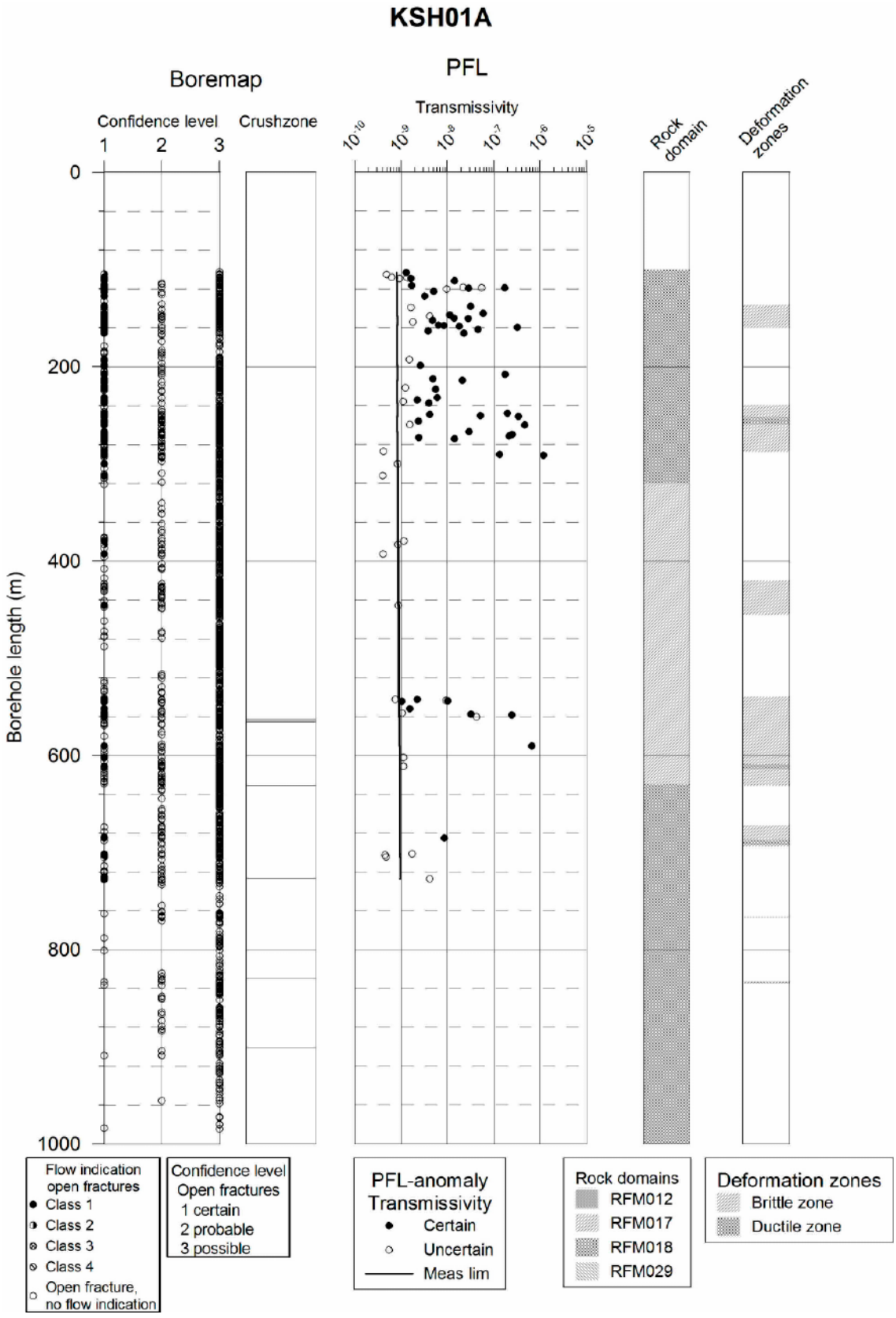

Figure 3-3. *Correlation of hydraulic fractures, based on PFL-f overlapping measurements, to mapped Open/Partly open fractures (all plotted as Open fractures above) or crush zones. Interpreted deformation zones (mainly brittle or ductile) and rock domains shown to the right. Fractures with PFL confidence (flow indication class) > 4 are not plotted /Forssman et al. 2005/.*

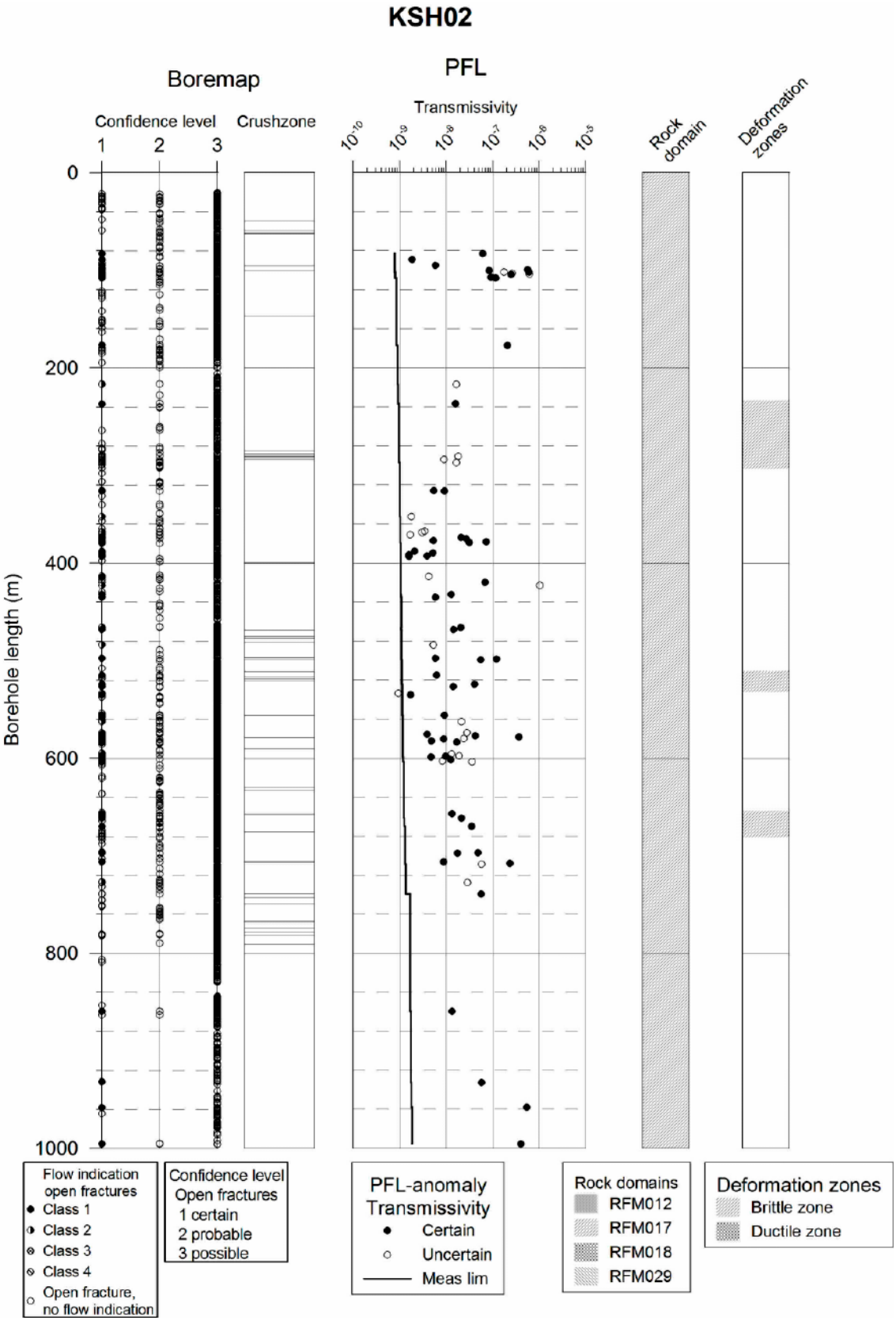

Figure 3-4. *Correlation of hydraulic fractures, based on PFL-f overlapping measurements, to mapped Open/Partly open fractures (all plotted as Open fractures above) or crush zones. Interpreted deformation zones (mainly brittle or ductile) and rock domains shown to the right. Fractures with PFL confidence (flow indication class) > 4 are not plotted /Forssman et al. 2005/.*

3.4 Comparing test methods and evaluation methodologies

The two cross plots in Figure 3-5 shows hydraulic test data for the KSH01A and KSH02 boreholes. Each plot shows three series of data:

- T5m_PFL–Σanom; aggregated radial flow, steady state, fracture transmissivities determined with the Posiva Flow Log (PFL) tool using an aggregation interval length of 5 m and an pumping period of c 2,000 minutes. The PFL-f fracture transmissivities underpinning the T5m_PFL–Σanom data are determined with a straddle interval of 5 m and an overlap of two consecutive measurements of 0.1 m (PFL-f; 5 m/0.1 m). The aggregation is made within the same 5 m intervals used in the PSS testing. The interpretation of the PFL-f transmissivities are made with Thiem's equation /Thiem 1906/.
- T_MOYE(5m–PSS); radial flow, steady state, test section transmissivities determined from data acquired with the Pipe String System (PSS) tool using a test section length of 5 m and an injection period of c 20 minutes. The interpretation of the steady state transmissivities are made with Moye´s equation /Moye 1967/.
- T_BC(5m–PSS); "best choice" test section transmissivities determined from data acquired with the Pipe String System (PSS) tool using a test section length of 5 m and an injection period of c 20 minutes.. A "best choice" transmissivity can either be a transient interpretation /Horne 1995/ or a steady state interpretation /Moye 1967/ depending on the investigators expert judgement. T_BC(5m–PSS) is generally synonymous to a transient interpretation.

Despite use of different test methods (PFL vs PSS) and different evaluation methods (transient vs steady state) most of the transmissivities plot close to the 1:1 line. Hence, from Figure 3-5 we conclude that fracture transmissivities determined by difference fracture flow logging (PFL-f) seem robust.

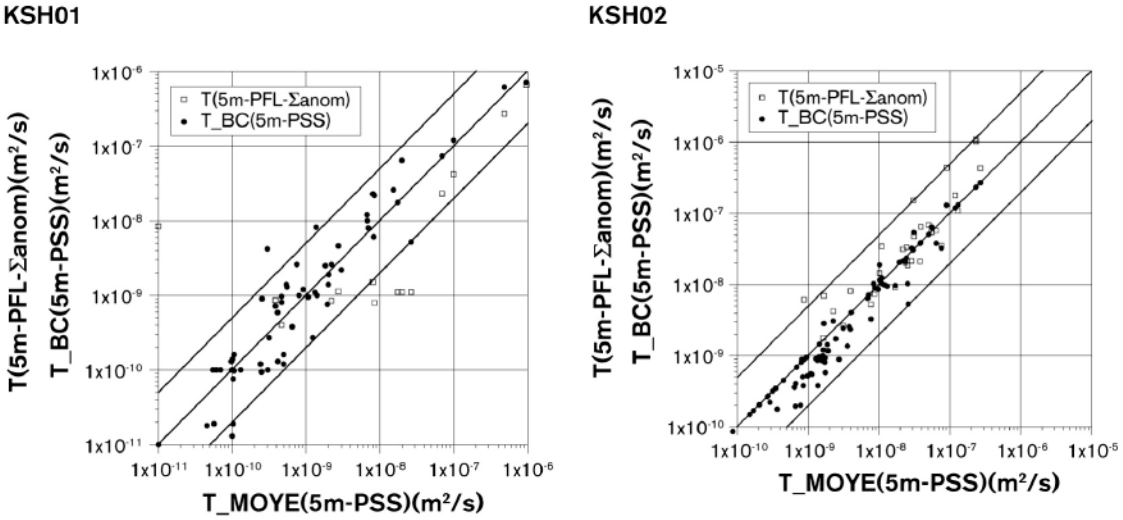

Figure 3-5. *Cross plots of 1) PFL-f transmissivities summed up 5 m sections (T(5m-PFL-Σanom) versus steady state PSS 5 m transmissivities (T_Moye), and 2) transient PSS 5 m transmissivities (T-BC(5 m-PSS) versus steady state PSS 5 m transmissivities (T_Moye). The bounding lines to the 1:1 line represent values that are 0.2 and 5 times the 1:1 value.*

4 Assessment of properties of the Hydraulic Conductor Domains (HCD)

4.1 Modelling methodology

The deterministically described deformation zones are modelled as three-dimensional features, the geometries of which were defined by geology and modelled in SKB's Rock Visualisation System /Curtis et al. 2003ab/. All deterministically described deformation zones in the Simpevarp regional model domain (cf Figure 1-3 and Figure 1-4) are modelled as potential HCDs. Single-borehole intervals with deformation zone type properties not modelled deterministically as deformation zones are handled as unconditional stochastic features in the Hydraulic Rock Domain (HRD) model.

4.2 Hydraulic properties

The deformation zones are mostly based on geological and/or geophysical indications. Some of the deformation zones are intercepted by old boreholes, and hydraulic test data from these boreholes were used the assignment of hydraulic properties in the 1.1 modelling stage, cf /SKB 2004/. A few boreholes only drilled during the 1.2 site investigations have penetrated the deterministically modelled deformation zones, e.g.:

- The ZSMNE024A deformation zone was penetrated by the KSH03A core drilled borehole and the HAV11 percussion drilled borehole,
- ZSMEW002A was penetrated by the HLX20,
- ZSMEW007A was penetrated by HLX11 and HLX13,
- ZSMNE012A was penetrated HAV13 and HAV14,
- ZSMNE018A was penetrated HSH02, and
- ZSMNE025A was penetrated by HSH01.

The assignment of hydraulic properties to the HCDs is based on single-hole hydraulic tests mainly. Data from cross-hole (interference) hydraulic tests are still very scarce at this stage. In conclusion, the site-specific data available for the 1.2 hydrogeological modelling consist of transmissivity and hydraulic thickness estimates, whereas general formulae are used for assigning equivalent parameter values of the storativity, the transport aperture and the kinematic porosity of the HCDs, cf Equations (2-1), (2-2) and (2-25). These formulae are taken from the findings reported in /Rhén et al. 1997, Rhén and Forsmark 2001, Andersson et al. 1998b, 2000, Dershowitz et al. 2003/. It is noted that the HCD storativity, transport aperture and kinematic porosity are all modelled as power law functions of the HCD transmissivity.

Table 4-1 summarises the hydraulic properties (hydraulic thickness and transmissivity) of the HCDs. The values are based on results from the pre-construction investigation and the construction of the Äspö HRL and the ongoing site investigations in the Simpevarp and Laxemar subareas. The geometric mean of the transmissivities of the HCDs in the Äspö HRL model /Rhen et al. 1997/ are used if no site specific value is available for a specific HCD. The hydraulic properties are assumed to be constant within each HCD.

Table 4-1. Compilation of the hydraulic thickness and transmissivity assigned to each HCD in the 1.2 hydrogeological modelling. General formulae are used for assignment of storativity (storage coefficient), transport aperture and kinematic porosity, cf Equations (2-1), (2-2) and (2-25). There are 22 high confidence HCDs in S1.2.

Name of HCD (RVS ID and/or ÄSPÖ HRL ID)	Geological confidence	Hydraulic thickness (m)	Transmissivity (m^2/s)
ZSMEW002A (Mederhult zone)	High	45	$1.0 \cdot 10^{-5}$
ZSMEW004A	High	30	$*1.3 \cdot 10^{-5}$
ZSMEW007A	High	2	$2.3 \cdot 10^{-4}$
ZSMEW009A (EW3)	High	12	$1.7 \cdot 10^{-5}$
ZSMEW013A	High	20	$4.0 \cdot 10^{-7}$
ZSMEW028A	High	10	$8.5 \cdot 10^{-8}$
ZSMNE005A (Äspö shear zone)	High	40	$6.6 \cdot 10^{-7}$
ZSMNE006A (NE1)	High	28	$2.2 \cdot 10^{-4}$
ZSMNE010A	High	20	$*1.3 \cdot 10^{-5}$
ZSMNE011A	High	10	$*1.3 \cdot 10^{-5}$
ZSMNE012A (NE4)	High	41	$1.1 \cdot 10^{-4}$
ZSMNE016A	High	13	$*1.3 \cdot 10^{-5}$
ZSMNE018A	High	30	$2.9 \cdot 10^{-6}$
ZSMNE024A	High	80	$3.6 \cdot 10^{-4}$
ZSMNE040A	High	15	$3.7 \cdot 10^{-6}$
ZSMNS001A	High	10	$*1.3 \cdot 10^{-5}$
ZSMNS001B	High	10	$*1.3 \cdot 10^{-5}$
ZSMNS001C	High	10	$*1.3 \cdot 10^{-5}$
ZSMNS001D	High	10	$*1.3 \cdot 10^{-5}$
ZSMNS009A	High	50	$*1.3 \cdot 10^{-5}$
ZSMNS017A	High	20	$6.5 \cdot 10^{-5}$
ZSMNW004A	High	50	$*1.3 \cdot 10^{-5}$
ZSMNW007B	High	50	$*1.3 \cdot 10^{-5}$
ZSMNW012A	High	40	$*1.3 \cdot 10^{-5}$
ZSMNW025A	High	5	$2.6 \cdot 10^{-7}$
ZSMxxxxxx (All other RVS zones)	Low	20	$*1.3 \cdot 10^{-5}$

* Geometric mean of the transmissivities of the HCDs in the Äspö HRL model /Rhen et al. 1997/.

5 Assessment of hydraulic properties of the Hydraulic Rock Domains (HRD)

5.1 Modelling methodology

Hydraulic properties are assigned to the HRDs by hydrogeological DFN analyses. /La Pointe and Hermanson 2005/ provided a geological DFN (GeoDFN) model for the fracturing of the rock mass within the Simpevarp subarea, see Section 5.3. The geological DFN model is based on lineament data, outcrop fracture data and cored borehole fracture data. In the hydrogeological modelling we integrate the geological DFN model with the fracture flow data presented in Chapter 3. The integrated analysis of structural and hydraulic data results in a so called hydrogeological DFN (HydroDFN) model. The hydrogeological DFN model is used for calculating block scale properties as well as for regional variable density flow simulations, cf Figure 2-2.

The hydrogeological DFN modelling approach carried out in the work presented here comprises four main steps:

1. Assessment of geological DFN data.
2. Assessment of hydrogeological DFN data.
3. Assessment of interconnected fracture intensity.
4. Assessment of parameter values for a correlated transmissivity-size model.

Step 1 covers an examination of the geological DFN and the geological single-hole interpretations followed by an analysis of the fracture properties and intensities as well as orientations within each deformation zone and each rock domain in the boreholes.

Step 2 includes an analysis of hydraulic data to obtain a representative value for each uncertain (stochastic) deformation zone treated as a part of the hydrogeological DFN model. The certain (deterministic) deformation zones are excluded from the analysis. A second component is to define the transmissivity distribution.

Step 3 aims at generating stochastic fracture models (realisations) that compare statistically with the mapped orientations and borehole fracture frequencies of Open and Partly open fractures in the core-drilled boreholes. Once the measured geological intensity of intercepts is matched, the interconnected fracture surface area per unit volume of rock mass is determined by a connectivity analysis. This to honour the anisotropy and heterogeneity of underlying DFN and to calculate the FWS.

Step 4 aims at deriving parameter values for the correlated transmissivity model in Equation (2-12).

The fourth step is a working hypothesis. Indeed, any transmissivity-size model can be brought into play, though a correlated model is considered the most intuitive in the work reported here, cf the reasoning in Section 5.2.5. The correlated transmissivity-size model is invoked by assuming that it is the largest interconnected fractures intercepting he borehole in each stochastic DFN realisation that correspond to the largest measured fracture transmissivities.

5.2 Conceptual assumptions

To derive a hydrogeological DFN model with DarcyTools it is necessary to make some conceptual assumptions. Below follows a short presentation of the assumptions used in the work reported here.

5.2.1 Conductive fractures

All naturally Open and Partly Open fractures, regardless of their aperture confidence (Certain, Probable and Possible) were considered to be potential candidates for flow from the onset in the connectivity analysis. Sealed fractures, on the other hand, were considered impervious. This assumption is largely supported by the PFL-anomalies correlating with Open fractures in the BIPS (Borehole Image Processing System). It is recognised to be incorrect on the scale of the fracture aperture, cf Section 5.2.2.

An Open fracture is by definition associated with a naturally broken core, i.e. the natural fracture is as large as or larger than the core diameter. Consequently, a Partly open fracture is by definition a fracture that does not break the core, but still have some kind of aperture associated to it. According to the method description for core mapping /SKB 2002b/, all Partly open fractures are mapped to the extent possible. Partly open and Open fractures are treated alike in the SICADA database as they both contribute to the concept of borehole fracture frequency (borehole fracture intensity) P_{10}. It is noted that the borehole fracture intensity P_{10} associated with Partly open fractures in the Simpevarp subarea is less than 1% of the total P_{10} of Open and Partly open fractures for the boreholes used in the geological DFN modelling /La Pointe and Hermanson 2005/.

5.2.2 Flow

Conductive fractures are assumed to be completely flat surfaces with homogenous macroscopic hydraulic properties, i.e. transmissivity and storativity. In case of heterogeneous fracture properties, equivalent homogeneous (effective) values are considered. In reality, the flow is distributed through channels across the fracture plane. Possibly, also inter-sections between fractures can be considered as potential channels. The physical channels are formed by the undulating fracture surfaces (spatial distribution of the fracture asperity) that do not exactly match, thus creating channels. The distribution of flow channels is, however, governed by the acting boundary conditions, which may be transient. The flow channels in the fracture plane occupy only a minor part of the fracture volume, and parts of the fracture surface are closed due to its undulating nature.

Exchange of solutes to stagnant pools of water, outside the flow channels, is governed by diffusion in more or less free water, which is faster than the diffusive exchange with the rock matrix. It can also be expected that parts of the fracture are filled with fault gauge material, i.e. fine-grained, clayey material, cf Figure 2-5. All these characteristics cannot, and need not always, be modelled in detail, but must be approximated in some way. For the diffusion processes, DarcyTools uses a multi-rate diffusion model.

5.2.3 Stochastic deformation zones

Large fractures of trace lengths on the order of 100 m may exist as single breaks. However, it is more common that discontinuities of trace lengths greater than about 50 m exist as deformation zones or ‘fracture swarms’. A number of fracture swarms are observed in the boreholes. Some of the swarms are treated (modelled) as deterministic deformation zones, other as uncertain, i.e. stochastic. Hence, it is useful to characterise these fractures to get

some indication of the width and fracture intensities within these zones. However, at this regional modelling stage, fracture swarms interpreted as certain or uncertain deformation zones will be approximated as large fracture planes in a continuous range of fracture sizes, as shown in Figure 5-1. It is important that data, such as fracture intensity and the PFL-f flow anomalies, are handled in a manner consistent with this concept. Also, transport parameters, such as fracture porosity and flow-wetted surface, may have to be enhanced in the larger fractures to reflect their zonal properties.

Figure 5-1 implies that the fracturing within a deformation zone is not studied in terms of its components, but treated as a single object. Both stochastic and deterministic deformation zones are treated in this way.

If N_{TOT} is the total number of Open and Partly open fractures in a borehole and N_{DZ} is the number of Open and Partly open fractures in an intercepted stochastic deformation zone, the remaining number of potentially flowing Open and Partly open fractures in the borehole to be matched in the modelling process N_{CAL} may be written as:

$$N_{CAL} = N_{TOT} - \sum (N_{DZ} - 1) \qquad (5\text{-}1)$$

The summation in Equation (5-1) is made over all intercepted stochastic deformation zones. The subtraction by 1 is made as the zone itself is one fracture to be included in the modelling process. This is found to be important in cases where the rock is sparsely fractured.

In analogy with Equation (5-1) the transmissivity of a potentially flowing stochastic deformation zone is considered equal to its geological thickness-hydraulic conductivity product and the storativity is equal to its geological thickness-specific storativity product. This implies that the transmissivity of a stochastic deformation zone, as determined at its intersection with a borehole, is equal to the sum of the transmissivities of the flowing fractures:

$$T_{DZ} = \sum (T_f) \qquad (5\text{-}2)$$

The summation in Equation (5-2) is made over all PFL-f anomalies belonging to the intercepted stochastic deformation zone. Hence, should the deformation zone properties be heterogeneous, then equivalent homogeneous values are assumed. It is noted that Equation (5-2) may overestimate the deformation zone transmissivity T_{DZ} if the flowing fractures intersecting the borehole merge at some distance away from the borehole. The similarity in results between the aforementioned test methods, the difference flow logging (PFL) and the double-packer injection tests (PSS), see Figure 3-5, does not suggest that this may be a major problem, however.

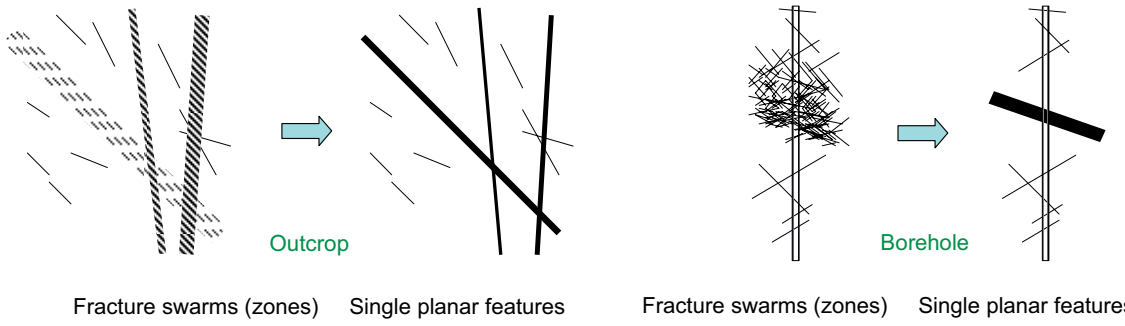

Figure 5-1. *An important assumption in the hydrogeological DFN analysis is the representation of fracture swarms (zones) as single planar fractures.*

5.2.4 Power law size distribution and intensity

One of the most difficult fracture characteristics to measure directly in the subsurface is fracture size. Fracture trace lengths can be measured on outcrops for fractures on the scale of centimetres to several metres, and data are available for lineaments on the scale of 500 m to several kilometres, but this leaves a gap between the scales. A widely used assumption in geology is one of a continuum of fractures that spans all scales and that can be described by a power law relationship between fracture intensity and size, see Figure 5-2. The DarcyTools code is adapted to this assumption, see Chapter 2.

Figure 5-2 illustrates the conceptual relationship between the deterministically treated deformation zones and the stochastic geological DFN. It is noted that fracture shapes are modelled as squares in DarcyTools with a side length L, whereas fracture shapes are modelled as circles of radius r in the geological DFN model. The equivalent radius r of a square of size L is shown in Equation (2-4).

The fracture surface area per unit volume of rock, $P_{32}[r > r_0]$, is a key parameter for the computation of the F-factor, the flow-related transport performance parameter defined in Equation (2-32). The determination of r_0 and hence $P_{32}[r > r_0]$ is a difficult task, however, because the numbers of fractures increase significantly for a power law distribution when the sizes of fractures get smaller. Observations of fracture trace lengths t on outcrops down

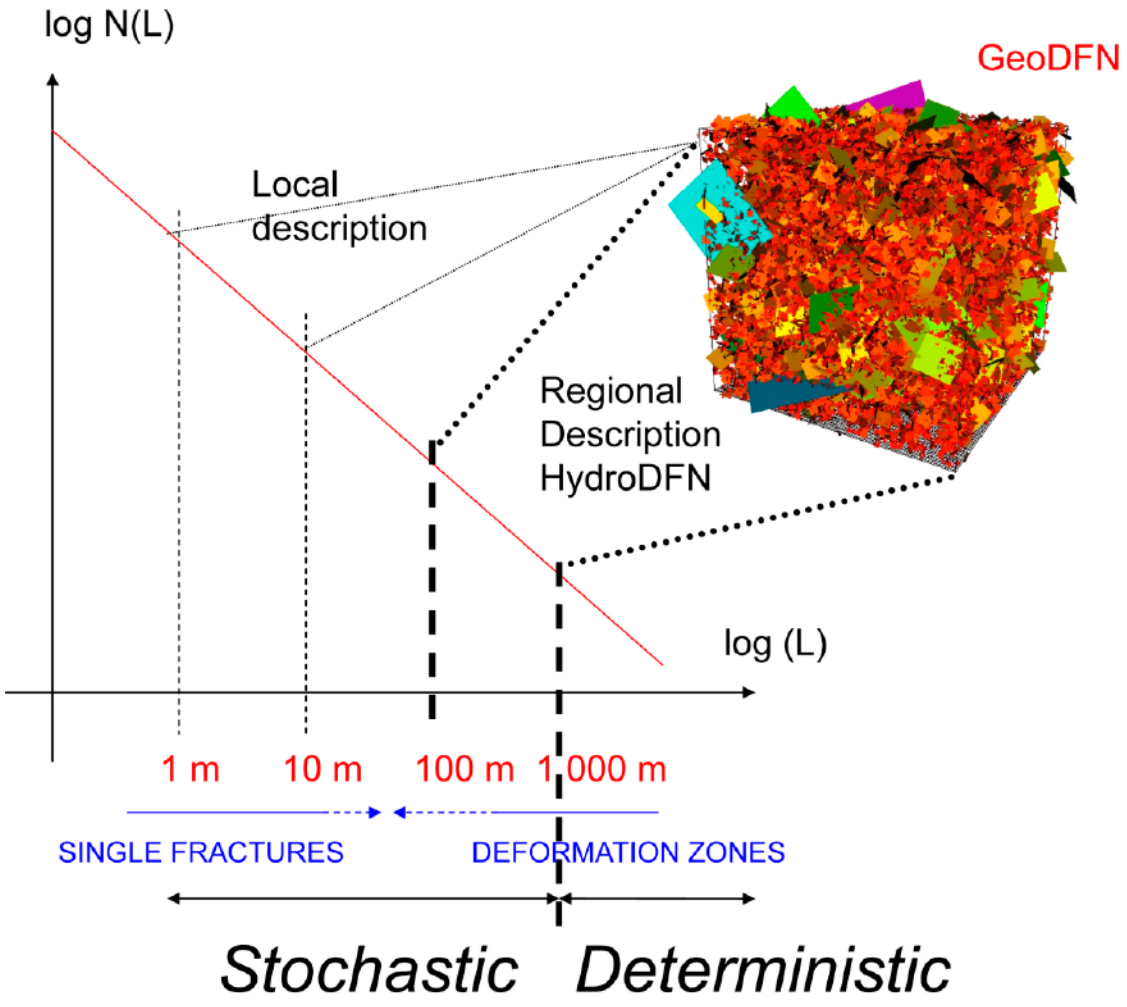

Figure 5-2. *Illustration of the power law size distribution and the conceptual relationship between deterministically treated deformation zones and the stochastic geological DFN.*

to 0.5 m can generally be mapped, whereas shorter trace lengths become quite cumbersome to map. The analysis is not trivial as large fracture sizes may also produce small trace lengths. It is also important to note that the fracture intensity seen on outcrops often differs significantly from the fracture intensity (frequency) seen in cored boreholes. The fracture frequency in boreholes generally decreases towards depth, cf Figures 3-3 and 3-4, which makes it difficult to match observed fracture intensities on outcrops if the fracture network simulations are calibrated against the observed borehole frequency. Moreover, both outcrop and borehole data are biased with regard to the frequency of gently dipping and steeply dipping fractures, respectively. For instance, outcrop fracture trace length data contain almost no observations of gently dipping fractures. Means for intensity correction of borehole data is discussed in Section 5.2.8.

In the work reported here we assume that the desired three-dimensional fracture intensity, $P_{32}[r > r_0]$, is better modelled by the borehole fracture frequency than by the fracture intensity seen on outcrops. A notion about the value of r_0 must be formed, however, in order to transform the observed fracture frequency (m^{-1}), which is a one-dimensional entity, into the desired three-dimensional fracture surface area per unit volume of rock.

The fracture size cannot be determined from borehole data and the statistical matching of simulated versus observed borehole fracture frequencies is insensitive to the chosen value of r_0 provided that the borehole is treated as a scanline, i.e. $r_w = 0$. If the borehole is simulated as a cylinder with a finite radius, i.e. $r_w > 0$, however, a portion of all fractures intersecting the perimeter of the cylinder will not intersect the centre line of the borehole regardless the value of R0. In effect, it is necessary to reduce the fracture surface area per unit volume to retain the match to the observed borehole fracture frequency, which accounts for all fracture intercepts.

The notion about the magnitude of the location parameter r_0 couples closely to the notion about the magnitude of the smallest fracture size that affect the borehole fracture frequency. In Section 2.3 we postulate that $r_0 \approx r_0^*$, where r_0^* is the smallest fracture radius treated in the site investigation with regard to the fracture statistics acquired in cored boreholes. That is, we assume that $r_0^* \approx r_w$, where r_w is the radius of a cored borehole used in SKB's site investigations, 0.038 m.

5.2.5 Transmissivity

An important topic concerns the relationship between the transmissivities of single conductive fractures and the transmissivities deduced from hydraulic single-hole double packer tests. The 5m PSS tests generally comprise a couple of fractures within each test section, whereas the resolution of the PFL-f tests is 0.1 m. This suggests that the latter kind of testing is much more suitable for a discrete statistical analysis such as the one addressed here.

Transmissivity data from single-hole tests often show a wide range of variability and it is common to use statistical distributions for the fracture transmissivity assignment, e.g. the power law distribution or the log-normal distribution. The statistical assignment of transmissivity to discrete fractures can be made in different fashions, e.g.:

1. Transmissivity T is uncorrelated to fracture radius r by a specified normal variability of mean $\mu_{\log 10(T)}$ and standard deviation $\sigma_{\log 10(T)}$:

   $$T = 10^{N(\mu,\sigma)} \qquad (5\text{-}3a)$$

2. Transmissivity is correlated to fracture radius by a factor c and an exponent d,

   $$T = c\, r^d \qquad (5\text{-}3b)$$

3. Transmissivity is semi-correlated to fracture radius by a factor c, an exponent d and a standard deviation $\sigma_{\log 10(T)}$:

$$T = 10^{\left[\log_{10}\left(c\, r^{d}\right) + \sigma\, N(0,1)\right]} \qquad \text{(5-3c)}$$

The three relationships in Equations (5-3a) through (5-3c) are illustrated in Figure 5-3.

From a hydraulic perspective one can advocate that a correlated model is logical. This comes from the consideration that hydraulic tests have different scales of support, i.e. radius of influence. A hydraulic test in a fracture of high transmissivity implies a large radius of influence and vice versa. If the physical radius (size) of the high transmissive fracture is less than its theoretical hydraulic radius of influence, the hydraulic test will sensor this limitation as a physical boundary and in effect a lower transmissivity may be interpreted if the "boundary" is constraining the flow. Larger fractures are more likely to contain one or more channels that link (intersect) boundaries with a difference in head and hence will see more flow.

Another argument for it is that, at least for deformation zones, the zone width often increases with size, and thus generally so does the number of individual conductive fractures associated with a zone. If the transmissivity distribution for individual fractures is the same, then based on the above assumption it follows that the effective transmissivity for the deformation zone should increase with the size of the fracture zone. These arguments are the primary motives for assuming that is the largest interconnected fractures intercepting the borehole in each stochastic DFN realisation that correspond to the measured fracture transmissivities.

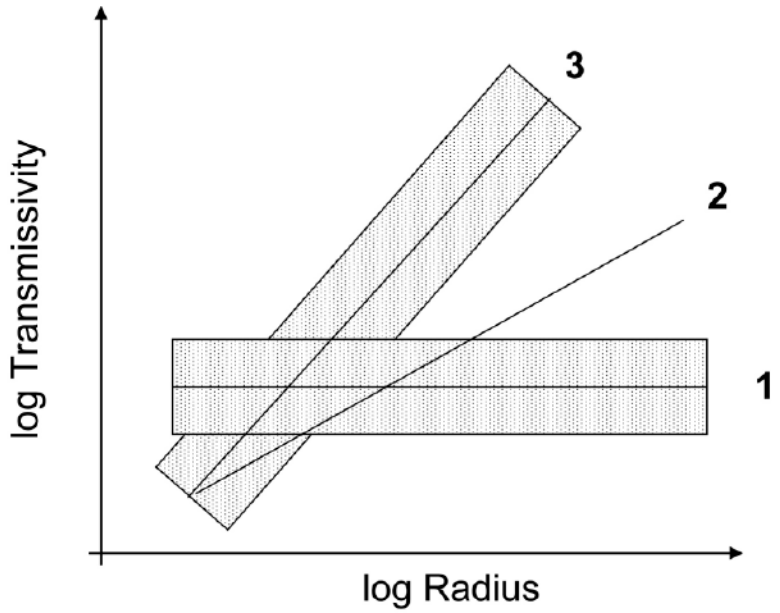

Figure 5-3. *Schematic of three statistical transmissivity models: 1) Uncorrelated with a specified uncertainty; 2) Correlated; 3) Semi-correlated, i.e. correlated with a specified uncertainty.*

5.2.6 Connectivity

The most transmissive of the potentially flowing Open and Partly Open fractures are assumed to be detected by the Posiva Flow Log:

$$N_{PFL} \leq N_{CAL} \tag{5-4}$$

N_{PFL} refers to the number of PFL-f flow anomalies above the lower transmissivity measurement limit and N_{CAL} is the number of potentially conductive features as defined in Equation (5-1). An important component of the connectivity-based approach used in the work reported here is the determination of N_{CON}, i.e. the number of connected fractures in a borehole, related to the geometrical connected feature intensity. N_{CON} is determined by sorting out all isolated features and isolated clusters of features. The intuitive relationship between N_{PFL}, N_{CON}, N_{CAL} and N_{TOT} becomes:

$$N_{PFL} \leq N_{CON} \leq N_{CAL} \leq N_{TOT} \tag{5-5}$$

The probabilistic framework between the simulated connected feature intensity and the interpreted transmissivities is illustrated in Figure 5-4.

In the work reported here we consider the ratio between N_{CON} and N_{CAL} as an estimator of the Open fracture connectivity. Hence, the connected fracture surface area per unit volume of Open fractures may approximately be written as:

$$P_{32}[r > r_0]_{CON} = \frac{N_{CON}}{N_{CAL}} P_{32}[r > r_0]_{CAL} \tag{5-6}$$

By the same token, the ratio between N_{PFL} and N_{CON} is an estimator of the fracture connectivity of flowing fractures with $T \geq T_{limit}$. Thus, the flowing fracture surface area per unit volume of fractures $T \geq T_{limit}$ may approximately be written as:

$$P_{32}[r > r_0]_{PFL} = \frac{N_{PFL}}{N_{CON}} P_{32}[r > r_0]_{CON} \tag{5-7}$$

We conclude this section by noting that Equations (5-5) through (5-7) must be broken into sets if the fracture sets have different length distributions.

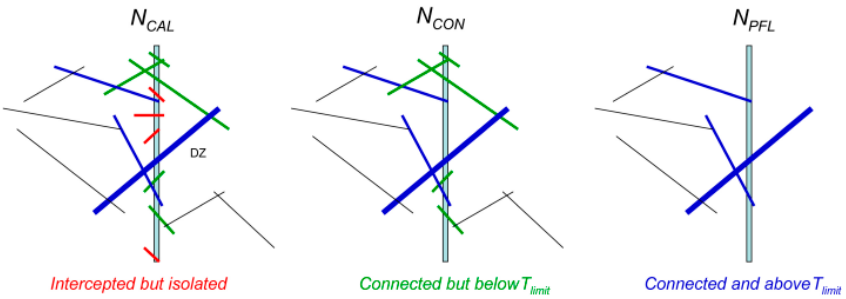

Figure 5-4. *Illustration showing the definitions of N_{CAL}, N_{CON} and N_{PFL}.*

5.2.7 Spatial distribution

The spatial pattern of all fractures in the rock mass outside the deformation zones is generally assumed to be uniformly distributed in space in the geological DFN, cf Section 5.3. The assumption of a Poisson process is a considerable simplification but it does not necessarily imply a uniform distribution of the fracture centres in space. Typically, individual realisations of a Poisson process often possess random clusters, i.e. statistical homogeneity is only valid for the ensemble of realisations. In practice, it is almost impossible to discriminate between a Poisson process and a fractal process, particularly for small data sets.

5.2.8 Intensity correction

To mitigate against under-predicting the intensity of fractures sub-parallel to the borehole trajectories it is common practice to use analytical correction methods. For instance, the analytical Terzaghi method /Terzaghi 1965/ was applied in the geological DFN modelling by /La Pointe and Hermanson 2005/. The correction is used as a weighting when calculating the percentage of fractures in each orientation set. That is, rather than just counting the number of fractures in each set, a weighted percentage is calculated by weighting each fracture by $1/\cos(\vartheta)$, where ϑ is the angle between the pole to the fracture plane and the borehole trajectory. It is up to modeller to decide the maximum weight to be used.

/Darcel et al. 2004/ consider the Terzaghi method to be a potential oversimplification because it does not take the effect of fracture size into account. For a power law size distribution this becomes a problem if $r_0 \leq r_w$ according to /Darcel et al. 2004/.

The Terzaghi method was not used in an explicit fashion in the work reported here. Instead we used exploration simulation, which means that we calibrated a numerical model, representing a fractured rock mass intersected by a borehole (scanline), by comparing the simulated and measured borehole set proportions. Details about the model set-up are presented in Section 5.3.

5.2.9 Block scale properties

The main assumptions in the calculation of block scale properties are:

1. The hydraulic conductivity in the rock mass is governed by the connected fracture system and can be modelled by the DFN concept.
2. Flow within fractures can be approximated by Darcy's law.
3. Fracture transmissivity can be described by a correlated model as envisaged by Equations (2-11) and (5-3b).
4. Fracture transport aperture is correlated to fracture transmissivity as envisaged by Equation (2-2).
5. The heterogeneity between grid blocks on a specified scale can be modelled by calculating the hydraulic conductivity of an array of sub blocks within a much larger domain and use this as an ensemble.

5.3 Assessment of geological DFN data

Table 5-1 presents primary statistics of Open and Partly open fractures in the KSH01A and KSH02 boreholes, respectively. Table 5-2 presents the final geological DFN model for the Simpevarp subarea inferred in the work reported here based on the analyses of data gathered in the KSH01A and KSH02 boreholes. Four sub domains are treated, C1, B1 and C2 in the KSH01A borehole and B2 in the KSH02 borehole, cf Figure 1-8.

Table 5-1. Primary statistics of Open and Partly open fractures in the KSH01A and KSH02 boreholes, respectively. Values of N_{TOT}, N_{CAL} and N_{PFL} are given in Table 5-5.

Object	KSH01A	KSH02
Adj secup/Adj seclow	102.36 m/984.2 m	80.35 m/995.73 m
Mean borehole inclination	c 15°	c 3°
Intervals with deformation zone type properties (DZ) [Modelled deterministically in RVS (DZ-RVS)] [Modelled stochastically as DZ-DFN]	13 [0] [13]	4 [0] [4]
Total no. of fractures [Open/Partly open] [DZ/rock mass (RM)]	2,176 [2,153/23] [1,086/1,090]	3,561 [3,559/2] [605/2,957]
Total no. of Certain [DZ/rock mass (RM)]	251 [152/99]	178 [42/136]
Total no. of Probable [DZ/rock mass (RM)]	291 [154/137]	278 [65/213]
Total no. of Possible [DZ/rock mass (RM)]	1,634 [1,090/1,086]	3,105 [498/2,607]
Total no. of PFL-f [DZ/rock mass (RM)] [Certain/Probable/Possible]	82 [41/41] [42%/18%/40%]	80 [10/70] [43%/18%/39%]

Table 5-2. Compilation of the geological DFN model for the Simpevarp subarea used in the work reported here. "All" means that the C1, B1 and C2 domains are lumped.

No.	Set	Fisher orientaion model (Trend/Plunge) Kappa	Power law size model (k; r_0) ($L_0 = r_0 \sqrt{\pi}$)	Intensity of all Open and Partly open fractures P_{32} ($r > r_0$) (C1; B1; C2) (B2)	Relative intensity Rel. P_{32}($r > r_0$) (C1; B1; C2; All) (B2)
		(°; °; –)	(–; m)	(m^2/m^3)	(%)
1	NNE-NE	(118; 2; 17)	(2.6; 0.038)	(3.274; 3.201; 2.296) (7.046)	(5; 6; 6; 7) (3)
2	EW-WNW	(17; 7; 11)			(16; 20; 16; 20) (13)
3	NW-NNW	(73; 5; 14)			(15; 12; 7; 11) (12)
4	BGNE	(326; 6; 18)			(13; 3; 19; 12) (15)
5	BGNS	(97; 4; 20)			(1; 6; 1; 1) (5)
6	BGNW	(22; 2; 6)			(8; 7; 3; 7) (3)
7	Sub HZ	(125; 75; 5)			(43; 47; 48;43) (48)

5.3.1 Deviations from the 1.2 geological DFN model

Some of parameter settings in Table 5-2 deviate from the parameter setting provided in the geological DFN model by /La Pointe and Hermanson 2005/. Below follows a list of the deviations and comments to the changes undertaken.

Fracture orientation

The original geological DFN provided by /La Pointe and Hermanson 2005/ consists of seven fracture sets, cf Table 5-1. We made two changes to the fracture set orientations:

First, we replaced the Bivariate Fisher distributions for sets 4 and 6 in the original geological DFN model by the best Uniform Fisher equivalents. The motive for this simplification was to facilitate the numerical simulations in DarcyTools, which can work with Uniform Fisher distributions only. Secondly, we changed the trend, plunge and concentration of set 7 to provide a better match to the data observed in the KSH01A and KSH02 boreholes, see Figure 5-5.

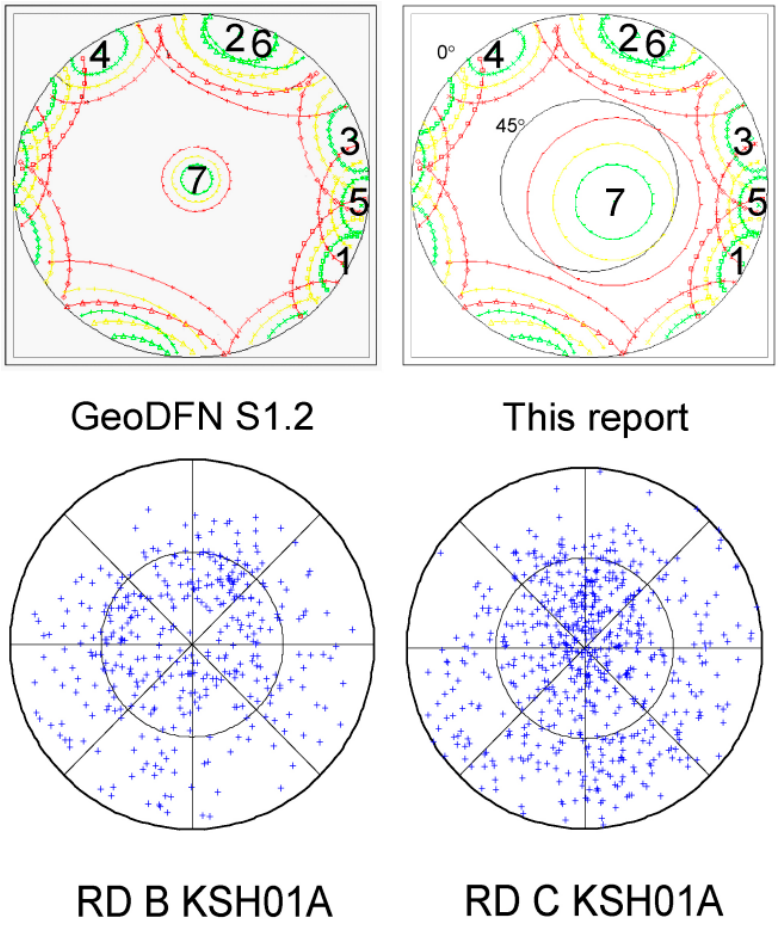

Figure 5-5. *Upper left: Stereo net diagram corresponding to the seven set geological DFN model suggested by /La Pointe and Hermanson 2005/. Upper right: Stereo net diagram of the geological DFN model as used in the work reported here, cf Table 5-1. Lower left and right: Stereo net diagrams corresponding to Open and Partly open fractures in the KSH01A borehole; rock domain B (left) and rock domain C (right). The green, yellow and red lines represent the 25%, 50% and 75% Fisher concentration contours associated with each set. A lot of fractures fall outside the 75% density contours in the set model suggested by /La Pointe and Hermanson 2005/.*

Figure 5-5 suggests that there is considerable overlap between fracture sets 2 and 6 and that sets 1, 3, 4 and 5 also very close to each other. From a core mapping point of view we consider the division of the rock mass fractures into seven fracture sets arbitrary. It is noteworthy that /Darcel et al. 2004/ does not address the issue of fracture sets but suggests bootstrapping in their modelling approach.

Fracture size and spatial distribution

The geological DFN model provided by /La Pointe and Hermanson 2005/ has different values of the shape parameter k and the location parameter r_0 for the six sub vertical fracture sets. In a macroscopic perspective, the values suggested range between 2.50–3.14 for k and between 0.08–0.69 m for r_0. For the sub horizontal fracture set a log normal size distribution with a common log mean and standard deviation of –0.73 and 1.03 were suggested, respectively. Moreover, the analysis carried out results in two different interpretations of the scaling of the number of fractures of different sizes:

- a *linear (Euclidian) scaling*, which suggests that a uniform (uncorrelated and random; Poissonian) spatial pattern can be seen in the data, and
- a *non linear (non Euclidian) scaling*, which means that a non uniform (correlated in some sense, e.g. fractal) spatial pattern can be seen in the data.

/La Pointe and Hermanson 2005/ provide descriptions to these findings but make no conclusion on the best setting for rock mechanical and hydrogeological DFN modelling.

The size analysis carried out in the alternative geological DFN modelling by /Darcel et al. 2004/ resembles the modelling by /La Pointe and Hermanson 2005/ to some extent. For instance, different power law size distributed DFN models are reported for the four outcrops excavated in the Simpevarp subarea. In summary, the value of k was concluded to be 2.20 ± 0.05 for two of the outcrops and 3.0 ± 0.00 for the other two. For the former pair of outcrops the transition of the size distribution from small objects to larger objects of observation (lineaments) was found to be non linear, whereas it was found to be linear for the latter pair of outcrops. For both pair of outcrops the value of the location parameter r_0 was reported to be equal or less than the borehole radius, i.e. 0.038 m, however.

We find the analysis of k and r_0 (including the scaling issue) fairly uncertain at this stage in the geological modelling. Probably there is a considerable heterogeneity in the data as well as uncertainties in the structural modelling undertaken. In particular, we find the motives for a log normal size distribution of the sub horizontal fracture set quite tentative. In our view there is no physical reason why sub horizontal fractures should have a different size distribution than sub vertical fractures. For instance, /Darcel et al. 2004/ make no distinction in this sense.

In the hydrogeological DFN modelling we take for granted that all fractures, regardless of set belonging, follow the same power law size distribution model and that the fracture centre points are distributed statistically uniform in space. We study the sensitivity of a postulated transmissivity-size correlation model (Equation (5-3b)) to three specific values of k (2.40, 2.60 and 2.80) and to two specific values of r_0 (0.038 m and 0.282 m).

Fracture intensity

The intensity of Open and Partly open fractures in the geological DFN model provided by /La Pointe and Hermanson 2005/ differs between different lithological rock domains. In terms of P_{32} [$r > r_0$], i.e. fracture surface area per unit volume of rock, the value for rock domain B is slightly higher than for rock domain C, 1.416 m^2/m^3 versus 1.085–1.365 m^2/m^3.

The intensity values are not claimed to vary in space and there is no particular difference observed in the fracture intensity between outcrop (surface) data and borehole (depth) data.

We consider variations in the fracture intensity versus depth to be important for the analysis of a transmissivity-size model. After all, the hydraulic data used in the hydrogeological DFN modelling is based on hydraulic tests conducted in core drilled boreholes at different depths. The values given for rock domain B and C in Table 5-1 are based on fracture frequency data gathered in the KSH01A and KSH02 boreholes and refer to a $k = 2.60$ and a $r_0 = 0.038$ m. Two values for each rock domain B and C are inferred as a result of spatial variability observed. In order to compare with the geological DFN we transform the intensity values for $r_0 = 0.038$ m to $r_0 = 0.302$ m, which is the mean value of location parameter for the range of r_0 values suggested in the geological DFN model. For the four rock domains B1, B2, C1 and C2 we get 0.920, 2.025, 0.941, and 0.660 m^2/m^3, respectively. In conclusion, the approach used in the work reported here suggest that the intensity of the geological DFN model is slightly less than the model provided by /La Pointe and Hermanson 2005/. The only exception to this observation is rock domain B2, which also differs much from the.fracture intensity observed in the KSH01A borehole.

To mitigate against under predicting the intensity of fractures sub parallel to the borehole trajectories /La Pointe and Hermanson 2005/ used the Terzaghi method /Terzaghi 1965/. Table 5-3 compares the relative intensities of the different fracture sets in rock domains B and C as reported by /La Pointe and Hermanson 2005/ with the relative intensities inferred in the work reported here (cf Table 5-2). The main reason for the discrepancies seen is due to lower value of the concentration factor (kappa) of the sub horizontal fracture set in geological DFN used in the work reported here. The motive for the lower value used is shown in Figure 5-5.

We used exploration simulation to calculate the fracture intensity $P_{32}[r > r_0]$ and the relative proportions between the sets. That is, we calibrated a numerical simulation model, representing a fractured rock mass intersected by a borehole (scanline), by comparing the simulated and measured borehole set proportions captured by boreholes with the same trajectories as the KSH01A and KSH02 boreholes.

The simulated and measured proportions were determined from a sector division of the geological DFN model used in the work reported here. The sector division is illustrated in Figure 5-6. The border between the sub horizontal set and the six sub vertical sets was set half way between the 75% Fisher concentration contours. This definition implies that the border dip between the sub-vertical fractures sets and the sub-horizontal fracture set varies between 45–65°.

Table 5-3. Compilation of relative fracture intensities for rock domains B and C /La Pointe and Hermanson 2005/ and sub domains B1, B2, C1 and C2 (this report).

Domain	Set 1 NNE-NE [%]	Set 2 EW-WNW [%]	Set 3 NW-NNW [%]	Set 4 BGNE [%]	Set 5 BGNS [%]	Set 6 BGNW [%]	Set 7 Sub HZ [%]
B and C	15	14	18	15	12	5	20
B1	6	20	12	3	6	7	47
B2	3	13	12	15	5	3	48
C1	5	16	15	13	1	8	43
C2	6	16	7	19	1	3	48

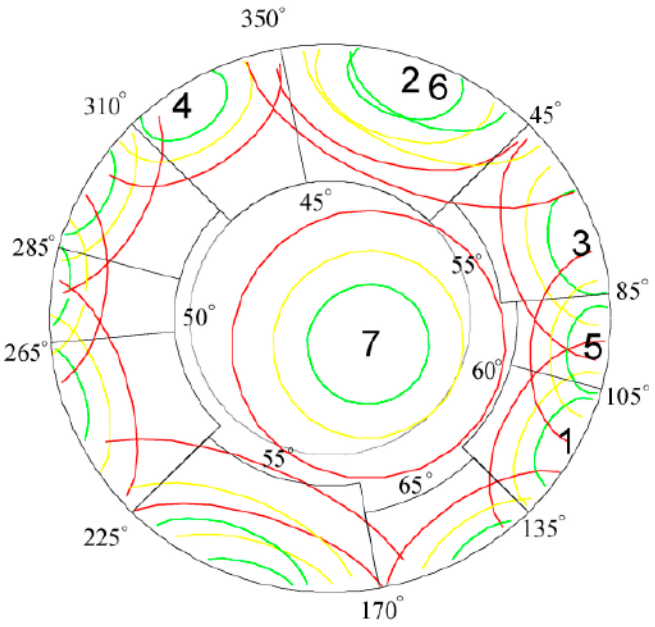

Figure 5-6. *Illustration of the sector division of the geological DFN model used in the work reported here. The border between the sub horizontal set and the six sub vertical sets was set half way between the 75% Fisher concentration contours (red lines). This definition implies that the border dip between the sub-vertical fractures sets and the sub-horizontal fracture set varies between 45–65°.*

The intensity analysis carried out in the alternative geological DFN modelling by /Darcel et al. 2004/ cannot be compared to the analysis carried out in the work reported here because /Darcel et al. 2004/ studied the intensity of all fractures rather than the intensity of the Open and Partly open fractures. However, their analysis can be compared to the analysis carried out by /La Pointe and Hermanson 2005/ as the latter authors analysed the intensity of all fractures as well. Indeed, the two intensity analyses are fairly consistent. In summary, /La Pointe and Hermanson 2005/ reported a total intensity of 3.02 m^2/m^3 for rock domain A, 7.66 m^2/m^3 for rock domain B and 4.93–5.28 m^2/m^3 for rock domain C. In comparison, /Darcel et al. 2004/ reported an intensity range of 5.79–8.44 m^2/m^3 in the region where the transition from small objects to large objects was inferred to be linear and an intensity range of 7.81–13.4 m^2/m^3 where the transition was found to be non linear. In order to make this comparison between the two geological DFNs we have transformed the original intensity values provided by /Darcel et al. 2004/ from a $r_0 \approx 0.05$ m to $r_0 \approx 0.302$ m, i.e. the mean value of location parameter for the range of r_0 values suggested in the geological DFN model by /La Pointe and Hermanson 2005/.

5.4 Assessment of hydrogeological DFN data

The PFL-f transmissivities not associated with the deterministically treated deformation zones are the main sources of information for the HydroDFN analysis reported here.
The PFL-f method has the best spatial resolution of all hydraulic test methods. The PFL-f method detects fractures that are flowing after several days of pumping, which implies that the fractures observed belong to a connected network that extends some distance from the borehole. The duration of the PSS method is 20 minutes only.

5.4.1 KSH01A

The KSH01A borehole penetrates two types of rock domains, B and C. The B rock domain occurs between 322.50 m and 631 m borehole length. The C rock domains occur above and below the B rock domain, i.e. between 100 m and 322.50 m borehole length and between 631 m and 1,001 m borehole length. The upper C rock domain is denoted by C1 and the lower by C2 in the work reported here. Correspondingly, the B rock domain is denoted by B1. Figure 5-7 shows the PFL-f transmissivities acquired in the KSH01A borehole together with inferred rock domain intervals C1, B1 and C2.

The open interval in the KSH01A borehole is c 901 m long and intersects 2,176 Open and Partly open fractures. 1,086 of these fractures are associated with 13 intervals that have deformation zone type properties, see Figure 3-3. The total thickness of the 13 intervals is

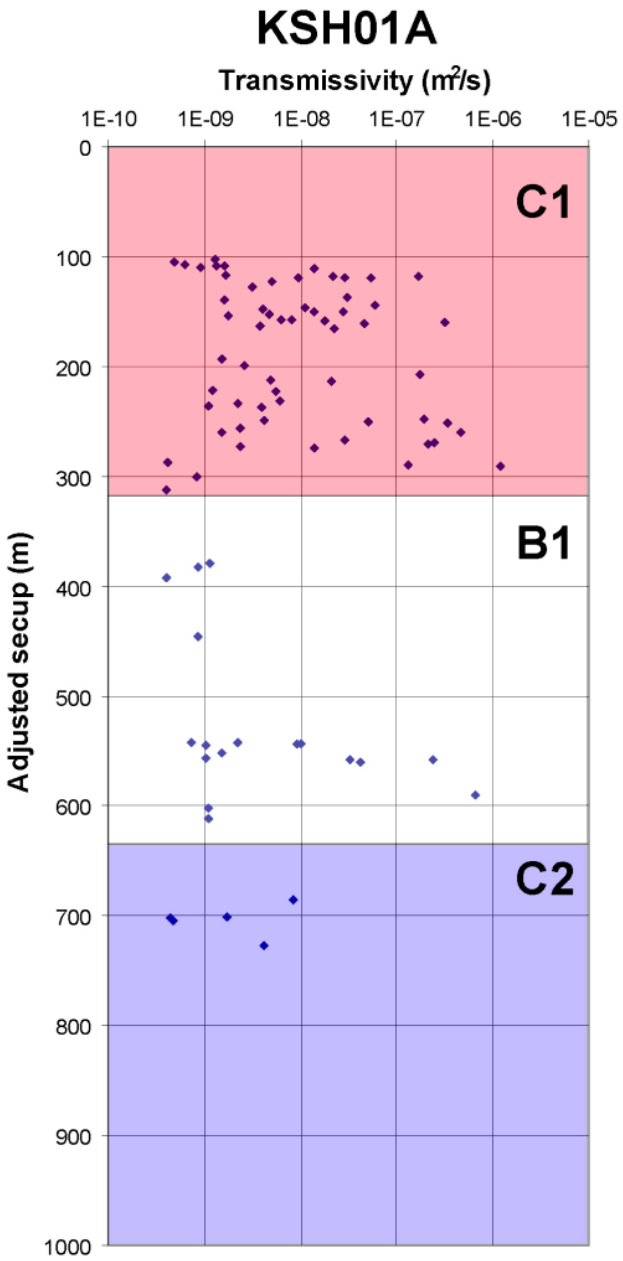

Figure 5-7. *PFL-f transmissivities acquired in the KSH01A borehole together with inferred rock domain intervals C1, B1 and C2.*

c 220 m leaving c 681 m of rock mass (RM) outside the deformation zone type intervals. None of the 13 intervals with deformation zone type properties is incorporated into the deterministically modelled deformation zone model. This means that the orientations and sizes of the deformation zone type intervals are undetermined and thus a part of the stochastically modelled features, cf Figure 5-2. Further, 8 of the deformation zone type intervals are interpreted to be brittle (BDZ) and 5 are interpreted to be ductile (DDZ). The total thickness of the brittle deformation zone type intervals is c 199 m, which means that the total thickness of the ductile deformation zone type intervals is c 21 m.

Table 5-4 summarises the Open fracture frequency statistics with regard to rock domain and kind of deformation zone type intervals. The ductile deformation type intervals are more intensely fractured than the brittle deformation type intervals. The rock mass outside the 13 deformation zone type intervals is much less fractured than the deformation zone type intervals and the rock masses in the C1 and B1 rock domains are significantly more fractured than the rock mass in C2 rock domain. It is difficult to say if the difference between B1 and C2 is related to depth rather than to rock domains, however.

There are 82 PFL-f anomalies in the KSH01A borehole with a minimum transmissivity value of $3.9 \cdot 10^{-10}$ m^2/s. 39 of the 82 PFL-f anomalies in the KSH01A borehole are found in the rock mass outside the 13 length intervals interpreted to have deformation zone type properties. 60 PFL-f anomalies are observed in the C1 rock domain among which 32 are associated with the rock mass. 17 flow anomalies are observed in the B1 rock domain among which 3 are associated with the rock mass. Finally, 5 flow anomalies are observed in the C2 rock domain among which 4 are associated with the rock mass.

Table 5-5 and Table 5-6 summarise the PFL-f and specific transmissivity ($\Sigma T/\Sigma b$) values with regard to rock domain and kind of deformation zone type interval. The data in the two tables are visualised in Figure 5-8. It is noted that the differences observed in Figure 5-8 between the three rock domains could also be indicative of a depth trend, e.g. at c 300 m.

Moreover, the brittle deformation zone type intervals are on the average two orders of magnitude more transmissive than the ductile deformation zone type intervals. If this difference is characteristic for the two kinds of deformations zones it will be important for the regional scale flow modelling.

Table 5-4. Open fracture frequency (P_{10}) statistics with regard to rock domain and kind of deformation zone type interval in the KSH01A borehole.

Rock domain	Depth below surface (m)	P10 Brittle DZ [m^{-1}]	P10 Ductile DZ [m^{-1}]	P10 Rock mass [m^{-1}]
C1	0–322	4.7	6.2	1.4
B1	322–631	5.8	7.8	1.3
C2	631–EOB	2.5	3.5	1.0

Table 5-5. NPFL-f frequency statistics ($P_{10,PFL}$) with regard to rock domain and kind of deformation zone type interval in the KSH01A borehole.

Rock domain	Depth below surface (m)	$P_{10,PFL}$ Brittle DZ [m^{-1}]	$P_{10,PFL}$ Ductile DZ [m^{-1}]	$P_{10,PFL}$ Rock mass [m^{-1}]
C1	0–322	0.44	0.13	0.21
B1	322–631	0.11	0.18	0.02
C2	631–EOB	0.07	0.00	0.01

Table 5-6. Specific transmissivity (Σ*T*/Σ*b*) with regard to rock domain and kind of deformation zone type interval in the KSH01A borehole. T_{tot} = 5.0·10^{-6} m^2/s.

Rock domain	Depth below surface (m)	ΣT/Σb Brittle DZ [m^2/s/m]	ΣT/Σb Ductile DZ [m^2/s/m]	ΣT/Σb Rock mass [m^2/s/m]
C1	0–322	5.3·10^{-8}	3.1·10^{-10}	4.0·10^{-9}
B1	322–631	8.4·10^{-9}	2.0·10^{-10}	1.3·10^{-11}
C2	631–EOB	5.6·10^{-10}	N/A	2.0·10^{-11}

Figure 5-9 shows the orientations of the fractures associated with the 82 PFL-f anomalies observed in the KSH01A borehole (blue figures). C. 90% of the PFL-f anomalies within the brittle (BDZ) and ductile (DDZ) deformation zone type intervals are encountered among the fracture sets denoted by (2+6), 3 and 7. The same percentage and set preferences are observed for the PFL-f anomalies in the rock mass (RM) outside the brittle and ductile deformation zone type intervals. This suggests a geometrical anisotropy in accordance with the main horizontal stress direction (NW).

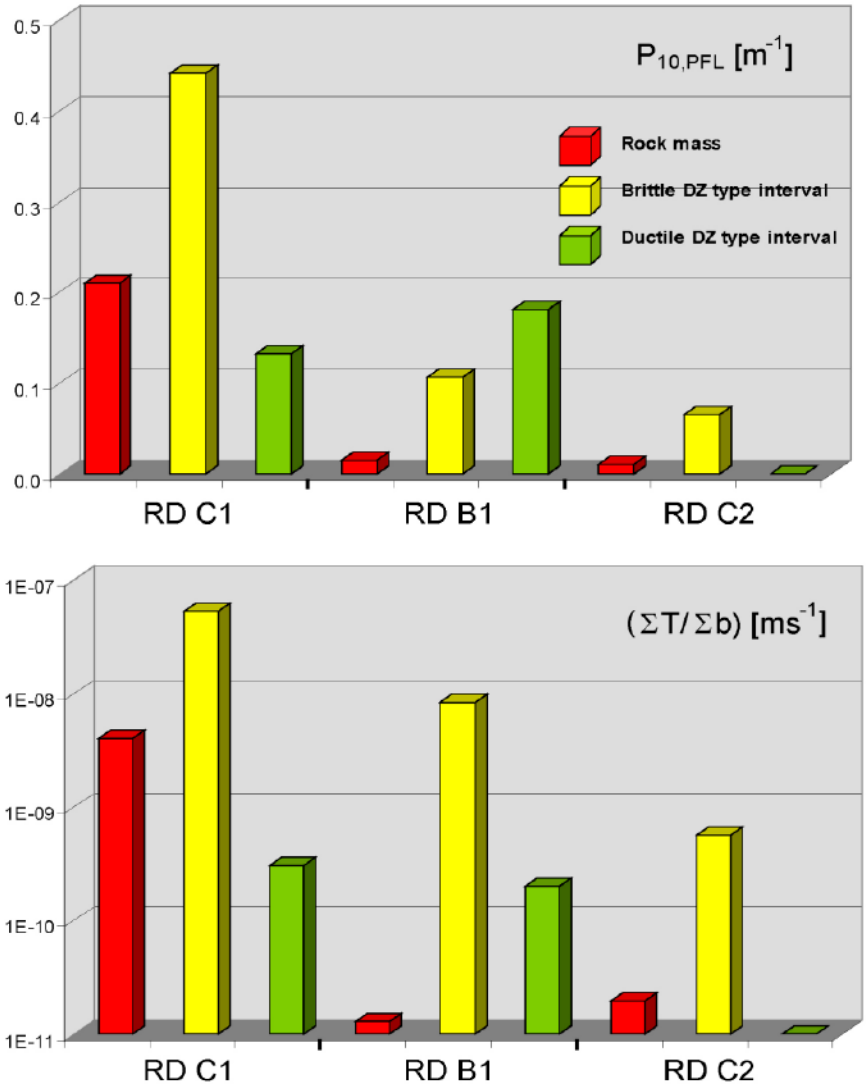

Figure 5-8. *Visualisation of PFL-f in Table 5-5 and the specific transmissivity (ΣT/Σb) in Table 5-6.*

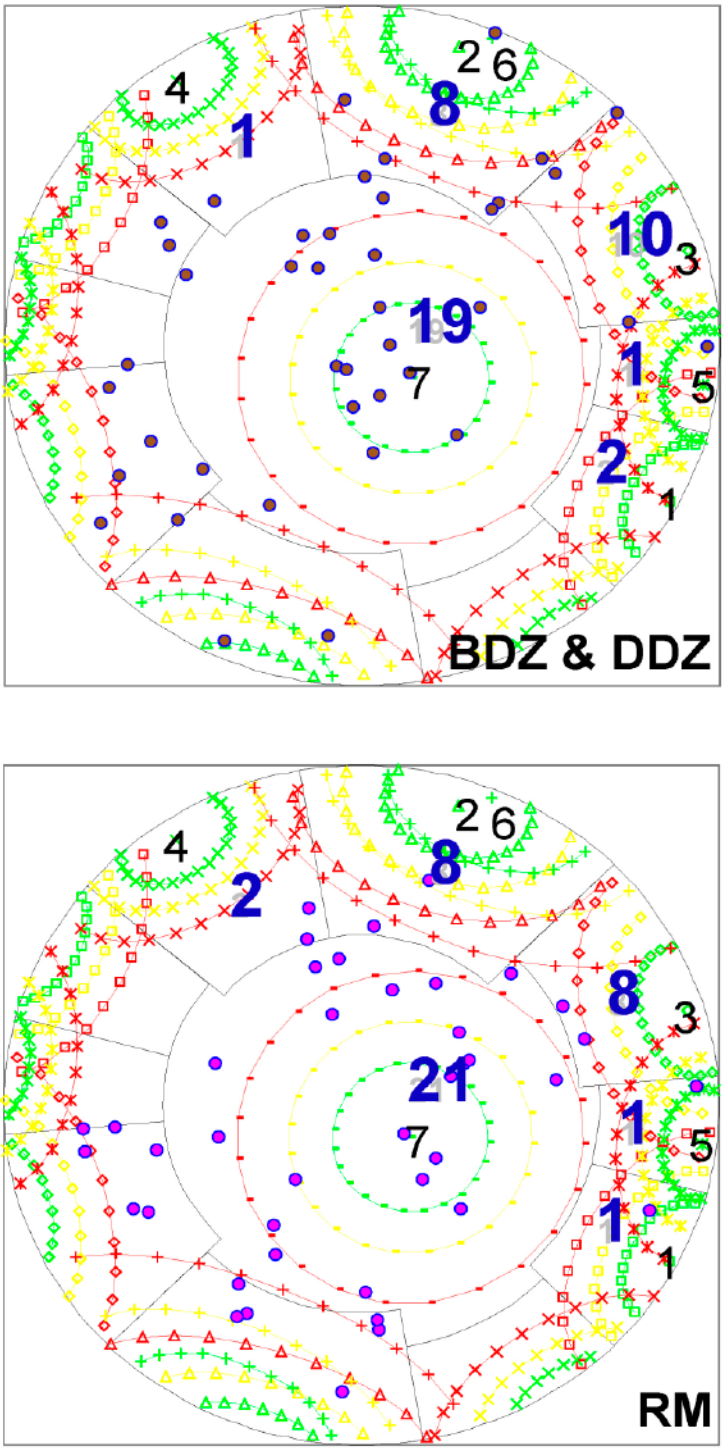

Figure 5-9. *Orientations of fractures associated with the 82 PFL-f anomalies observed in the KSH01A borehole (blue figures). Three fracture sets dominate, (2+6), 3 and 7.*

5.4.2 KSH02

Figure 5-10 shows the PFL-f transmissivities acquired in the KSH02 borehole, which penetrates the B type of rock domain only. Figure 5-10 does not suggest a depth trend.

The open interval in the KSH02 borehole is c 915 m long and intersects 3,561 Open and Partly open fractures. 605 of these fractures are associated with 4 intervals that have brittle

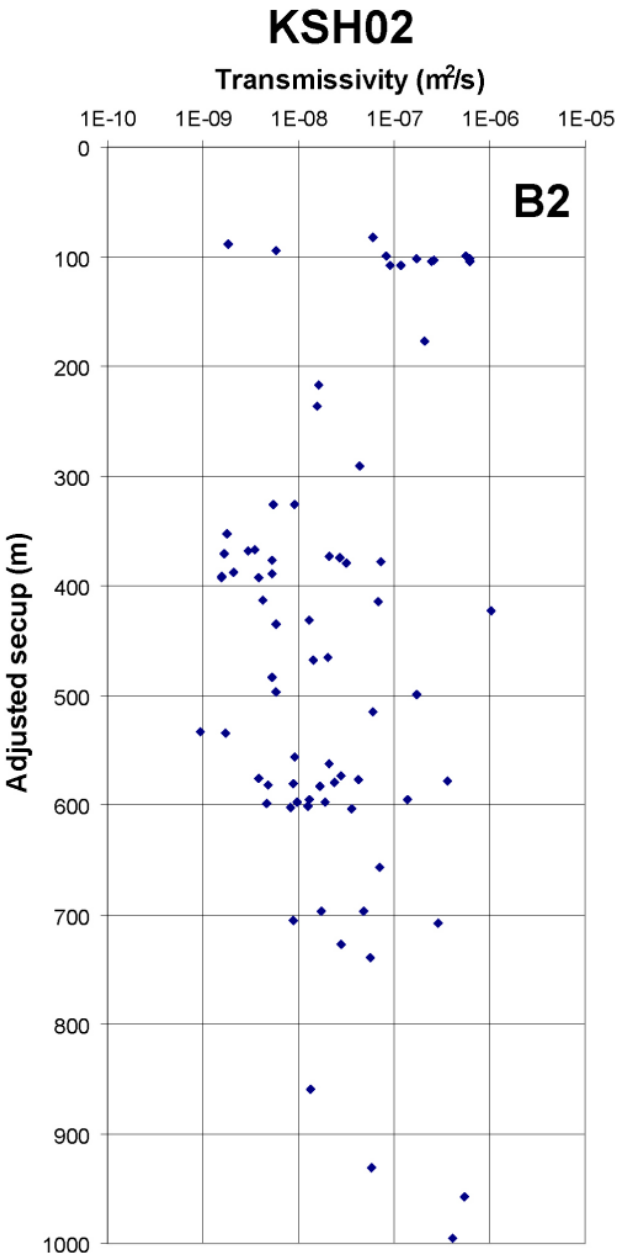

Figure 5-10. *PFL-f transmissivities acquired in the KSH02 borehole together with inferred rock domain B2.*

deformation zone type properties, see Figure 3-4. The total thickness of the 4 intervals is c 118 m leaving c 797 m of rock mass (RM) outside the deformation zone type intervals. None of the 4 intervals with deformation zone type properties is incorporated into the deterministically modelled deformation zone model. This means that the orientations and sizes of the deformation zone type intervals are undetermined and thus a part of the stochastically modelled features, cf Figure 5-2.

Table 5-7 summarises the Open fracture frequency statistics with regard to rock mass and deformation zone type intervals. Both entities have significantly higher magnitudes in the B2 rock domain than in the B1 rock domain, cf Table 5-4.

There are 80 PFL-f anomalies in the KSH02 borehole with a minimum transmissivity value of $9.4 \cdot 10^{-10}$ m^2/s. 70 of the 80 PFL-f anomalies in the KSH02 borehole are found in the rock mass outside the 4 length intervals interpreted to have deformation zone type properties. Table 5-8 and Table 5-9 summarise the PFL-f and specific transmissivity statistics with regard to rock domain and kind of deformation zone type interval.

The rock mass PFL-f frequency and specific transmissivity ($\Sigma T/\Sigma b$) have higher magnitudes in the B2 rock domain than in the B1 rock domain, cf Table 5-5 and Table 5-6, respectively. In our view, the KSH02 borehole seems to be drilled in, or very close to, a deformation zone, cf Figure 1-5.

Figure 5-11 shows the orientations of the fractures associated with the 80 PFL-f anomalies observed in the KSH02 borehole (blue figures). C 60% of the PFL-f anomalies within the brittle (BDZ) deformation zone type intervals are encountered among the fracture sets denoted by (2+6), 3 and 7, whereas c 91% of the PFL-f anomalies observed the rock mass (RM) outside the deformation zone type intervals have these set preferences. This suggests that the geometrical anisotropy observed in the KSH01A borehole remains also for the KSH02 borehole.

Table 5-7. Open fracture frequency (P_{10}) statistics with regard to rock mass and deformation zone type interval in the KSH02 borehole.

Rock domain	P10 Brittle DZ [m^{-1}]	P10 Ductile DZ [m^{-1}]	P10 Rock mass [m^{-1}]
B2	5.1	N/A	3.7

Table 5-8. PFL-f frequency statistics ($P_{10,PFL}$) with regard to rock domain and kind of deformation zone type interval in the KSH02 borehole.

Rock domain	P10,PFL Brittle DZ [m^{-1}]	P10,PFL Ductile DZ [m^{-1}]	P10,PFL Rock mass [m^{-1}]
B2	0.09	N/A	0.09

Table 5-9. Specific transmissivity ($\Sigma T/\Sigma b$) with regard to rock domain and kind of deformation zone type interval in the KSH02 borehole. $T_{tot} = 7.0 \cdot 10^{-6}$ m^2/s.

Rock domain	ΣT/Σb Brittle DZ [m^2/s/m]	ΣT/Σb Ductile DZ [m^2/s/m]	ΣT/Σb Rock mass [m^2/s/m]
B2	$8.5 \cdot 10^{-10}$	N/A	$7.5 \cdot 10^{-9}$

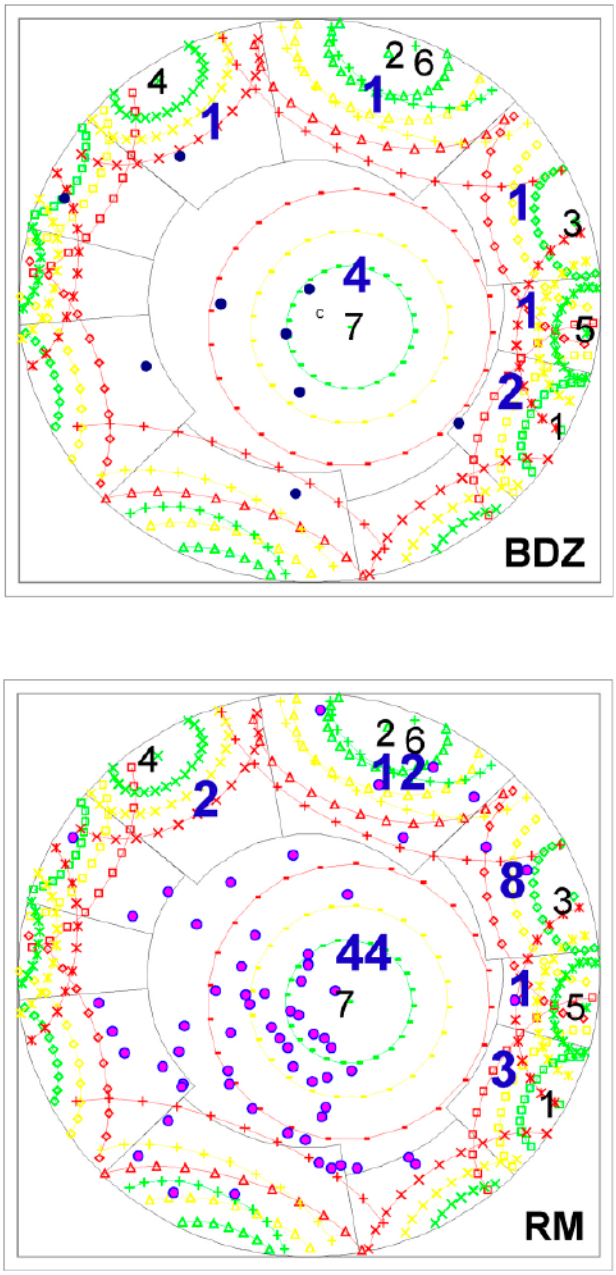

Figure 5-11. *Orientations of fractures associated with the 80 PFL-f anomalies observed in the KSH02 borehole (blue figures). Three fracture sets dominate, (2+6), 3 and 7.*

5.4.3 Transmissivity distributions

Figure 5-12 presents counter cumulative density function plots of the PFL-f transmissivities interpreted from the difference flow measurements in the KSH01A and KSH02 boreholes, respectively. The two sets of data have similar slopes but slightly different minimum values (c. an order of magnitude). In Figure 5-13 the counter cumulative density function plot for KSH01A shown in Figure 5-12 is broken up plotted with regard to the transmissivity data in the C1, B1 and C2 rock domains.

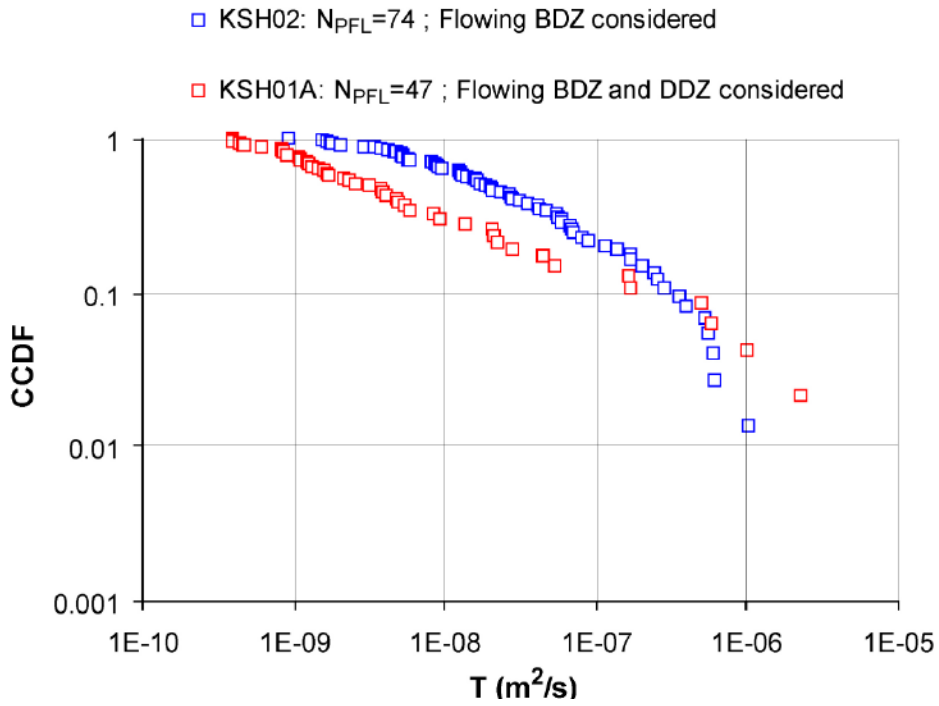

Figure 5-12. *Complementary cumulative density function plots of the PFL-f transmissivities interpreted from the difference flow measurements in the KSH01A and KSH02 boreholes, respectively. The two sets of data have similar slopes but slightly different minimum values (c. half an order of magnitude).*

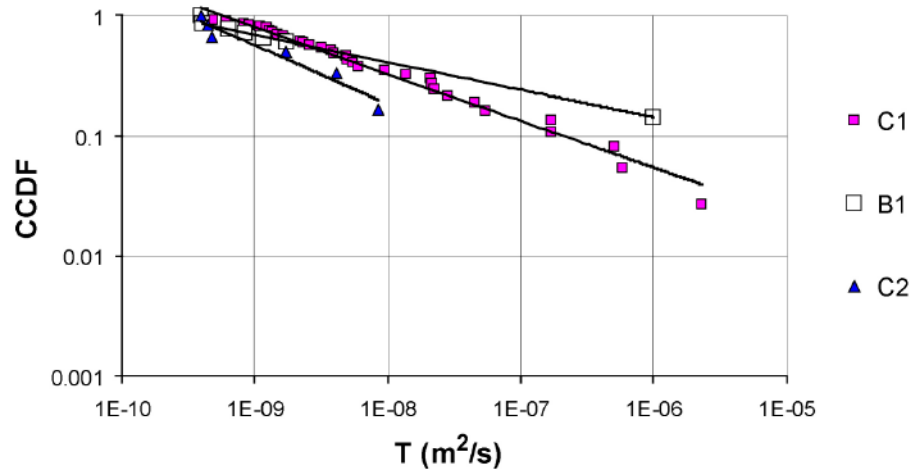

Figure 5-13. *The complementary cumulative density function plot for KSH01A shown in Figure 514 is broken up plotted with regard to the transmissivity data in the C1, B1 and C2 rock domains. The slopes of the regression lines are c –0.39 (C1), –0.23 (B1) and –0.49 (C2).*

5.4.4 Summary of observations

The main observations made in the data screening presented above are:

- Some fracture sets overlap significantly in the geological DFN model provided by /La Pointe and Hermanson 2005/. In our mind three "fracture" sets are sufficient to model the fracture network statistics seen in the rock mass as well as in the deformation zone type intervals. That is, fracture sets (2+6), 3 and 7 gather c 90% of the PFL-f anomalies observed in the KSH01A and the KSH02 boreholes.
- The frequency and transmissivity of the PFL-f anomalies in the KSH02 borehole (B2) differ significantly from the observations made in the KSH01A borehole (B1). We question if the KSH02A borehole is representative for the rock mass in the B rock domain. In our view, the KSH02 borehole seems to be drilled in, or very close to, a deformation zone, cf Figure 1-5.
- The fracture frequency and the hydraulic properties in the rock mass in the KSH01A borehole suggest a depth trend. For instance, the rock mass above c –300 m above sea level are c 100 times more transmissive than the rock mass below this elevation. Possibly, there is another step at c –600 m above sea level.
- The brittle deformation zone type intervals are c 100 times more transmissive than the ductile deformation zone type intervals at all depths in the KSH01A borehole.
- Complementary cumulative density function plots of the PFL-f transmissivities interpreted from the difference flow measurements in the KSH01A and KSH02 boreholes suggest that the transmissivity data acquired in the C1, B1, C2 and B2 rock domains can be power law distributed. The data range is close to four orders of magnitude, from $4 \cdot 10^{-9}$ to $2 \cdot 10^{-6}$ m^2/s. The slopes of the fitted regression lines are c –0.39 (C1), –0.23 (B1), –0.49 (C2) and –0.23 (B2). The slope of the regression line in the B2 rock domain is the most uncertain.

5.5 Assessment of connected fracture intensity

In Section 5.2.3 we define N_{CAL} , i.e. the number of Open and Partly open fractures to be used for the inference of N_{CON}, the connected number of Open and Partly open fractures. N_{CON} is defined in Section 5.2.6. Figure 5-14 defines the input parameters for the calibration process.

Table 5-10 presents the basic fracture frequency data outside the deformation zones that is used in the connectivity analysis. N_{CAL} is the number of potentially flowing Open and Partly open fractures in each rock domain to be matched in the modelling process and N_{PFL} is the number of flow anomalies in the connected network of flowing features above the lower measurement limit of the PFL-f tests. T_{PFLmin} is the smallest transmissivity value measured and may be considered as an estimate of the lower measurement limit T_{lim}. As noted previously, the lower measurement limit of the PFL-f measurements is not a threshold with a fixed magnitude, but varies in space dependent on the in situ borehole conditions.

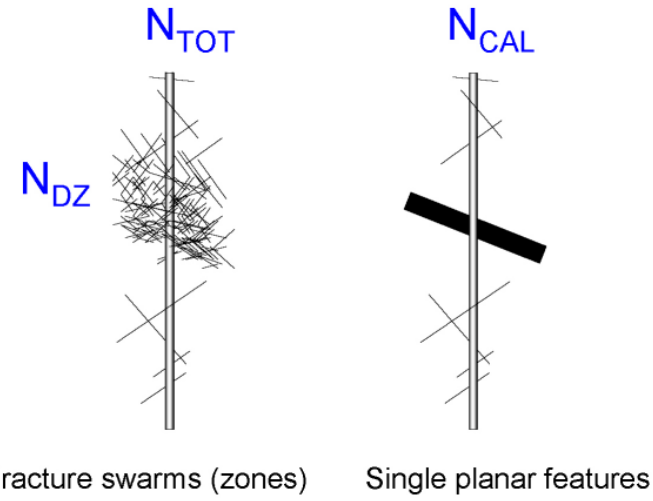

Figure 5-14. *Definition of N_{TOT}, N_{DZ} and N_{CAL}, cf Section 5.2.3.*

Table 5-10. Input data to connectivity analysis presented in Section 5.2.6.

Object	Rock domain C1	Rock domain B1	Rock domain C2	Rock domain B2
Length [m]	220	309	353	797
N_{TOT}	670	1,034	472	3,561
N_{DZ}	363 (4 DZ)	630 (3 DZ)	93 (1 DZ)	605 (4 DZ)
N_{CAL}	311 (= 307+4)	407 (= 404+3)	380 (= 379+1)	2,957 (= 2,953+4)
N_{PFL}	36 (= 32+4)	6 (= 3+3)	5 (= 4+1)	74 (= 70+4)
T_{PFLmin}; T_{PFLmax} [m^2/s]	4.0E-10; 2.3E-06	4.0E-10; 1.0E-06	4.4E-10; 8.5E-09	9.4E-10; 1.0E-06

5.5.1 Modelling procedure

The connected fracture intensity is assessed by means of four stochastic realisations that match the statistics of the mapped orientations and borehole fracture frequencies of Open and Partly open fractures in the KSH01A and KSH02 boreholes, see Table 5-10. These boreholes penetrate rock domains C1, B1 and C2 (KSH01A) and B2 (KSH02) in the Simpevarp subarea. Once the measured geological intensity of Open and Partly open fractures is matched, the connected fracture intensity is determined by a connectivity analysis. A connected fracture is defined as a fracture that directly or indirectly connects to two hydraulic boundaries, e.g. a deterministically modelled deformation zone in RVS, the the bedrock surface, a scanline representing a borehole. The methodology used is illustrated in Figure 5-4.

The simulation domain consists of three concentric shells; one large (outer), one intermediate large (middle) and one small (inner). In the centre of the simulation domain there is a scanline mimicking a core-drilled borehole. The model set-up and dimensions of the shells are shown in Figure 5-15. Within the outer shell stochastic fractures in the size range L = 20–1,000 m (r = 11.3–564 m) are generated, within the middle shell L = 1–20 m (r = 0.564–11.3), and within the inner shell $L = L_0$–1 m ($r = r_0$–0.564) m. The motive for the outer shell is based on the deformation zones, see Figure 5-16. All six boundaries are used for the connectivity analyis. Dead-end fractures are not removed, only isolated fractures or isolated clusters of fractures.

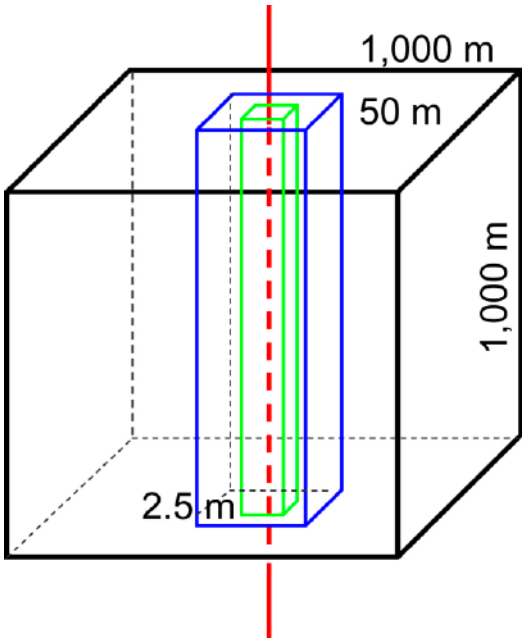

Figure 5-15. *Simulation model set-up and dimensions of the three fracture shells; outer (black), middle (blue) and inner (green).*

Figure 5-16. *Left: Close up of the geological map presented in Figure 1-1. We have centred a fictive simulation model domain close to the KSH01A borehole. Right: Close up of the simulation domain with the outer, middle and inner shells for each rock domain C1, B1 and C2.*

The fractures are generated in order beginning with the outer shell. The approximate procedure of generating an interconnected network is done as follows:

- the interconnected stochastic fractures within the outer shell are retained while the stochastic fractures in the middle shell are generated, and
- the interconnected stochastic fractures within the outer and middle shells are retained while the stochastic fractures in the inner shell are generated.

The stochastic simulations are done twice for each seed. In the first run there is a scanline in the centre representing the borehole or borehole interval to be matched and in the second run there is no scanline. When the scanline (borehole) acts as a boundary it sees not only the connected fractures but also the isolated fractures. In the second run the borehole does

not act as a boundary, but inserted first when the isolated fractures are discarded. This approximate procedure enables a matching against N_{CAL} and a determination of N_{CON} , where N_{CAL} is the total number of potentially flowing Open and Partly open fractures that intersects the scanline and N_{CON} is the connected (non isolated) number of potentially flowing Open and Partly open fractures that intersects scanline, see Figure 5-6. The relationship between N_{PFL}, which is the number of PFL-f flow anomalies above the lower measurement limit for transmissivity, N_{CON} and N_{CAL} is given by Equation (5-5).

5.5.2 Demonstration of the simulation process for the C1 rock domain

The picture to the left in Figure 5-16 shows a close up of the geological map presented in Figure 1-1. We centred a fictive simulation model domain close to the KSH01A borehole. The picture to the right in Figure 5-16 shows a close up of the simulation domain with the outer, middle and inner shells for each rock domain C1, B1 and C2.

By trial an error we adjusted the intensity parameter in DarcyTools, α, until we matched the right number of intercepts with the scanline (borehole), i.e N_{CAL}. We repeated the simulations three more times. Table 5-11 summarises the results for the C1 rock domain using the power law size model presented in Table 5-2, i.e. $k = 2.6$ and $r_0 = 0.038$ m.

Figure 5-17 shows, as an example, the size distribution of the $N_{CON} = 243$ fractures that intercepted the scanline in the first realisation, cf Table 5-11. The fitted line has a slope of c –0.63. The slopes of the other 3 realisations are c –0.57, –0.56 and –0.56, respectively.

Table 5-11. Compilation of simulation results for the C1 (L = 220 m) rock domain using the power law size model presented in Table 5-2, i.e. k = 2.6 and r_0 = 0.038 m.

Object	Mean	Real. # 1	Real. # 2	Real. # 3	Real. #4
Sim. N_{CAL}	306	335	278	323	289
Sim. N_{ISO}	101	92	107	109	97
Sim. N_{CON}	205	243	171	214	192
Connectivity [%]	65	72	62	60	66

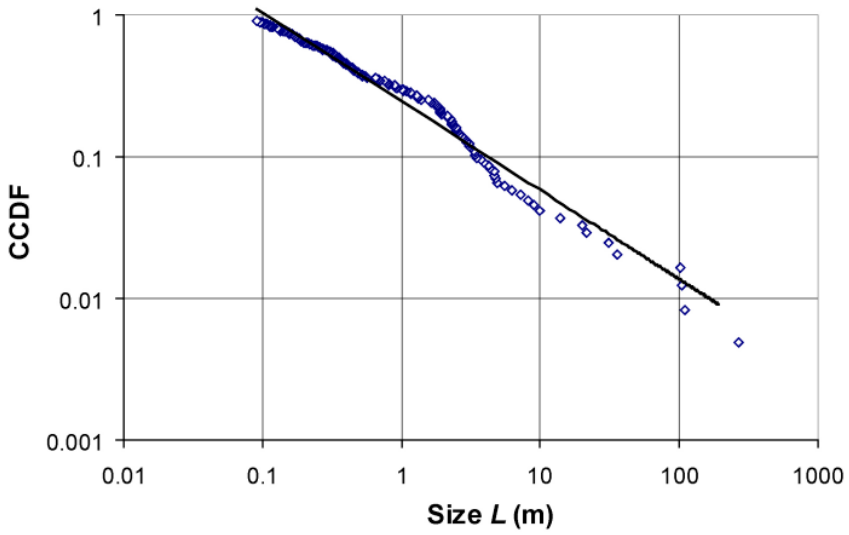

Figure 5-17. *Size distribution of the N_{CAL} = 335 fractures that intercepted the scanline in the first simulation for the C1 rock domain. Note that L is shown and not r.*

5.5.3 Sensitivity to *k* and r_0

Two different values of r_0 are used in work reported here, 0.038 m and 0.282 m, as a means to assess the uncertainty in the location parameter, cf the discussion in Section 5.2.4 and Section 5.3.1. Further, the simulations are conducted for three different values of *k*, 2.6 ± 0.2, as a means to assess the uncertainty in the shape parameter, cf the discussion in Section 5.3.1. Table 5-12 summarises the results from the simulations undertaken in the C1 rock domain. Each case was run four times (4 realisations) and the values shown are mean values.

Table 5-12. Compilation of simulation results for the C1 rock domain using different power law size distribution models. The values shown are mean values of four realisations for each power law size parameter combination.

Object	Mean **k = 2.6** **r_0 = 0.038 m**	Mean **k = 2.6** **r_0 = 0.282 m**	Mean **k = 2.4** **r_0 = 0.038 m**	Mean k = 2.8 r_0 = 0.038 m
Simulated N_{CAL}	306	316	304	307
Simulated N_{ISO}	101	1	73	194
Simulated N_{CON}	205	315	231	113
Connectivity [%]	65	100	76	37

5.5.4 Sensitivity to the fracture frequency (intensity)

From Table 5-12 we conclude that the simulated DFN connectivity is highly dependent on the values chosen for the shape parameter and the location parameter. The sensitivity of the connectivity to these parameters is greater if the intensity is low than if it is high, however. This is demonstrated in Table 5-13, which summaries the results from the simulations undertaken in the C1, B1, C2 and B2 rock domains. The four rock domains have different fracture frequencies $P_{10,CAL}$. Each case was run four times (4 realisations) and the values shown are mean values.

Table 5-13. Compilation of simulation results for the C1, B1, C2 and B2 rock domains using the power law size model presented in Table 5-2, i.e. *k* = 2.6 and r_0 = 0.038 m. The values shown are mean values of four realisations for each rock domain.

Object	Rock domain C1	Rock domain B1	Rock domain C2	Rock domain B2
Interval length [m]	220	309	353	797
N_{CAL}	311	407	380	2,957
$P_{10,CAL}$ [m^{-1}]	1.41	1.32	1.08	3.71
Mean connectivity [%]	65	42	29	83
NPFL	36 (= 32+4)	6 (= 3+3)	5 (=4+1)	74 (=70+4)
T_{PFLmin}; T_{PFLmax} [m^2/s]	4.0E-10; 2.3E-06	4.0E-10; 1.0E-06	4.4E-10; 8.5E-09	9.4E-10; 1.0E-06

5.5.5 Compilation of simulation results

Table 5-14 summaries the simulation results from the connectivity analysis presented above. The results shown in Table 5-14 suggests that the vertical spacing between the connected fractures is c 1 m in the C1 rock domain, c 1.8 m in the B1 rock domain, c 3.2 m in the C2 rock domain and c 0.3 m in the B2 rock domain. The last result brings up the question asked

Table 5-14. Compilation of simulation results from the connectivity analysis presented above. The values shown are mean values of four realisations.

Model	r_0 [m]	k_r [–]	N_{CON} [–]	P_{10CON} [100 m]	P_{32} [m^2/m^3]	P_{32CON} [%]	P_{32CON} [m^2/m^3]	$P_{32CON} < T_{min}$ [% of P_{32CON}]	$P_{32CON} > T_{min}$ [% of P_{32CON}]
C1	0.038	2.6	205	93	3.274	65	2.128	82	18
B1	0.038	2.6	171	55	3.201	42	1.344	96	4
C2	0.038	2.6	110	31	2.296	29	0.666	96	4
B2	0.038	2.6	2,440	306	7.046	83	5.848	97	3

previously, see Section 5.4.4. That is, we question if the KSH02A borehole is representative for the rock mass in the B rock domain. In our view, the high fracture frequency suggests that the KSH02 borehole seems to be drilled in, or very close to, a deformation zone.

It is noteworthy that the body of the connected fractures have transmissivities below the practical lower measurement limit of the PFL-f method. In fact, the average spacing between the PFL-f fractures in Table 5-13 is c 6 m in the C1 rock domain, c 52 m in the B1 rock domain, c 71 m in the C2 rock domain and c 11 m in the B2 rock domain.

5.6 Assessment of parameter values for a correlated transmissivity-size model

5.6.1 Methodology

Figure 5-18 shows a schematic illustration of a complementary cumulative density function (CCDF) plot of ordered fracture transmissivity measurements in a borehole. The CCDF equation for the fracture transmissivity may be written as:

$$G[T > T] = (1 - P[T' \le T]) = \left(\frac{m_T}{T}\right)^{k_T} \quad (5\text{-}8)$$

where m_T is the transmissivity value where the power law regression intersects $G[T' > T] = 1$ and k_T is the slope of the power law regression:

$$m_T = T^{\{1/k_T\}}\sqrt{G[T' \ge T]} = T_{PFL\,\min}\left(\frac{N_{PFL}}{N_{CON}}\right)^{(k_T)^{-1}} \quad (5\text{-}9)$$

In order to compute the value of the transmissivity m_T we make use of T_{PFLmin} and N_{PFL} in Table 5-13, the simulated values of N_{CON} in Table 5-14 and the deduced values of k_T from Figure 5-13 and Section 5.4.4.

Furthermore, we assume that the largest fractures among the N_{CON} connected fractures in each realisation correspond to the flow in the N_{PFL} PFL-f flow anomalies. Since the borehole is a one dimensional object (scanline) the slope of the power law regression k_r in the CCDF plots is:

$$k_r = k - 2 \quad (5\text{-}10)$$

where k is the shape parameter of the parent fracture size distribution, cf Equation (2-3).

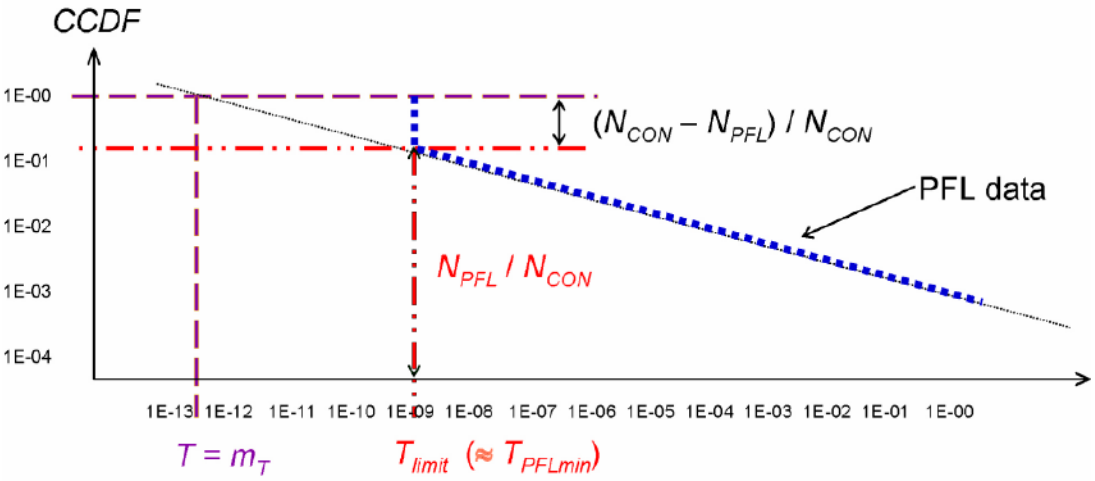

Figure 5-18. *Illustration showing the evaluation of a CCDF plot of ordered fracture transmissivity measurements in a borehole.*

The magnitude of m_r, i.e. the fracture size where the power law regression intersects $G[r' \geq m_r] = 1$ is evaluated as:

$$m_r = r^{\{1/k_r\}}\sqrt{G[r' \geq r]} = r_{N_{PFL}} \left(\frac{N_{PFL}}{N_{CON}} \right)^{(k_r)^{-1}} \tag{5-11}$$

where $r_{N_{PFL}}$ denotes the size of the smallest fracture among the N_{PFL} largest interconnected fractures.

The inferred values of the four variables $\{m_T, k_T\}$ and $\{m_r, k_r\}$ make it possible to derive the values of the coefficient c and the exponent d in Equation (2-9) by assuming that the complementary cumulative density functions are correlated:

$$G[T' \geq T] = G[r' \geq r] \tag{5-12}$$

By substituting both sides of Equation (5-12) by their corresponding power law expressions we get the desired variables into play:

$$\left(\frac{m_T}{T} \right)^{k_T} = \left(\frac{m_r}{r} \right)^{k_r} \tag{5-13}$$

and

$$T = m_T \left(\{m_r\}^{-1} r \right)^{\left(\frac{k_r}{k_T} \right)} \tag{5-14}$$

Thus, the coefficient c and the exponent d in Equation (2-12) can be computed from:

$$d = \frac{k_r}{k_T} \tag{5-15}$$

$$c = \frac{m_T}{(m_r)^b} \tag{5-16}$$

5.6.2 Demonstration of the methodology for the C1 rock domain

Table 5-15 shows values of c and d for 4 realisations in the C1 rock domain. The values are based on the assumption that $k = 2.6$ and $r_0 = 0.038$ m. The only input parameter to the calculations behind Table 5-15 not based on numerical simulations, but taken directly from the analysis of field observations, is k_T , the values of which are deduced from the PFL-f flow anomalies by fitting a power law regression model to the transmissivity data, cf Figure 5-15. The values deduced are shown in Section 5.4.4.

Figure 5-19 shows simulated transmissivities versus measured PFL-f transmissivities in the C1 rock domain using c and d values for the 4 realisations shown in Table 5-15.

Table 5-15. Values of c and d in the C1 rock domain using $k = 2.6$ and $r_0 = 0.038$ m.

Object	Mean	Real. # 1	Real. # 2	Real. # 3	Real. #4
C	8.2E-10	4.8E-10	1.2E-09	6.8E-10	8.9E-10
D	1.541	1.541	1.541	1.541	1.541
ΣT(C1) = 4.0E-6 [m²/s]	3.1E-06	1.7E-06	4.4E-06	2.0E-06	4.3E-06

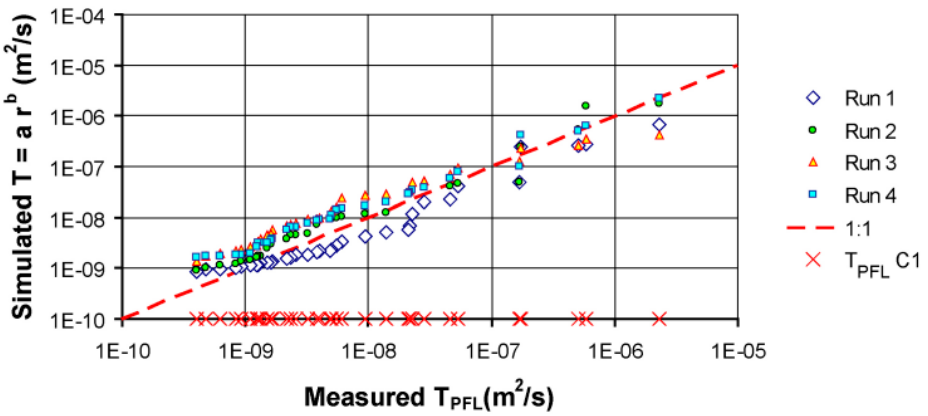

Figure 5-19. *Simulated transmissivities versus measured PFL-f transmissivities in the C1 rock domain using c and d values for the 4 realisations shown in Table 5-15.*

5.6.3 Sensitivity to *k* and r_0

Simulations were conducted for two values of r_0, 0.038 m and 0.282 m, and three different values of k, 2.6 ± 0.2, as a means to assess the uncertainty in the location parameter and the shape parameter, cf the discussion in Section 5.3.1. Figure 5-20 shows a comparison between r_0 = 0.038 m and 0.282 m for k = 2.6 and Figure 5-21 shows a comparison between k = 2.6 ± 0.2 for r_0 = 0.038 m. Each data series represents the mean of 4 realisations.

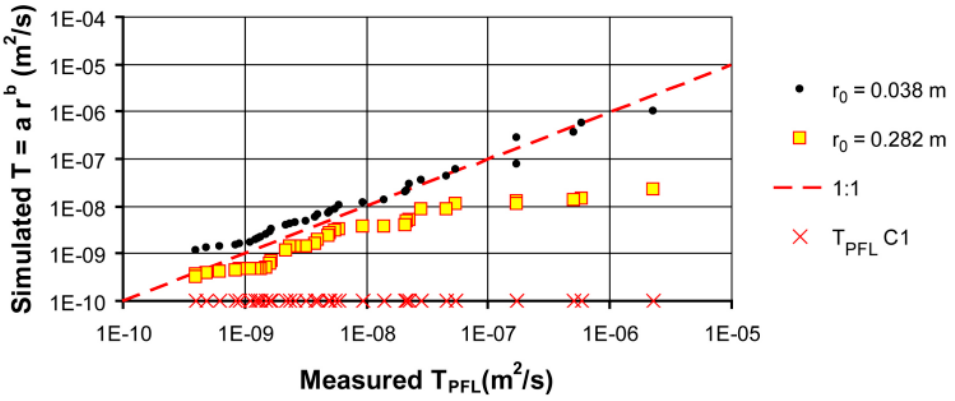

Figure 5-20. *Simulated transmissivities versus measured PFL-f transmissivities in the C1 rock domain using mean values of c and d values from 4 realisations with r_0 = 0.038 m and 4 realisations with r_0 = 0.282 m. k = 2.6 in both cases. The c value was adjusted when the r_0 value was changed.*

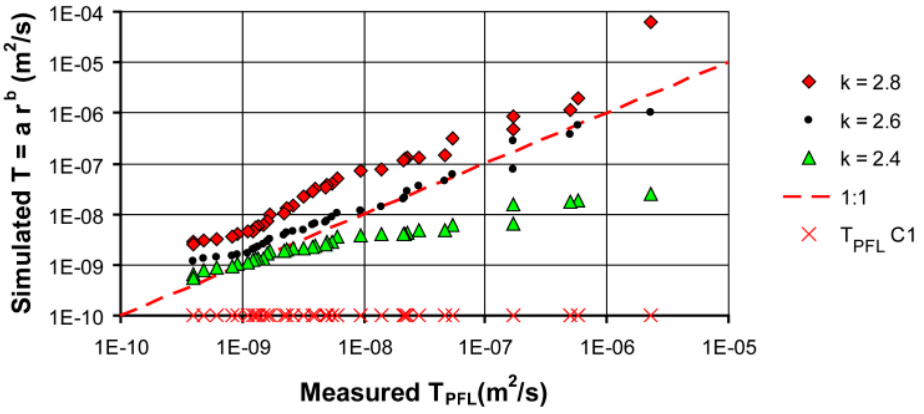

Figure 5-21. *Simulated transmissivities versus measured PFL-f transmissivities in the C1 rock domain using mean values of c and d values from 4 realisations each for k = 2.6 ± 0.2 and r_0 = 0.038 m.*

5.6.4 Sensitivity to the fracture frequency (intensity)

Table 5-16 shows a compilation of mean values of *c* and *d* from 4 realisations in each of the C1, B1, C2 and B2 rock domains. The four rock domain have different intensities and transmissivity distributions. The bottommost Table 5-16 shows the ratio between the cumulative simulated transmissivity and the cumulative transmissivity of the PFL-f measurements.

The mean values of *c* and *d* for the (C1+B1+C2) combination is calculated for the sake of the block scale simulations reported in Section 5.7 and the regional flow simulations shown in Chapter 7.

The mean values of *c* and *d* for the B2 rock domain are assumed to be similar to the mean values for the B1 rock domain. The reason for this assumption is that it was difficult to infer the k_T value from the transmissivity measurements in the B2 rock domain, see Figure 5-12. Figure 5-22 demonstrates the outcome of this assumption. That is, Figure 5-22 shows simulated transmissivities versus measured PFL-f transmissivities in the B2 rock domain using calculated mean *c* and *d* values for the C1, B1 and C2 rock domains, respectively, shown in Table 5-15. From Figure 5-22 we conclude that the aforementioned assumption is reasonable.

Table 5-16. Compilation of mean values of *c* and *d* from 4 realisations in each of the C1, B1, C2 and B2 rock domains. The bottommost row shows the ratio between the cumulative simulated transmissivity and the cumulative transmissivity of the PFL-f measurements.

Object	C1	B1	C2	C1+B1+C2	B2
C	8.0E-10	9.5E-13	1.2E-11	1.6E-11	9.5E-13
d	1.541	2.629	1.225	2	2.629
ΣTsim/ΣTmeasured [%]	78	54	136	89	72

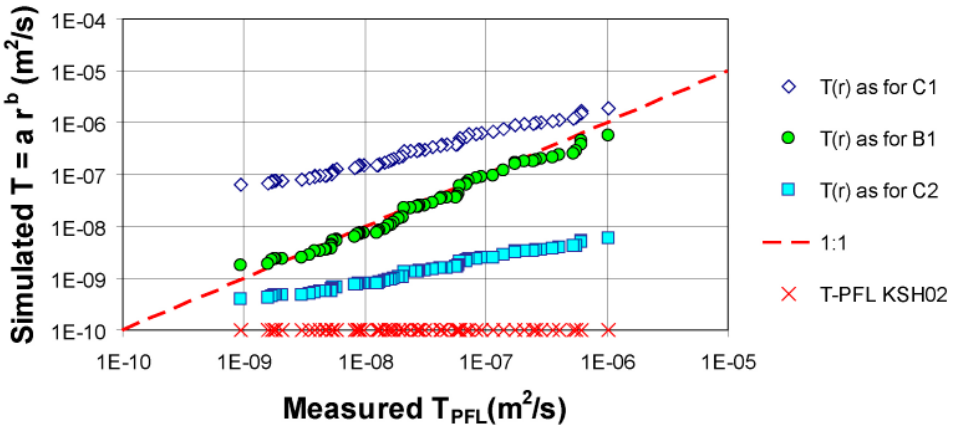

Figure 5-22. *Simulated transmissivities versus measured PFL-f transmissivities in the B2 rock domain using calculated mean c and d values for the C1, B1 and C2 rock domains, respectively, shown in Table 5-15.*

5.6.5 Summary of observations

The main observations made in the transmissivity-size analysis are:

- Field data conform fairly well to the assumption of power law size and transmissivity distribution.
- The methodology developed by the DarcyTools team for the analysis of a correlated transmissivity size model appears to be robust for practical applications.
- The parameter combination $r_0 = 0.038$ m and $k = 2.6$ gives the best simulation results in the work reported here.
- For the block scale simulations in Section 5.7 and the variable density flow simulations in Chapter 7 we suggest that $1.6 \cdot 10^{-11}$ is used for c and that 2.0 is used for d. This means that a fracture with a radius of 0.564 m ($L = 1$ m) has a transmissivity of c $5 \cdot 10^{-10}$ m^2/s, which is below the measurement limit, and that a zone with a radius of 564 m ($L = 1{,}000$ m) has a transmissivity of c $5 \cdot 10^{-6}$ m^2/s.

5.7 Assessment of block scale properties

The remit for this study, as specified by Repository Engineering, is to calculate block size statistics of the hydraulic conductivity tensor of 20 m and 100 m blocks using the results from the hydrogeological DFN. The block size simulations are useful also for the implementation of the DFN findings into a regional scale groundwater flow model.

Figure 5-23 and Figure 5-24 illustrate the methodology used. A huge DFN realisation is generated into which a 1 km^3 large cube is inserted. The cube in Figure 5-23 is divided into 1,000 grid cells (ten 100 m grid cells in each direction) and in Figure 5-24 the cube is divided into 125,000 grid cells (fifty 20 m grid cells in each direction). Following the GEHYCO technique presented in Section 2.4 fractures in the size range $L = 100$–$1{,}000$ m are to be generated for the 100 m mesh and $L = 20$–$1{,}000$ m are generated for the 20 m mesh. However, we decided to exclude the 100 m block size in this work and to generate fractures for the 20 m mesh only. The reason for this was that the 100 m mesh becomes quite isotropic and homogeneous due to the high fracture intensities observed, thus of little information.

5.7.1 Demonstration of the simulation process for the C1 rock domain

Two 1,000 m long scanlines pointing NS (parallel to the y-axis) and WE, respectively, are inserted into the computational domain representing the C1 rock domain. The left picture in Figure 5-25 shows fractures in a realisation intersecting the NS scanline and the right picture shows fractures in the same realisation intersecting the WE scanline.

The approach taken was to compute the grid cell conductivities in three orthogonal directions using the GEHYCO technique presented in Section 2.4. By rotating the axes in small increments the anisotropy of the fracture network was studied, see Figure 5-26.

The results for the realisation shown in Figure 5-25 are visualised in Figure 5-27.

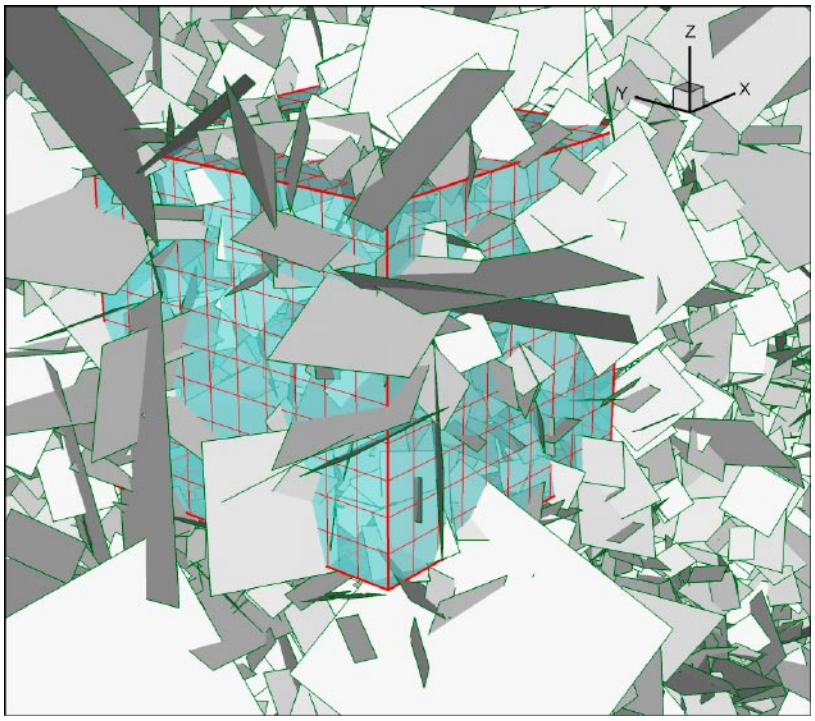

Figure 5-23. *Illustration of the methodology used in the work reported here for the computation of block scale properties. The picture shows a huge DFN realisation into which a 1 km³ large cube is inserted. The cube is divided into 1,000 grid cells (ten 100 m grid cells in each direction). The fractures shown are in the size range L = 100–1,000 m.*

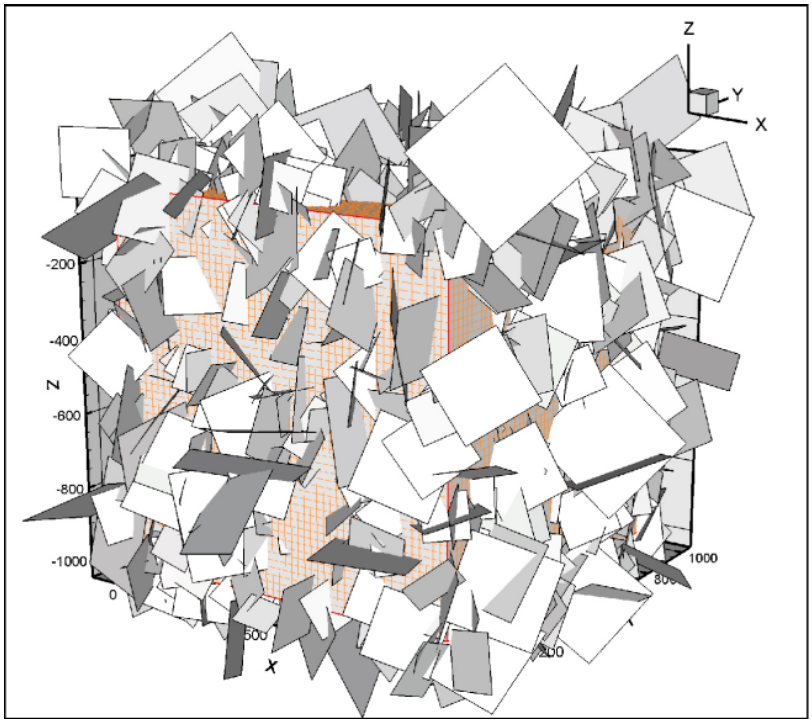

Figure 5-24. *Illustration of the 20 m mesh together with the generated fractures that intersect the 1 km³ cube only. All fractures less than L = 100 m are excluded in this picture to improve its readability.*

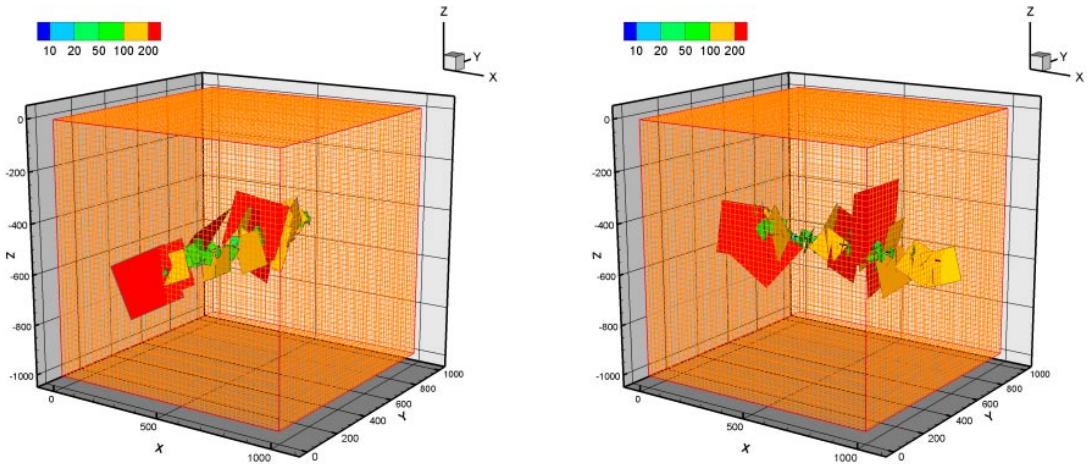

Figure 5-25. *Two 1,000 m long scanlines pointing NS (parallel to the y-axis) and WE, respectively, are inserted into the computational domain. The left picture shows fractures in a realisation intersecting the NS scanline and the right picture shows fractures in the same realisation intersecting the WE scanline.*

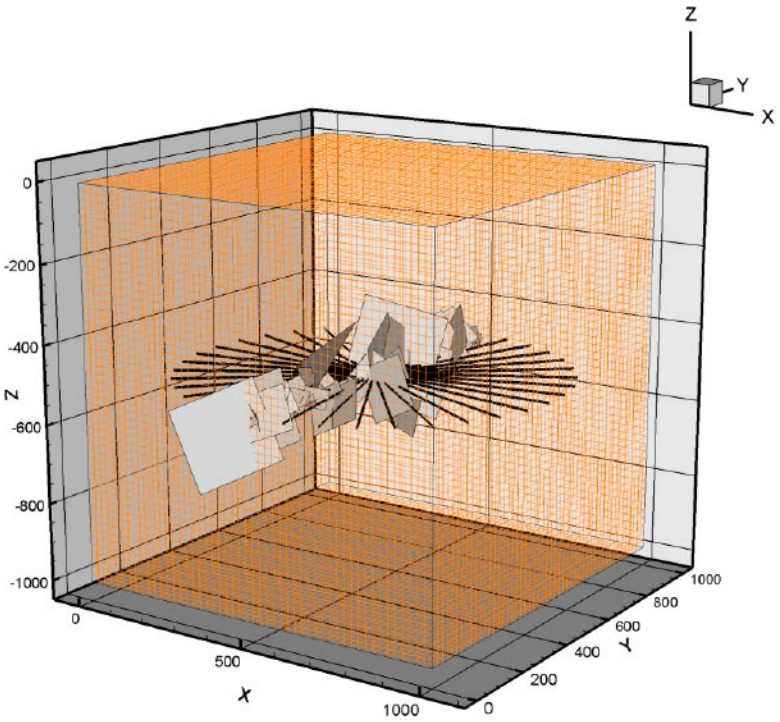

Figure 5-26. *The anisotropy of the fracture network was studied by rotating the axes in small increments.*

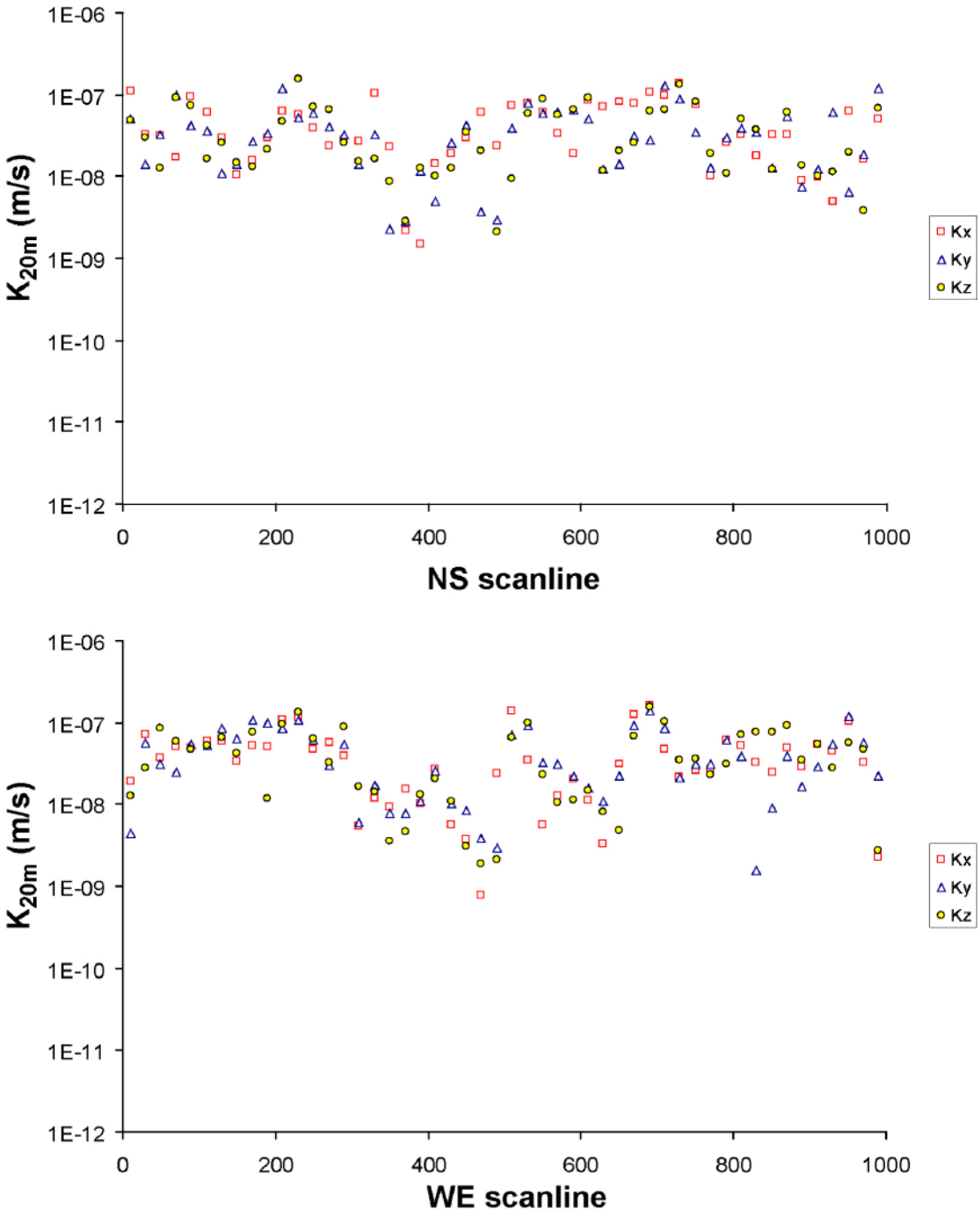

Figure 5-27. *Directional grid cell conductivities for the realisation shown in Figure 5-25.*

5.7.2 Sensitivity to the rock domain

Table 5-17 summarises the results from the simulations undertaken in the C1, B1, C2 and B2 rock domains. The four rock domains have different hydrogeological DFN properties. The statistics shown represent the spatial variance along the scanlines for a single DFN realisation in each rock domain.

Table 5-17. Compilation of simulation results for the C1, B1, C2 and B2 rock domains.

Object	Rock domain C1	Rock domain B1	Rock domain C2	Rock domain B2
Geometric mean of K_x [m/s] [NS/WE]	[3.2E-08/2.7E-08]	[1.2E-09/1.1E-09]	[8.1E-11/1.1E-10]	[9.0E-09/8.5E-09]
$\log_{10}$ standard deviation of K_x [–] [NS/WE]	[0.42/0.48]	[0.69/0.85]	[0.34/0.45]	[0.37/0.41]
Geometric mean of K_y [m/s] [NS/WE]	[2.6E-08/2.8E-08]	[1.2E-09/1.8E-09]	[7.8E-11/1.2E-10]	[7.7E-09/8.7E-09]
$\log_{10}$ standard deviation of K_y [–] [NS/WE]	[0.44/0.46]	[0.67/0.70]	[0.42/0.39]	[0.47/0.42]
Geometric mean of K_z [m/s] [NS/WE]	[2.6E-08/2.7E-08]	[1.1E-09/8.4E-10]	[8.3E-11/1.2E-10]	[7.4E-09/7.7E-09]
$\log_{10}$ standard deviation of K_z [–] [NS/WE]	[0.42/0.50]	[0.67/0.86]	[0.45/0.47]	[0.50/0.47]

5.7.3 Summary of observations

The main observations made in the 20 m block scale analysis are:

- The differences in geometric means between the rock domains are greater than the directional differences within any rock domain. Indeed, the simulated anisotropy is very weak in work reported here. Probably this is due the fact that the geological DFN model suggests seven fracture sets of moderately different intensities and that all facture sets in a given rock domain are assigned the same transmissivity-size correlation in the work reported here. In effect, the differences seen in the geometric means between the rock domains probably reflect both the observed differences in the fracture intensities and the observed differences in the PFL-f measurements.
- The C1 rock domain is the most conductive and the C2 rock domain the least. The conductivity of the B1 rock domain falls in between. Probably, this is due to the depth trend observed in the PFL-f measurements. Further, the B2 rock domain is more conductive than the B1 rock domain. We question if the KSH02A borehole is representative for the rock mass in the B rock domain. In our view, the KSH02 borehole seems to be drilled in, or very close to, a deformation zone, cf Figure 1-5.

6 Assessment of hydraulic properties to the Hydraulic Soil Domains (HSD)

6.1 The surface distribution and stratigraphy of Quaternary deposits in the Simpevarp regional model area

The regolith, also referred to as the overburden, includes all unconsolidated Quaternary deposits, both glacial deposits such as till, glaciofluvial sediment and clay, as well as postglacial deposits such as marine and lacustrine sediment and peat. The upper part of the overburden, affected by soil-forming processes, is referred to as *the soil*.

All known Quaternary deposits in the Simpevarp regional model area were formed during, or after, the latest glaciation. The oldest deposits are of glacial origin and have been deposited either directly by the ice, or by water from the melting ice. The whole regional model area is located below the highest coastline and fine-grained water-laid glacial and post-glacial sediments have been deposited in sheltered localities. In more exposed positions, the overburden has been partly eroded and redeposited by waves and streams when the water depth became shallower, as a consequence of the isostatic land uplift. The Simpevarp regional model area, in its present state, is a relatively flat area with a coastline highly exposed to the Baltic Sea. Isostatic land uplift is still an active process (1 mm yr^{-1}) and coastal processes are continuously changing the properties and distribution of the overburden. Accumulation of gyttja clay is an ongoing process in the present narrow bays along the coast. For a more detailed account of the present knowledge of Quaternary deposits in the Simpevarp regional model area the reader is referred to /Lindborg 2005/.

A relatively large part of the Simpevarp subarea is characterised by exposed bedrock, see Figure 6-1. The areas situated at the highest altitudes are almost entirely characterised by exposed bedrock. There are probably several reasons for the relatively low coverage of Quaternary deposits in this area. One reason may be that a relatively small amount of glacial till was deposited in the area during the latest ice age. Another reason is that large parts of the investigated area are exposed towards the open Baltic Sea. This condition has caused erosion and redeposition of overburden by waves.

Glacial till is the oldest known component of the overburden in the area and was deposited directly by glaciers during Quaternary. It may be assumed, but not concluded, that most of the till in the regional model area was deposited during the latest glaciation and rests directly on the bedrock surface. Till is the dominant Quaternary deposit and covers about 35% of the Simpevarp subarea. The morphology of the till in the subarea normally reflects the morphology of the bedrock surface. The thickness of the till varies between 0.5 and 4 m in the Simpevarp subarea. Most of the till has a sandy matrix, but gravelly till also occurs. The distribution of bedrock and fine-grained deposits in the Laxemar subarea and its surroundings are shown in /Lindborg 2005/. Areas in between the two surveyed subareas are probably dominated by till. An old map of Quaternary deposits in the whole regional model area /Lindborg 2005/, indicates that there is a more coherent till coverage in the south-western and western part of the regional model area. The marine geological map indicates that only a small fraction of the seafloor is covered by till.

Glaciofluvial deposits are restricted to the western and northern parts of the regional model area. These deposits may have hydrological importance and will be a focus for studies during the forthcoming investigations. Special focus will be put on studying the properties and extension of a glaciofluvial deposit found in the northern part of the Laxemar subarea.

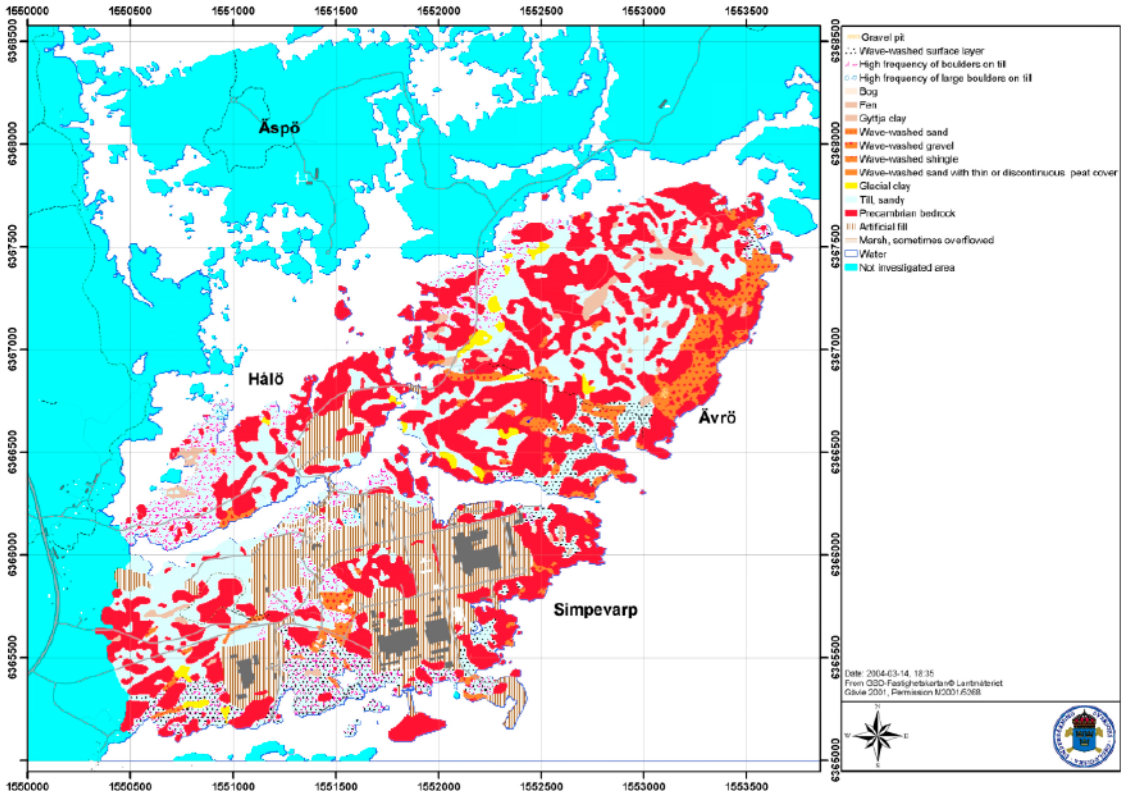

Figure 6-1. *The superficial distribution of Quaternary deposits and bedrock exposures in the Simpevarp subarea. Areas with a wave-washed surface layer and the superficial boulder frequency of the till are also shown. The map has been produced at the scale 1:10,000 and shows deposits with an area larger than 10 by 10 square metres.*

Peat covers c 2% of the Simpevarp subarea and is restricted to some of the narrower valleys. The peat is often found in mires, which are distinguished into two types: bogs and fens. The bogs are poorer in nutrients than the fens. Fen peat is the most common peat type in the Simpevarp subarea. There are, however, a number of small, but not raised, bogs, which often occur in depressions in areas dominated by exposed bedrock. The bog peat is often underlain by fen peat. Results from the soil investigation have shown that several wetlands in the Simpevarp regional model area consist of peat.

The total depth of overburden, observed at 15 soil drillings and two weight soundings in the Simpevarp subarea varies between 1.5 and 8.6 m. The average thickness of these observations is 3.6 m. The drillings were, however, carried out in the lowest topographical areas where the total depth of overburden probably exceeds the average for the whole area.

The results from the marine geological investigation show that the thickest overburden cover is restricted to long narrow valleys, but even here the total thickness of overburden is often less than 10 m. Also, according to the geophysical investigations carried out in the regional model area, the thickest overburden is situated in the valleys.

The overburden cover in the higher topographical areas, characterised by numerous bedrock exposures, is probably only one or a few metres thick at most. Further drillings, excavations and geophysical investigations will give more information regarding the thickness of overburden, especially in the Laxemar subarea.

Most of the stratigraphical information is at present concentrated to the Simpevarp subarea. A general tentative stratigraphy for the whole regional model area has, however, been constructed, see Table 6-1. This stratigraphy is based on results from the marine geological

survey and older stratigraphical investigations in the Simpevarp regional model area, e.g. /Borg and Paabo 1984, Risberg 2002/ and its surroundings e.g. /Svantesson 1999, Rudmark 2000/.

Table 6-1. The stratigraphical distribution of Quaternary deposits in the Simpevarp regional model area.

Quaternary deposit	Relative age
Bog peat	Youngest
Fen peat	↑
Gyttja clay/clay gyttja	
Sand/gravel	↑
Glacial clay	
Till	↑
Bedrock	Oldest

6.2 Conceptual model and hydraulic properties

No site specific values of the hydraulic properties were available on the outset of the regional variable-density flow modelling. The limited hydraulic information on the overburden in Simpevarp regional model area has led to use of a simplified two-layer model for the regional hydrogeological flow models. Below, the compiled results used as a basis for input to the regional variable-density flow modelling are shown.

Table 6-2. Hydraulic properties assigned to Hydraulic Soil Domain (HSD). Based on /Knutsson and Morfeldt 2002/ and /Carlsson and Gustafson 1997/.

Layer	Type of Quaternary deposits	Thickness (m)	Hydraulic conductivity (m/s)	Expected range of hydraulic conductivity (m/s)
1	Sandy till , near surface	1	$1{\cdot}10^{-5}$	$1{\cdot}10^{-7}$ to $1{\cdot}10^{-3}$
2	Sandy till, below layer 1	2	$1{\cdot}10^{-7}$	$1{\cdot}10^{-8}$ to $1{\cdot}10^{-6}$
Layer	**Type of Quaternary deposits**	**Thickness (m)**	**Specific storage (m^{-1})**	**Expected range of Specific storage (m^{-1})**
1	Sandy till , near surface	1	$1{\cdot}10^{-4}$	$1{\cdot}10^{-5}$ to $1{\cdot}10^{-3}$
2	Sandy till, below layer 1	2	$1{\cdot}10^{-4}$	$1{\cdot}10^{-5}$ to $1{\cdot}10^{-3}$
Layer	**Type of Quaternary deposits**	**Thickness (m)**	**Specific yield (–)**	**Expected range of Specific yield (SY) (–)**
1	Sandy till , near surface	1	$1{\cdot}10^{-1}$	$1{\cdot}10^{-2}$ to $3{\cdot}10^{-1}$
2	Sandy till, below layer 1	2	$1{\cdot}10^{-1}$	$1{\cdot}10^{-2}$ to $3{\cdot}10^{-1}$
Layer	**Type of Quaternary deposits**	**Thickness (m)**	**Kinematic porosity (%)**	**Expected range of Kinematic porosity, ne (%)**
1	Sandy till , near surface	1	$5{\cdot}10^{-2}$	$1{\cdot}10^{-2}$ to $1{\cdot}10^{-1}$
2	Sandy till, below layer 1	2	$5{\cdot}10^{-2}$	$1{\cdot}10^{-2}$ to $1{\cdot}10^{-1}$

7 Regional variable-density flow simulations

7.1 Numerical constraints for regional flow modelling

The final two steps of the workflow shown in Figure 2-2 involve calibration of a regional variable density flow model against available hydraulic and hydrogeochemical measurements and, subsequently, perform palaeo-hydrogeological simulations and particle tracking. The latter task comprises flow path simulations and sensitivity tests.

In practice, there is not a clear distinction between the two tasks. Indeed, calibration becomes meaningful only if the flow model is free from major uncertainties, e.g. concerning the size of model domain, choice of boundary conditions and the resolution of the computational grid. The latter issue is difficult in regional flow problems as the grid resolution generally is much coarser than the discrete fractures tested hydraulically and sampled chemically. The grid size also affects the heterogeneity (spatial variability) that can be addressed. Ideally, one should adapt the grid resolution to the properties of the deterministically modelled deformation zones and to the stochastically modelled hydrogeological DFN. The resolution of the computational grid used for regional flow modelling with DarcyTools in the work reported here is limited to 100 m due to computational constraints. Figure 7-1 shows a few examples of the shortcomings associated with this grid size (cf Appendix A for higher resolutions).

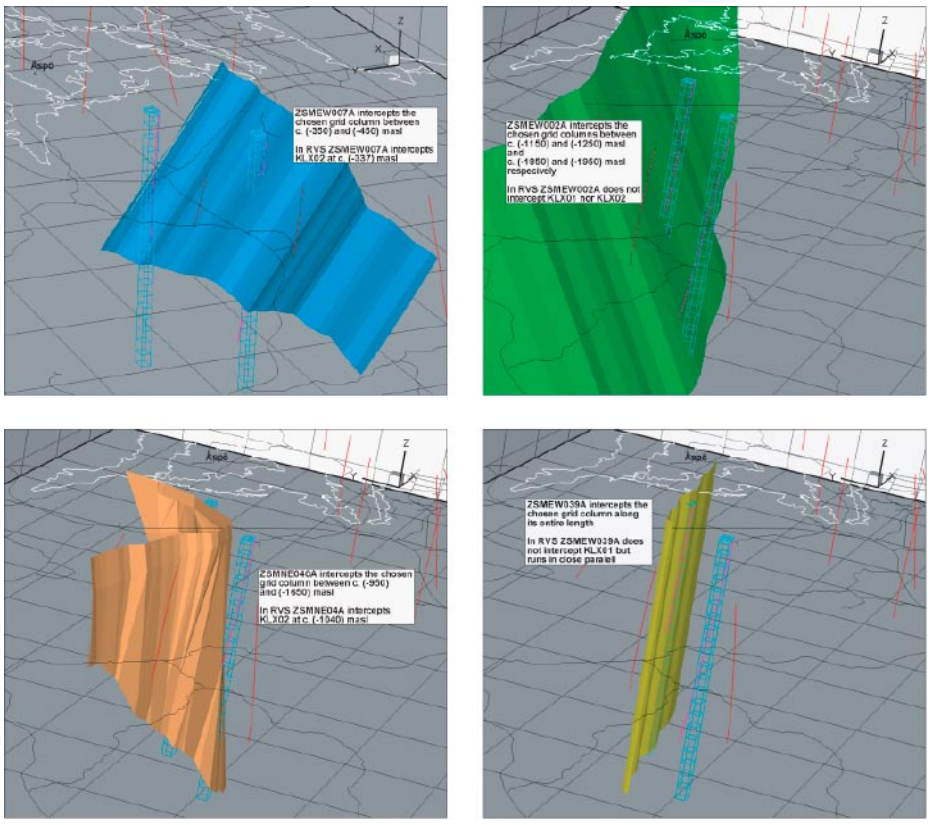

Figure 7-1. *The grid size affects the resolution near boreholes and may also significantly affect the hydraulic connection between the borehole and nearby deformation zones (less discrete connections than in reality).*

In conclusion, a finer grid resolution than 100 m within the local model area, and probably down to a depth of 1,000 m, where most of the hydrogeochemistry data are available, is probably required to capture the heterogeneity that is present. Hence, a finer grid resolution is probably vital for model calibration and the long-time and large-scale simulations of the groundwater flow after the last glaciation.

However, simulations with a coarse grid can also be of importance provided that the questions asked are correct vis-à-vis the hydrogeological simplifications made. For example, if regional hydrogeological uncertainties can be shown to have little effect on the flow paths from a particular model area, the conclusions drawn from the simulations still ought to be of significance. Of particular interest here are the size of the model domain, the variable fluid density and the role of the deterministically modelled deformation zones, see Figure 7-2.

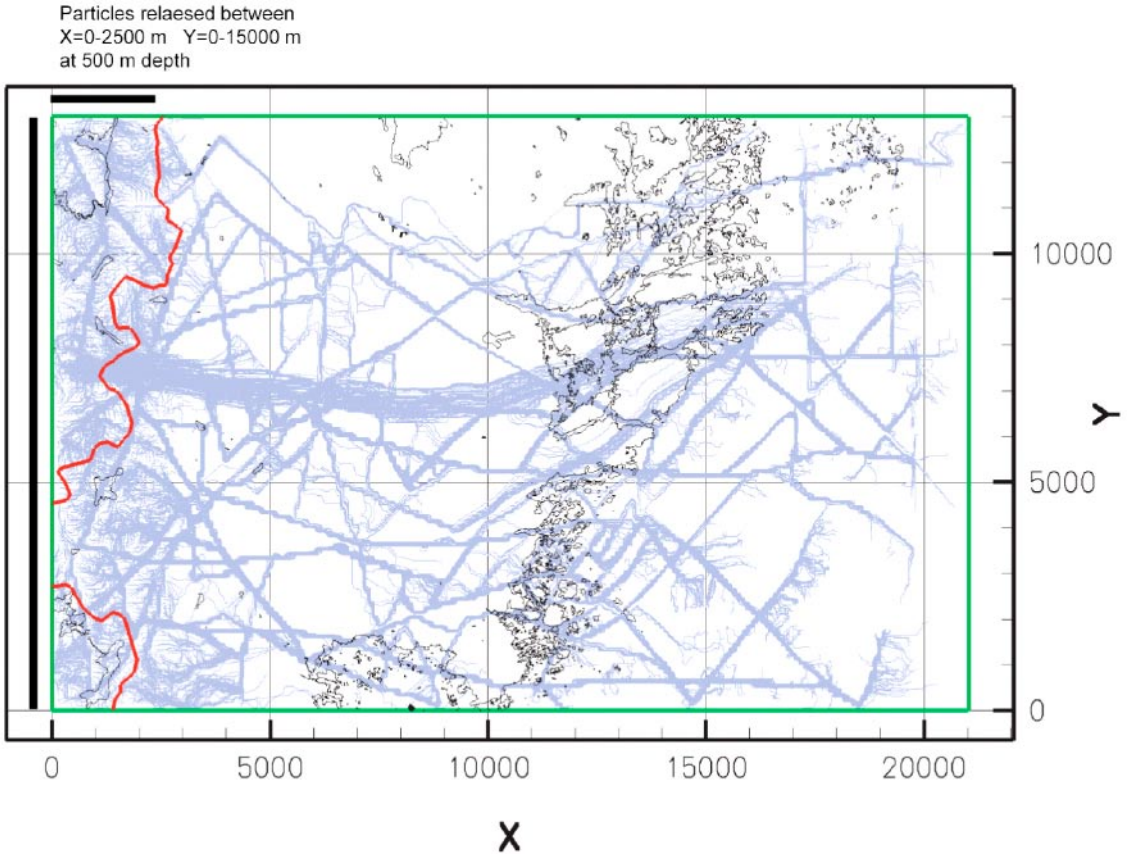

Figure 7-2. */Follin et al. 2004/ concluded in the 1.1 modelling stage that the local topography, the variable fluid density and the regional deformation zones are all important for the flow and discharge pattern. For instance, in this picture c 70% of the particles (blue traces) released at 500 m depth on both sides of a water divide (red line) close to the western (artificial no flow) boundary (at x = 0) discharge locally due to local gradients. Particles not captured by the local flow cells enter fairly soon the deterministically modelled deformation zones, which control the regional flow and discharge pattern in the model. The thickness of the model domain is 2,100 m.*

7.2 Comparison with the 1.1 hydrogeological model setup

The 1.1 hydrogeological modelling in the Simpevarp area conducted by /Follin et al. 2004/ was quite hypothetical since there were no geological DFN model and no hydraulic test data to take into account, cf /SKB 2004/. Many of the parameter values chosen were based on expert judgement, e.g. from the experiences gained in the Äspö HRL and True Block Scale projects and the ongoing site investigation in Forsmark. For the setup of the 1.2 hydrogeological modelling it is of interest to compare the findings and assumptions discussed in the work reported here with the assumptions used in the 1.1 hydrogeological modelling.

7.2.1 Deformation zones

There are 188 deterministically modelled deformation zones within the regional model domain. All zones are postulated to be more or less steeply dipping and have trace lengths greater than 1,000 m /SKB 2005/. The deformation zones have different levels of geological confidence, and most likely the number of true deformations zones is less than 188. For instance, 22 deformation zones only have a high confidence. In comparison, the 1.1 deformation zone model consisted of 177 deformations zones, 13 of which had a high geological confidence /SKB 2004/.

The transmissivity of the deterministically modelled deformation zones was set to $1.3 \cdot 10^{-5}$ m^2/s in the 1.1 modelling stage. In the 1.2 modelling stage 13 of the high confidence zones are assigned specific transmissivity values based on available information, e.g. field tests. In effect, some of the 13 zones are assigned a higher transmissivity value and some of the others a lower. The maximum and minimum values used in the 1.2 hydrogeological modelling stage are $3.6 \cdot 10^{-4}$ m^2/s and $8.5 \cdot 10^{-8}$ m^2/s, respectively.

7.2.2 Fracture orientation

There was no geological DFN model available for use in the 1.1 hydrogeological modelling. As a consequence it was decided to use the geological DFN model developed on behalf of the "Laxemar Methodology Project" /Andersson et al. 2002, Follin and Svensson 2002, SKB 2004/. The Laxemar geological DFN model consisted of four Fisher distributed fracture sets one of which was sub horizontal. The sub horizontal fracture set had a relative intensity of 17%. The Fisher concentrations of the four sets were quite low (kappa: 7–9.4), which means that there was no particular geometrical anisotropy prescribed. For the 1.2 geological DFN seven sets are used, and so as for the 1.1 hydrogeological modelling, fracture orientations are quite diffuse, and so these differences in fracture orientation are not expected a significant effect.

7.2.3 Fracture size and spatial distribution

The power law size distribution model used in the 1.1 modelling stage assumed a value of 2.6 for the shape parameter k. Moreover, a linear (Euclidian) scaling suggesting a uniform (uncorrelated and random; Poissonian) spatial pattern was postulated. None of these two assumptions are in contradiction with the settings for the 1.2 hydrogeological modelling discussed in the work reported here.

7.2.4 Fracture intensity

The hydrogeological modelling conducted by /Follin et al. 2004/ in the 1.1 modelling stage studied the role of the intensity of Open and Partly open features on a regional scale. The size range of the stochastically modelled features ranged from r = 56.4–564 m

(L = 100–1,000 m). Two hypothetical intensities were studied, $3.71 \cdot 10^{-2}$ m^2/m^3 and $7.42 \cdot 10^{-3}$ m^2/m^3. The higher value rendered on the average c 740,000 features, whereas the lower c 131,000 features. It was concluded that the magnitude of the intensity had a crucial impact on the heterogeneity and anisotropy in the resulting conductivity field in the flow model. For instance, the lower intensity rendered that c 3.5% of the 100 m large grid cells were not intersected by stochastic features in any direction and that c 13.5% grid cells were not intersected by stochastic deformation zones in at least one direction. For the higher intensity all grid cells were intersected by stochastic features in all directions. Hence, the lower intensity resulted in a flow model that was less conductive and much more heterogeneous and anisotropic, cf /Follin et al. 2004/.

From a hydrogeochemical point of view the lower intensity model showed indications of isolated volumes of glacial melt water and Littorina Sea water at 2000 AD. In contrast, the high intensity model did not show any indications of isolated ancient water types. That is, the high intensity model was completely flushed by meteoric water during the shoreline displacement leaving no ancient water types at depth in the terrestrial part of the regional model domain.

There were no particular motives for the chosen magnitudes of the two intensity models used by /Follin et al. 2004/ in the 1.1 modelling stage. Fairly tentative information from the 1.1 modelling stage in Forsmark was used as a reference for the higher intensity.

For the set-up of the 1.2 hydrogeological modelling in the Simpevarp subarea it is of interest to compare the deduced intensities shown in Table 5-1 with the aforementioned intensities used in the 1.1 modelling stage. For the four sub domains treated in the work reported here, i.e. B1, B2, C1 and C2, the intensity values shown in Table 5-1 render the following values for stochastic features in the postulated size range r = 56.4–564 m (L = 100–1,000 m): $3.83 \cdot 10^{-2}$, $8.42 \cdot 10^{-2}$, $3.92 \cdot 10^{-2}$, and $2.74 \cdot 10^{-2}$ m^2/m^3. Interestingly, these magnitudes compare quite well with the high intensity model studied in the 1.1 modelling stage ($3.71 \cdot 10^{-2}$ m^2/m^3). Also, the transmissivities are similar, as shall be seen in Section 7.2.5, and hence, a regional flow model based on an equivalent porous medium representation of the geological DFN model derived in the work reported here will most likely be fairly conductive and only weakly heterogeneous and anisotropic. Moreover, the flushing by meteoric water will probably be complete.

Upscaling of borehole fracture intensity and transmissivity data to represent a regional scale flow system is a provisional assumption. An alternative approach is downscaling, i.e. calculate the intensity that matches the number of large geological objects, e.g. the deterministically modelled deformation zones, cf Figure 5-2. From a scaling point of view the number of steeply dipping stochastic features with trace lengths greater than 1,000 m within the regional model domain can be calculated from Equation (2-5) provided that the relative intensity of steeply dipping fractures can be estimated. According the results reported in Table 5-2 the relative intensity of steeply dipping fractures in the KSH01A borehole is c 57%. If we assume this value to be representative on a regional scale Equation (2-5) renders 620 steeply dipping features with trace length greater than 1,000 m. However, there are “only” 188, which suggest that the calculated intensity from borehole data is far too large.

For the sake of the modelling work reported here we treat below two intensity models, $3.13 \cdot 10^{-2}$ m^2/m^3 and $9.49 \cdot 10^{-3}$ m^2/m^3. The intensity of the first model is based on a weighted average of the three rock domains penetrated by the KSH01A borehole, i.e. C1, B1, and C2. The intensity model of the second model is simply 30% of the first model, i.e. 188/620 times $3.13 \cdot 10^{-2}$ m^2/m^3. The first intensity model renders c 600,000 features, whereas the second renders c 192,000 features.

7.2.5 Fracture transmissivity

The correlated transmissivity-size model (cf Equation (5-4b)) used in the 1.1 modelling stage postulated a value of $2.47 \cdot 10^{-12}$ for the coefficient a and a value of 1.791 for the exponent b. For a stochastic feature of L = 100 m or L = 1,000 m these values implies a transmissivity value of $9.4 \cdot 10^{-9}$ m^2/s and $5.8 \cdot 10^{-7}$ m^2/s, respectively.

The correlated transmissivity-size model deduced in the work reported here (cf Section 5.6) a value of $5.0 \cdot 10^{-12}$ for the coefficient a (with regard to L) and a value of 2.00 for the exponent b. For a stochastic feature of L = 100 m or L = 1,000 m these values implies a transmissivity value of $5.0 \cdot 10^{-8}$ m^2/s and $5.0 \cdot 10^{-6}$ m^2/s, respectively. Hence, the transmissivities of the stochastic fractures are moderately more transmissive in the 1.2 modelling stage compared to the correlated transmissivity-size model used in the 1.1 modelling stage.

7.2.6 Discussion

The deformation zones and the hydrogeological properties used for regional variable density flow simulations and particle tracking in the 1.1 modelling stage are very similar to the deformation zones suggested for the 1.2 modelling stage as well as the hydrogeological properties inferred from the assessment of a hydrogeological DFN model based on the data acquired from the investigations in the KSH01A and KSH02 boreholes. The implication of this observation is that the results from the regional variable density flow simulations and particle tracking reported from the 1.1 modelling stage by /Follin et al. 2004/ are relevant also for the regional flow modelling with DarcyTools in the 1.2 modelling stage.

The considerable overlap between the 1.1 and 1.2 modelling stages in terms of input model parameters inevitable limits the novelty of the work reported here since the overall tasks (cf Figure 2-2) for the two modelling stages are the same. Indeed, the major contribution of this report to the site descriptive modelling is the development of the hydrogeological DFN methodology reported in Chapter 5. To a large extent the regional variable density flow modelling presented below is a refined analysis of the sensitivity study carried out by /Follin et al. 2004/ in the 1.1 modelling stage.

It is noted that there is no particle tracking and analysis of flow related transport parameters incorporated into the work reported here due to the decision made by SKB at the onset of simulations. The only exception made to this limitation is when the sensitivity to a larger size of the model domain is studied, cf sensitivity case B. below.

7.3 Definition of Base Case and sensitivity cases

Table 7-1 summarises the hydraulic parameters and conditions used for the Base Case model setup. Table 7-1 also shows the five sensitivity cases treated. The sensitivity cases are:

A. Higher fracture intensity.

B. Larger and smaller size of the model domain.

C. Depth dependence in the transmissivity field.

D. Later start of the Littorina Sea period.

E. Different values of the global capacity ratio.

Table 7-1. Compilation of model assumptions and hydraulic properties used for the Base Case model setup. The rightmost column shows the sensitivity cases treated.

Parameter	Base Case	Sensitivity Case
Model domain	210·130·2.1 km^3.	260·130·2.1 km^3.
Grid resolution	100 m.	No alternative tested.
Initial condition	Full Glacial between 0–950 m; then a linear salinity gradient to no Glacial, full Brine at 1,450 m; full Brine below 1,450 m.	Glacial has to go to about 1 km depth then full Brine by 1,500 m. Hence, no alternative tested.
Flow BC	Top: transient specified pressure. Lateral and bottom: no flux.	No alternative tested.
Salinity BC	Top: Baltic Ice Lake (Glacial) → Yoldia Sea (Marine/Glacial) → Ancylus Lake (Glacial) → Littorina Sea (Marine) → Baltic Sea → Meteoric (precipitation) → Rain 1960 (Meteoric after 1960) Lateral and bottom: no flux and spec. concentration, respectively.	Tested the sensitivity of the flow model to a later start of the Littorina Sea period.
HydroDFN	Orientation and size: Table 5-2 Intensity: 9.49E-03 m^2/m^3 (Section 7.2.4) Transmissivity: Table 5-16 (C1+B1+B2).	Tested also a model with a much higher fracture intensity, 3.13E-2 m^2/m^3, see Section 7.2.4.
Depth dependence in the transmissivity of the HCDs	None. Tmin = 8.5E–08 m^2/s. Tave = 1.3E–05 m^2/s. Tmax = 3.6E–04 m^2/s.	Tested also an alternative model where the conductivity decreased by a factor of 10 per kilometre.
Minimum hydraulic conductivity and kinematic porosity of the background rock mass	1E–11 m/s. 1E–04.	No alternative tested. No alternative tested.
Maximum kinematic porosity of the RVS deformation zones the stochastic DFN	1E–02. 5E–03.	No alternative tested. No alternative tested.
Matrix porosity	Used a multi-rate diffusion model instead. A global value of the capacity ratio βG between the immobile to mobile pore volume of 2 was assumed.	Tested also βG = 0.1 and βG = 10.
Flow wetted surface per unit volume of rock	Computed internally from the assumption of 2 m^2 flow wetted surface area per unit fracture area (cf Chapter 2).	No alternative tested
Maxtrix diffusion	Used a multi-rate diffusion model with 10 storage volumes of different time scales.	No alternative tested.
Multi-rate diffusion mass transfer coefficients	α_{max} = 1E–03 s^{-1} α_{min} = 1E–10 s^{-1}	No alternative tested.

7.4 Comparisons with measured data

An improved understanding of the palaeo-hydrogeological conditions is necessary in order to gain credibility for the site descriptive model in general and the hydrogeological description in particular. This requires modelling of the groundwater flow from the last glaciation up to present-day with comparisons against measured hydrogeochemical data.

7.4.1 Premises for comparisons

Hydraulic properties are generally estimated from the evaluation of hydraulic test results related to the geological domains as shown in Chapters 4, 5 and 6. The next phase is to set up a numerical groundwater flow model by combining the geometric information associated with the geological domains with the preliminary hydraulic properties and evaluate the flow model results versus relevant data sets, e.g. natural heads, interference and tracer test responses, and hydrogeochemical profiles. Some of these data sets come into play as calibration targets during the course of the development of the hydrogeological model. However, at this point the matching of simulations against detailed measurements is above all indicative as the data sources for conclusive comparisons are quite limited and the regional model domain is treated with a significant imperfection in terms of detailed discretisation, see Figure 7-3. Still, the main objective of the flow modelling is to focus on what is going on at repository depth within the Simpevarp and Laxemar subareas.

The quantity of hydrogeochemical data available for modelling in the 1.2 modelling stage are still quite limited, in particular at depth. This is an important constraint as the simulation of variable density flow is a key task in the work reported here. For instance, there are samples from depths greater than one kilometre in KLX02A borehole only, where presumably a significant amount of Brine has been encountered. Hence, data on the dense saline water are quite sparse. From a regional perspective there is a risk of bias if the comparison of salinity is made with data from just one or a few deep boreholes. Moreover, most of the boreholes are located near to the coast in very low topographic areas. So, there is an additional risk of bias due to sampling essentially in a single hydrogeological environment.

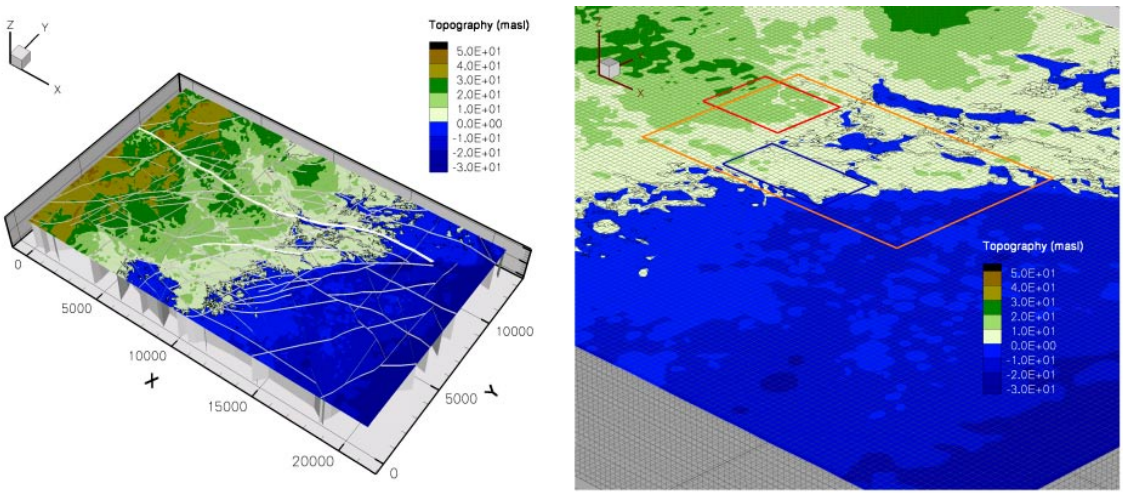

Figure 7-3. *Left: The regional hydrogeological model treats a flow system that is 2.1 km deep, 21 km long and 13 km wide. Right: In order to cope with this huge volume, a coarse a grid resolution of 100 m is used in the numerical simulations. It is important to recall these shortcomings when comparing simulations with detailed measurements. The rectangles represent the local model domain (orange) and the Laxemar (red) and Simpevarp (blue) subareas.*

Finally, the KLX02 borehole is interpreted to be intercepted by at least two steeply dipping and deterministically modelled deformation zones (ZSMEW007A and ZSMNE040A), see Figure 7-1, which means that the influence of the properties of the stochastic hydro-geological DFN properties on the groundwater chemistry is most likely limited, which is a drawback from a calibration point of view, see Section 7.4.

Bearing these risks in mind the primary data used for comparisons with the regional groundwater flow simulations in the work reported here are the present-day (2000 AD) hydrogeochemical data available from the KLX02 borehole. More precisely, comparisons are made with the measured TDS concentrations and with the mixing proportions calculated with the M3 method /Laaksoharju et al. 2004/, see Figure 7-4. It is noted that the uncertainty in the calculated M3 mixing proportions is significant, see Figure 7-5.

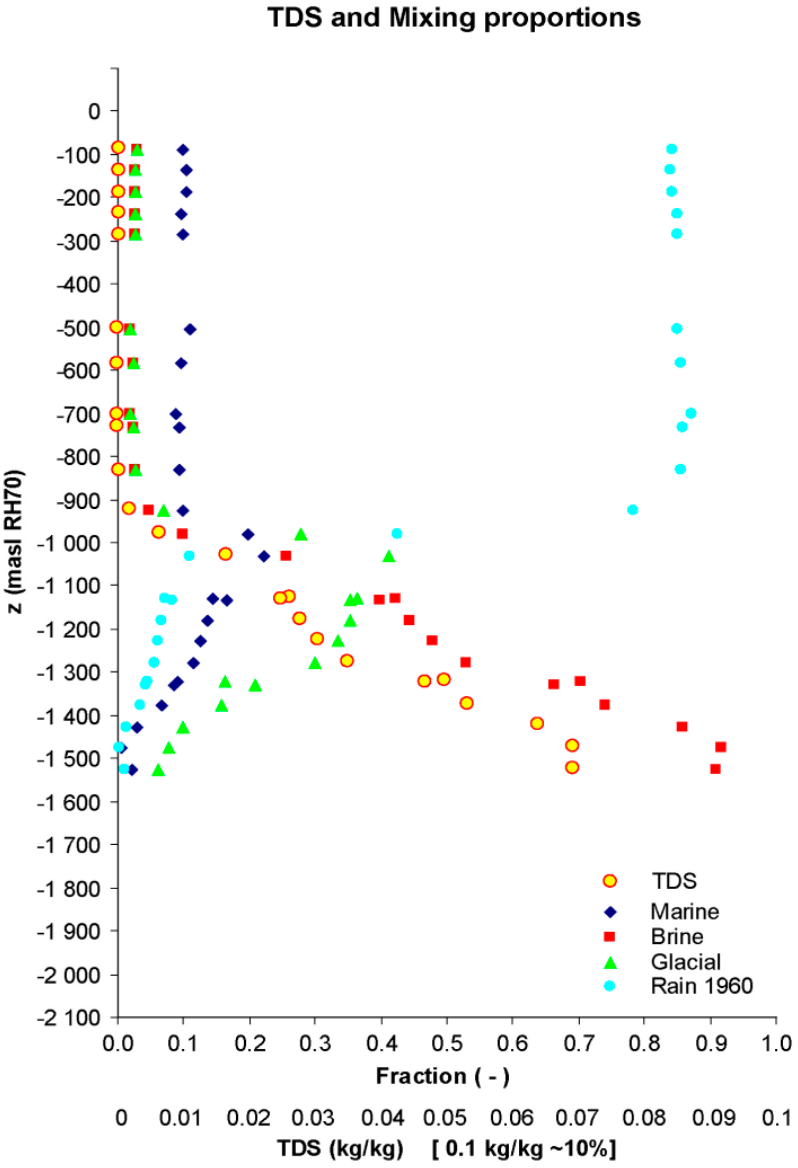

Figure 7-4. *Measured TDS concentrations and calculated M3 mixing proportions of four reference waters in the KLX02 borehole. This information is the primary data used in the work reported here for the comparison between regional groundwater flow simulations (representing different cases) and site specific data.*

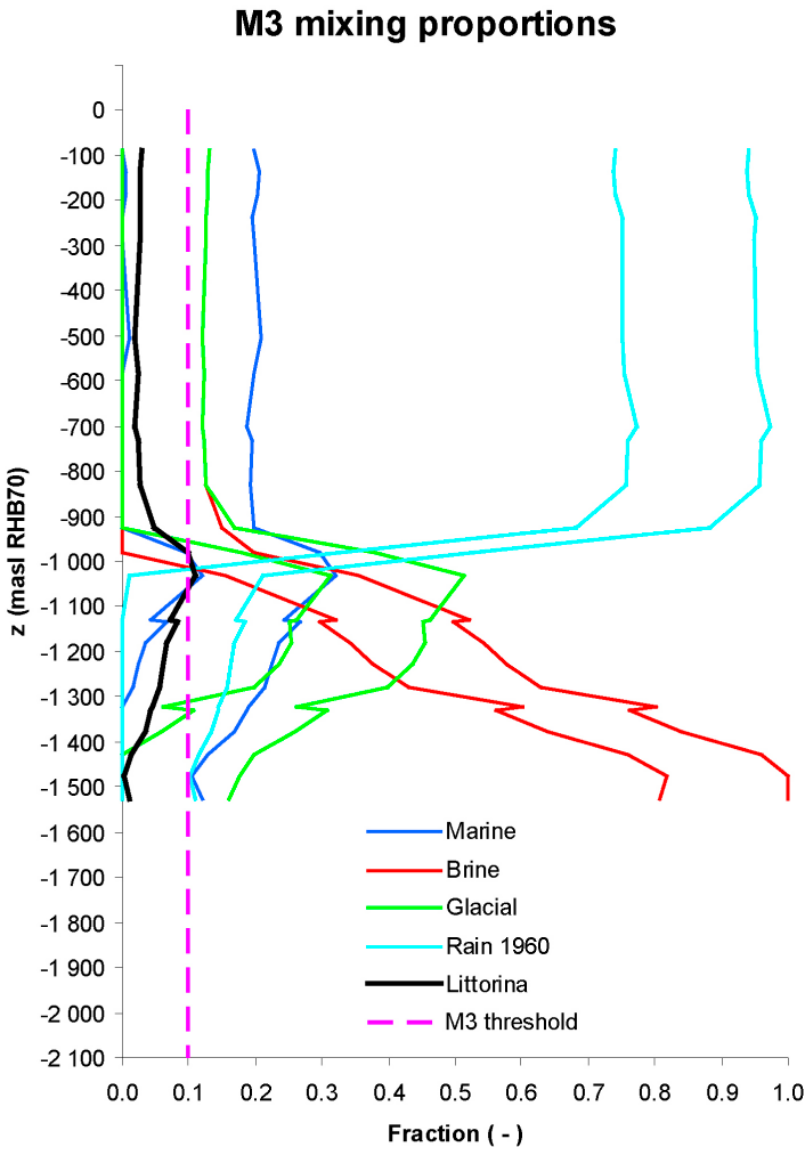

Figure 7-5. *The measurement threshold of the M3 calculations is c 10% and the uncertainty in the calculations is typically ± 10%. The double graphs indicate the range of what can be considered to be an acceptable match from a simulation point of view for the different water types.*

The M3 method uses a simplified system of four reference (or end-member) waters; Brine, Glacial, Marine and Rain 1960, see /Laaksoharju et al. 1999, 2004/ to describe groundwater composition. The end-member mixing fractions give several different tracers that have entered the groundwater system at different times and with different densities. Not all tracers are conservative though. As such, they give the possibility to quantify sensitivities of transient simulations to initial conditions, boundary conditions and hydraulic properties, which are not possible with salinity data alone. Salinity, on the other hand, gives an indication of the balance in driving forces between hydraulic gradients at the surface and buoyancy effects of the dense brine, and how this balance has changed over time due to land rise. Hence, it acts as a natural tracer for transient variable-density flow.

A single density driven advection-dispersion equation is solved in the DarcyTools simulations, where the variable density flow is governed by specified boundary and initial conditions for the pressure and salinity on the top boundary, see Figure 7-6 and Figure 7-7.

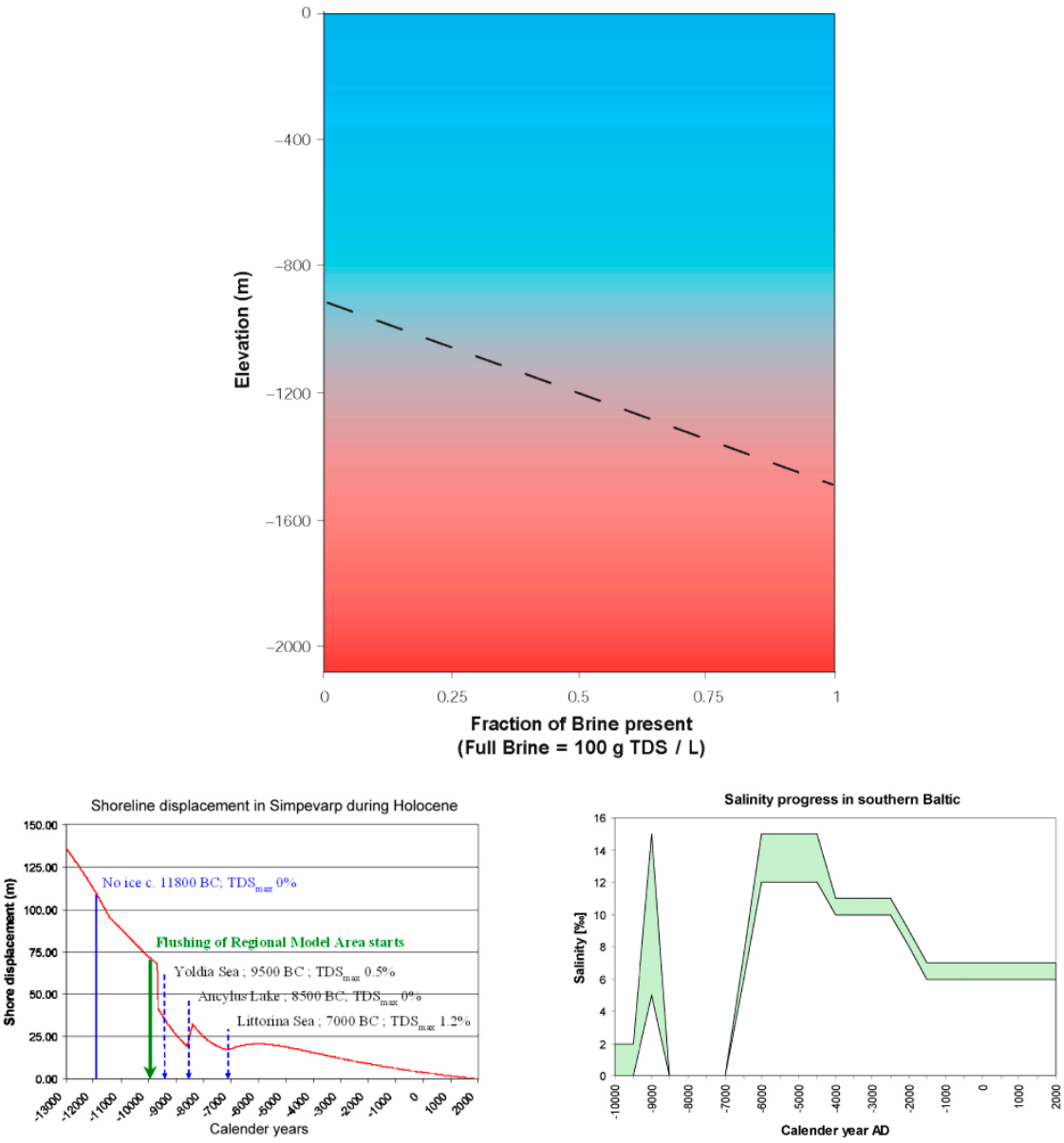

Figure 7-6. *Top: Initial condition for the salinity in the fracture system and in the matrix 10,000 BC. Lower left: Top boundary head during Holocene (the last 10,000 years). Lower right: Top boundary sea water salinity during Holocene. See Appendix A for close-ups.*

The transport of water parcels representing different water types (note the difference in the wording) is made by solving several independent non-reactive advection-dispersion equations in parallel, one for each water type, cf Section 2.6. It should be noted that in the DarcyTools simulations ”Rain 1960” represents meteoric water infiltrated after 1960, whereas “Meteoric” represents meteoric water infiltrated before 1960. Thus, in order to compare the DarcyTools simulation results with the “Meteoric” component in Figure 7-4 and Figure 7-5, the values of “Rain 1960” and “Meteoric” in the DarcyTools simulations should be added together.

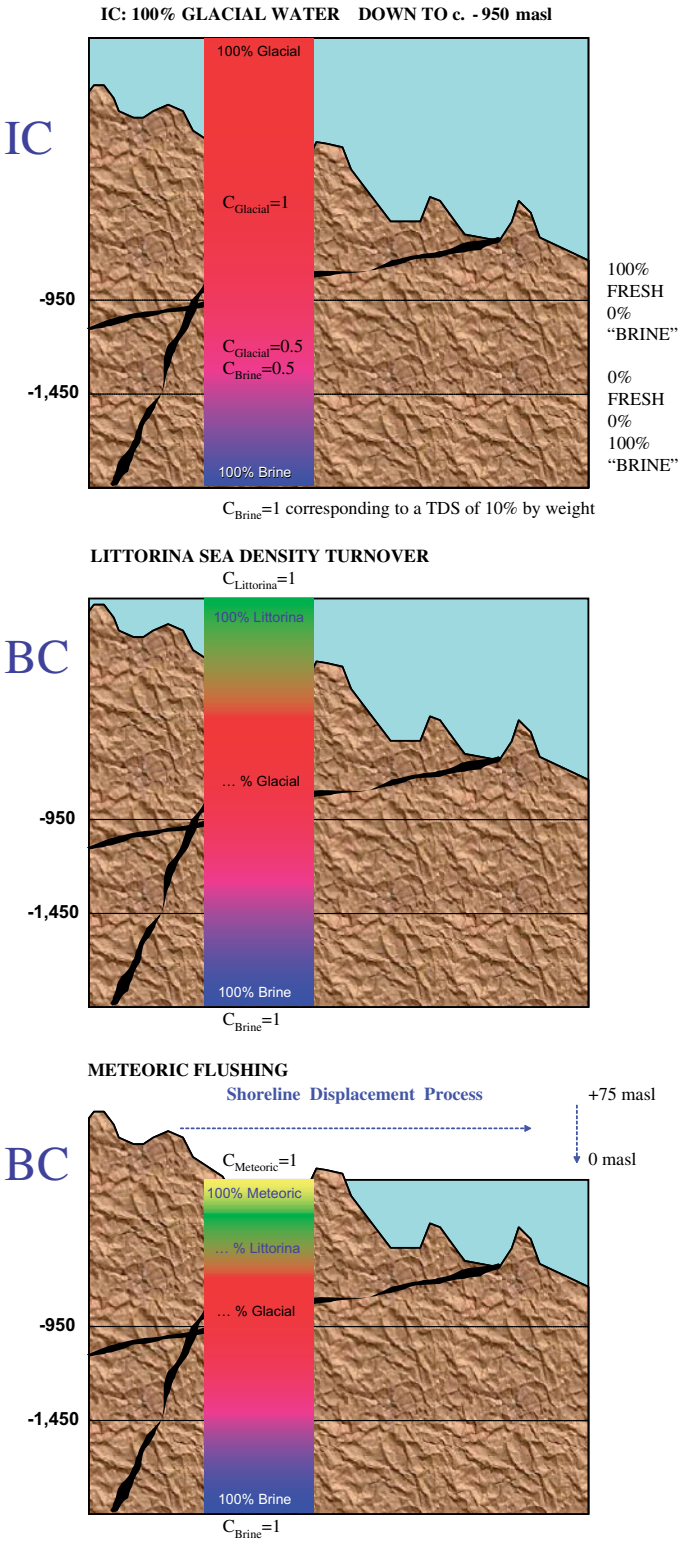

Figure 7-7. *Illustration of the water type initial condition 10,000 BP, the water type boundary condition during the Littorina Sea period, and the water type boundary condition during the Meteroric flushing.*

7.5 Sensitivity study

Figure 7-8 shows the 1.2 Simpevarp regional model domain, the deterministically modelled deformation zones and the computational grid.

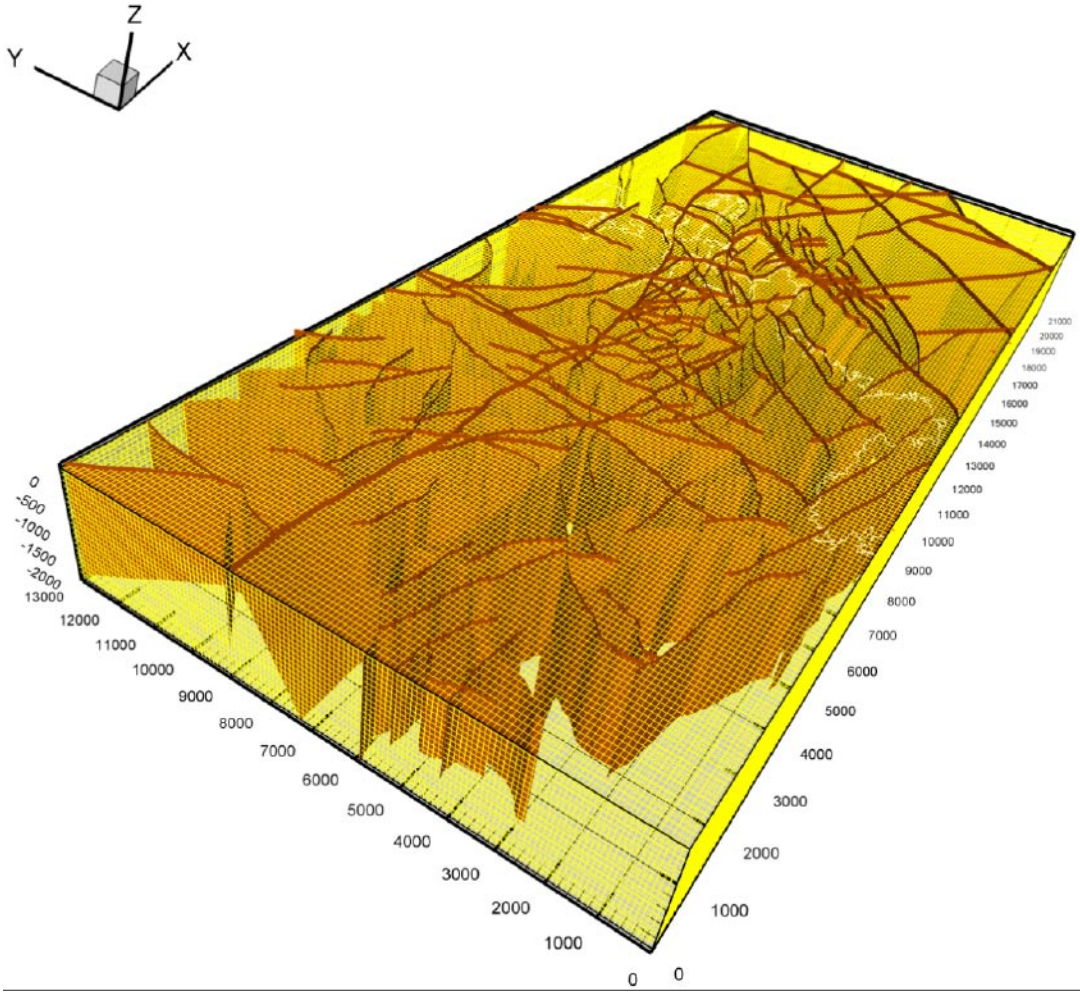

Figure 7-8. *The 1.2 Simpevarp regional model domain looking from SW towards NE and the Baltic Sea. The dark brown shadows are the 188 deterministically modelled deformation zones (RVS-DZ). The white line is the coast line. The resolution of the computational grid is 100 m below 100 m depth and finer above. In total the model domain consists of 655,200 grid cells.*

7.5.1 Base Case

In Section 7.2.4 we concluded that upscaling the fracture intensity seen in boreholes (cf the hydrogeological DFN presented in Chapter 5, e.g. Table 5-14) renders a considerably more fractured computational 100 m grid, with little heterogeneity and anisotropy, compared to the downscaling approach discussed in Section 7.2.4.Figure 7-9 illustrates the difference in fracture intensity and Figure 7-10 shows histograms for the hydraulic conductivity tensor and the kinematic porosity of all 100 m grid cells below 100 m depth (546,000). Table 7-2 presents data on the grid cell connectivity for the two fracture intensity cases. In the work reported here we use the downscaling approach as the Base Case for the fracture intensity. This decision implies that the value of N_{CAL}, i.e. the total number of Open and Partly Open fractures in a rock mass intercepted by a core drilled borehole, is overestimated by a factor of three (3).

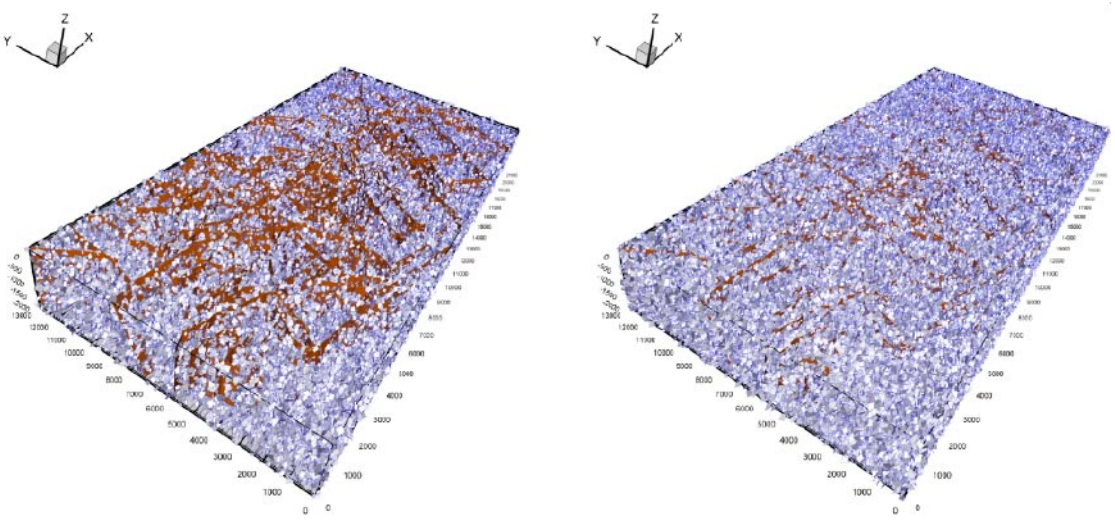

Figure 7-9. *The 1.2 Simpevarp regional model domain looking from SW towards NE and the Baltic Sea. The dark brow shadows are the 188 deterministically modelled deformation zones (RVS-DZ). Left: A low DFN intensity. Right: A high DFN intensity. The low intensity DFN renders c 190,000 connected fractures in the size interval L = 100–1,000 m, whereas the high intensity renders c 600,000 fractures.*

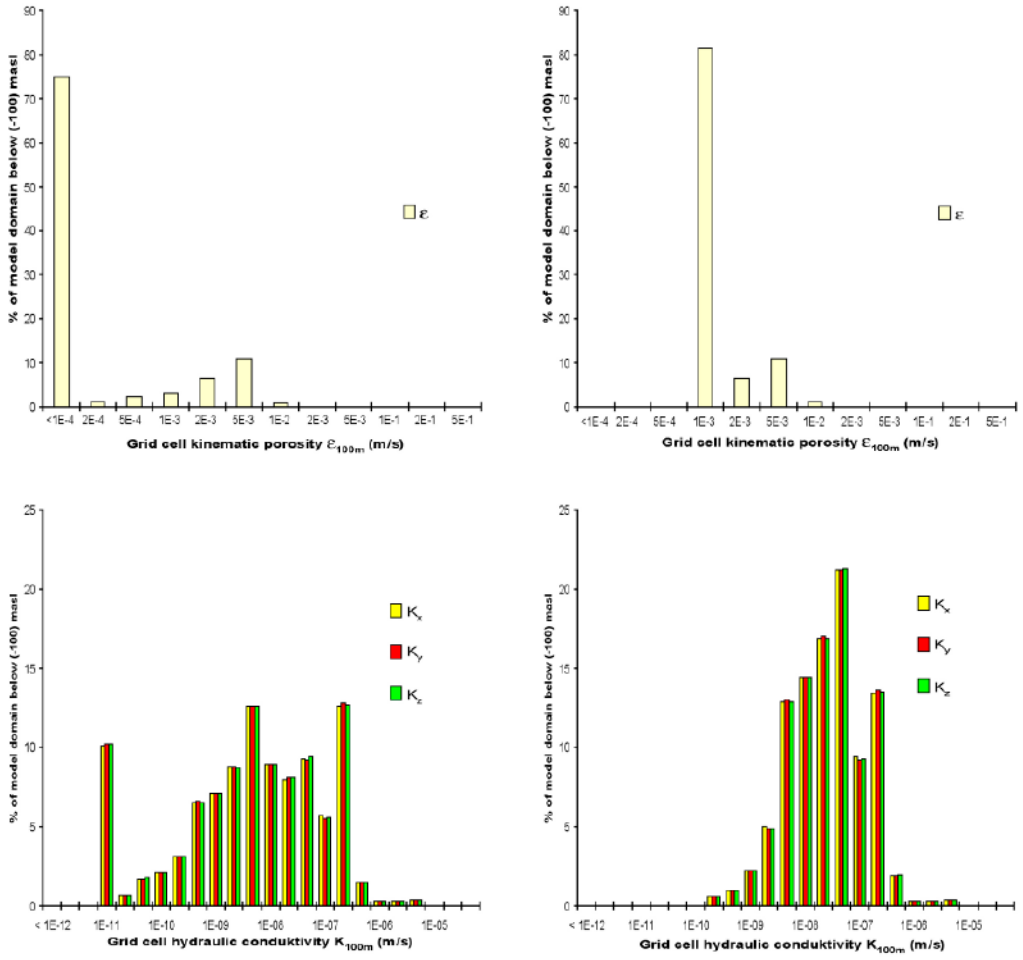

Figure 7-10. *Histograms of the grid cell kinematic porosity and hydraulic conductivity for the realisations shown in Figure 5-7. Left: Low DFN intensity. Right: High DFN intensity. Data on the connectivity is presented in Table 7-2.*

Table 7-2. Data on the grid cell connectivity for the two intensity cases. The low intensity case has one third the intensity of the high intensity case and a considerably greater grid cell disconnectivity.

DFN Intensity L = 100-1,000 m	No. of 100 m grid cells below 100 m depth	No. of cells with no connectivity in 1 flow direction	No. of cells with no connectivity in 2 flow directions	No. of cells with no connectivity in 3 flow directions
Low	546,000	166,535	76,282	16,041
High	546,000	5,272	537	40

7.5.2 Sensitivity Case A – Fracture intensity

The water type and TDS simulation results for the Base Case (low DFN intensity) and the high intensity case (Sensitivity Case A) are compared with measured TDS concentrations and calculated M3 mixing proportions in Figure 7-11. There are no significant differences between the two cases visible with regard to the salinity (TDS) and the calculated M3 mixing proportions, in particular not if one takes the uncertainty band in the calculated M3 mixing proportions shown in Figure 7-5 in account. This observation is probably due to the two steeply dipping deformation zones that runs sub parallel to the KLX02 borehole. That is, the high transmissivities of the two deformation zones govern large parts of the grid cell hydraulic conductivity along the borehole trajectory, thus overruling the differences in the rock mass fracture intensity. This conclusion was confirmed by running a second realisation of the low DFN intensity case, i.e. no significant differences were observed between the two realisations, see Figure 7-12.

From Figure 7-11 we note that the postulated initial interface between Glacial (fresh) water and Brine (saline) at the start of the simulation period (10,000 BC) is fairly stable. This observation, however, is slightly affected by the setting of the capacity ratio of the multi-rate diffusion model, see the discussion in Section 7.4.6 (Sensitivity Case E).

In Figure 7-13 through Figure 7-18 we visualise the TDS and water type simulation results in three-dimensions by means of five profiles, four parallel to the mean regional topographic gradient and one parallel to the coast line:

Figure 7-13: Simulated TDS concentrations.
Figure 7-14: Simulated Brine water type concentrations.
Figure 7-15: Simulated Glacial water type concentrations.
Figure 7-16: Simulated Littorina water type concentrations.
Figure 7-17: Simulated Meteoric water type concentrations.
Figure 7-18: Simulated Rain 1960 water type concentrations.

The simulated TDS concentrations in Figure 7-13 are very similar with inland discharges of saline groundwater in topographic lows. Figure 7-13 suggests that the present-day conditions may be close to a steady-state situation. The simulated water type concentrations reveal a pronounced Meteoric flushing, however more heterogeneously distributed in the Base Case.

Figure 7-19 and Figure 7-20, finally, show the Base Case distribution of volumes with Littorina and Glacial water types, where the residual relative concentrations are greater than 50%, respectively. For the high DFN intensity case there are no patched patterns of residual volumes of such large relative concentrations, see Figure 7-15 and Figure 7-16.

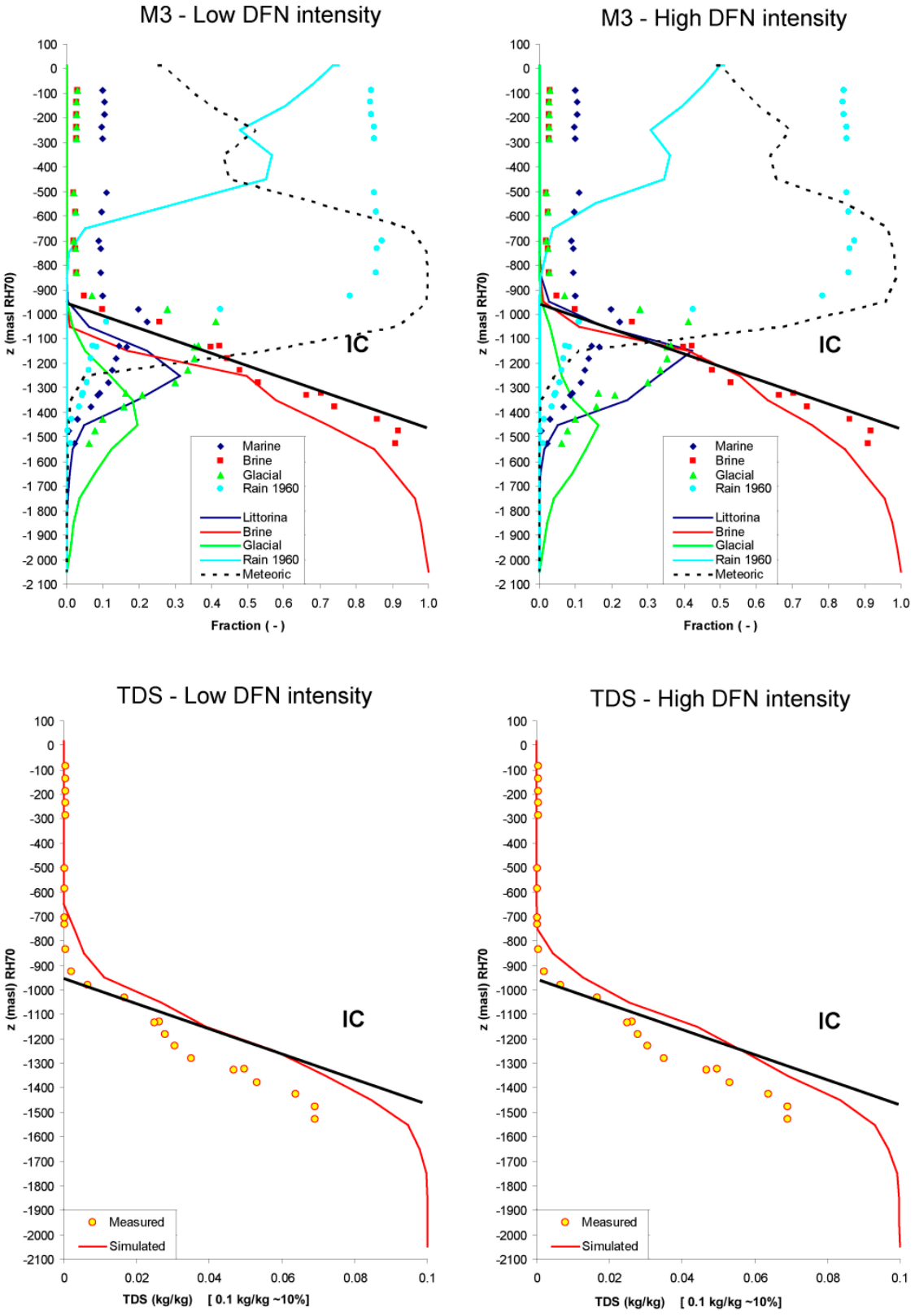

Figure 7-11. *Water type and TDS simulation results (lines) from the Base Case (low DFN intensity) and the high intensity case (Sensitivity Case A) together with measured TDS concentrations and calculated M3 mixing proportions (dots).*

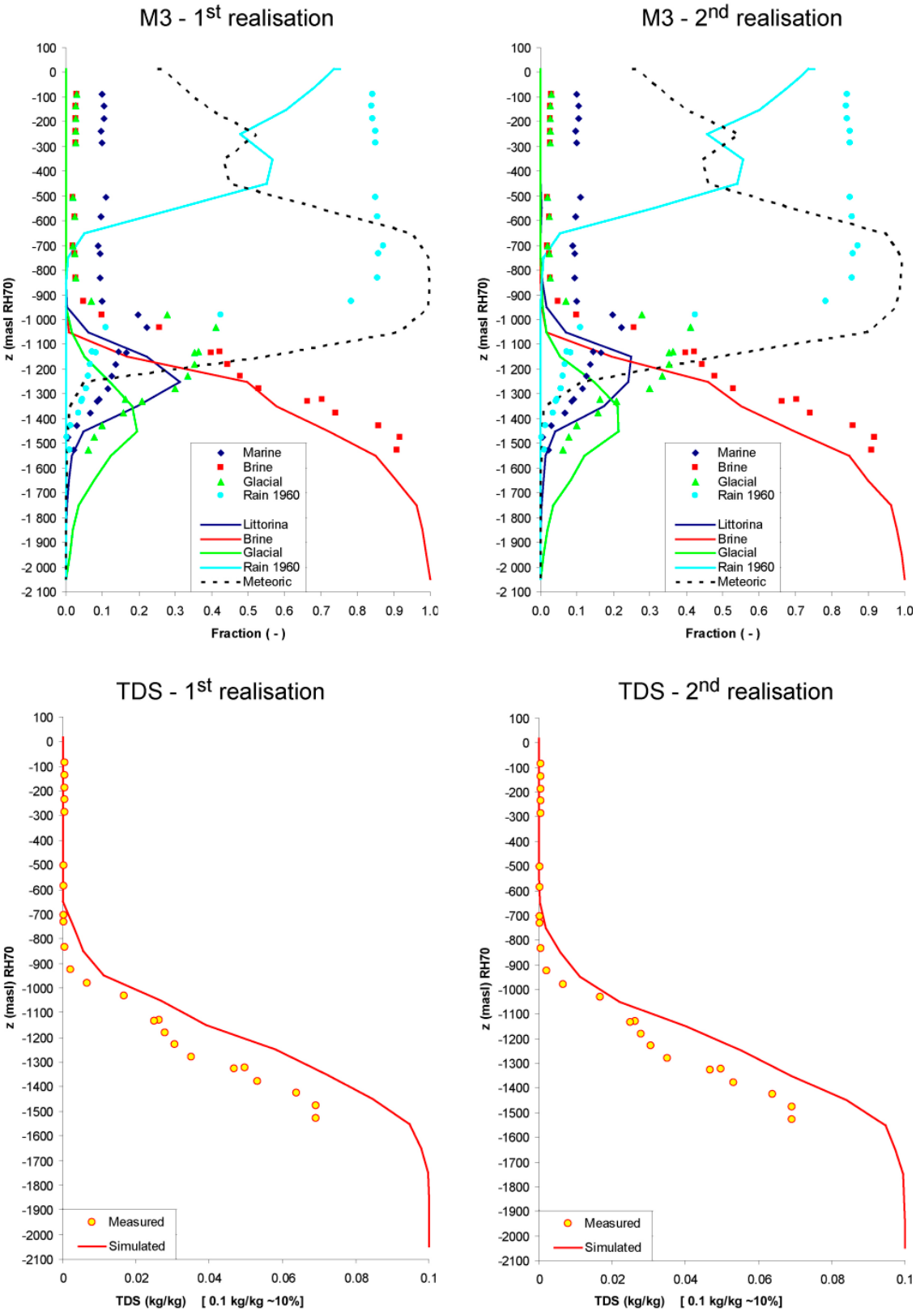

Figure 7-12. *Two realisations of the Base Case.*

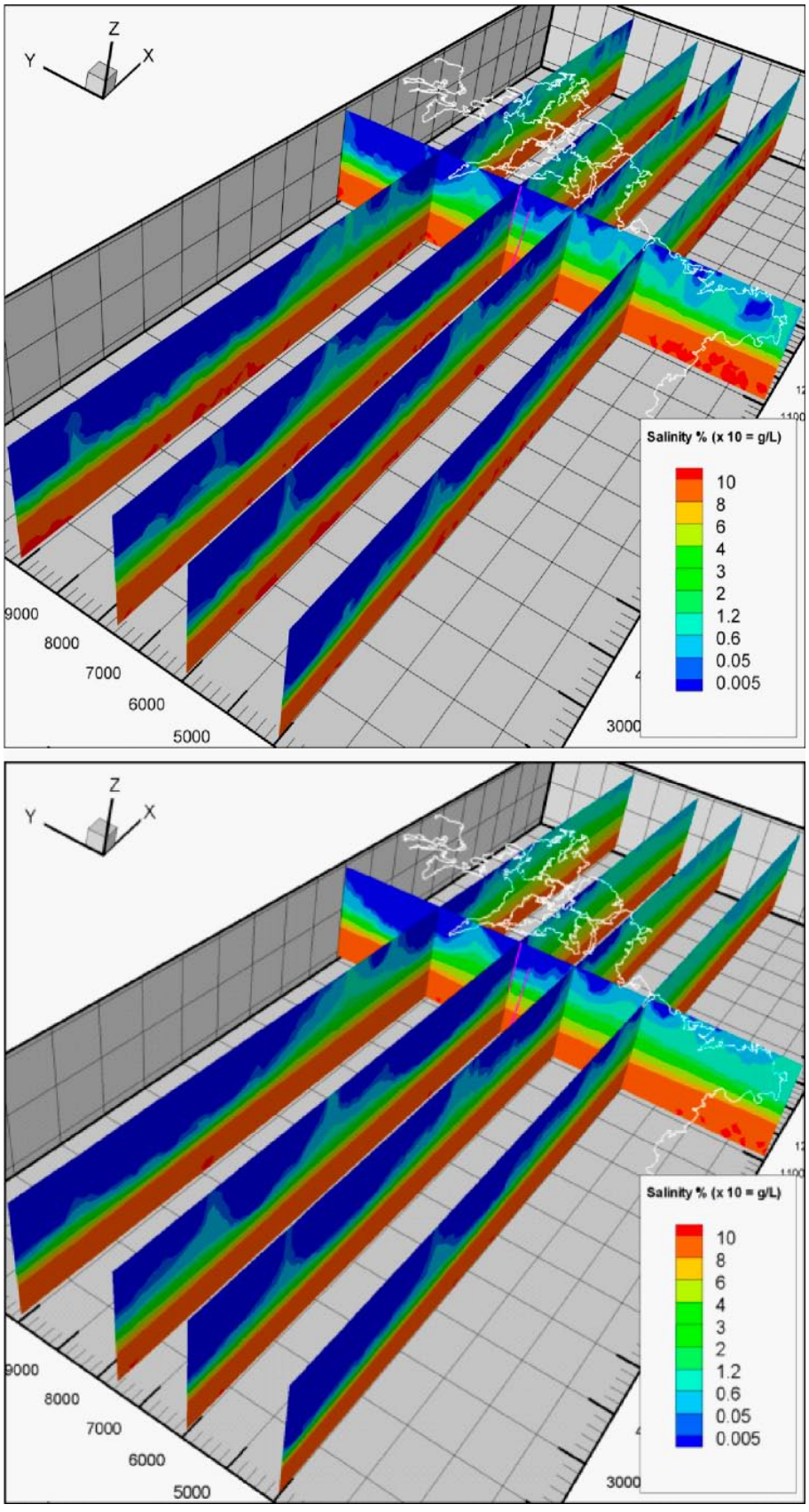

Figure 7-13. *Simulated TDS concentrations. Top: Base Case (low DFN intensity). Bottom: High DFN intensity.*

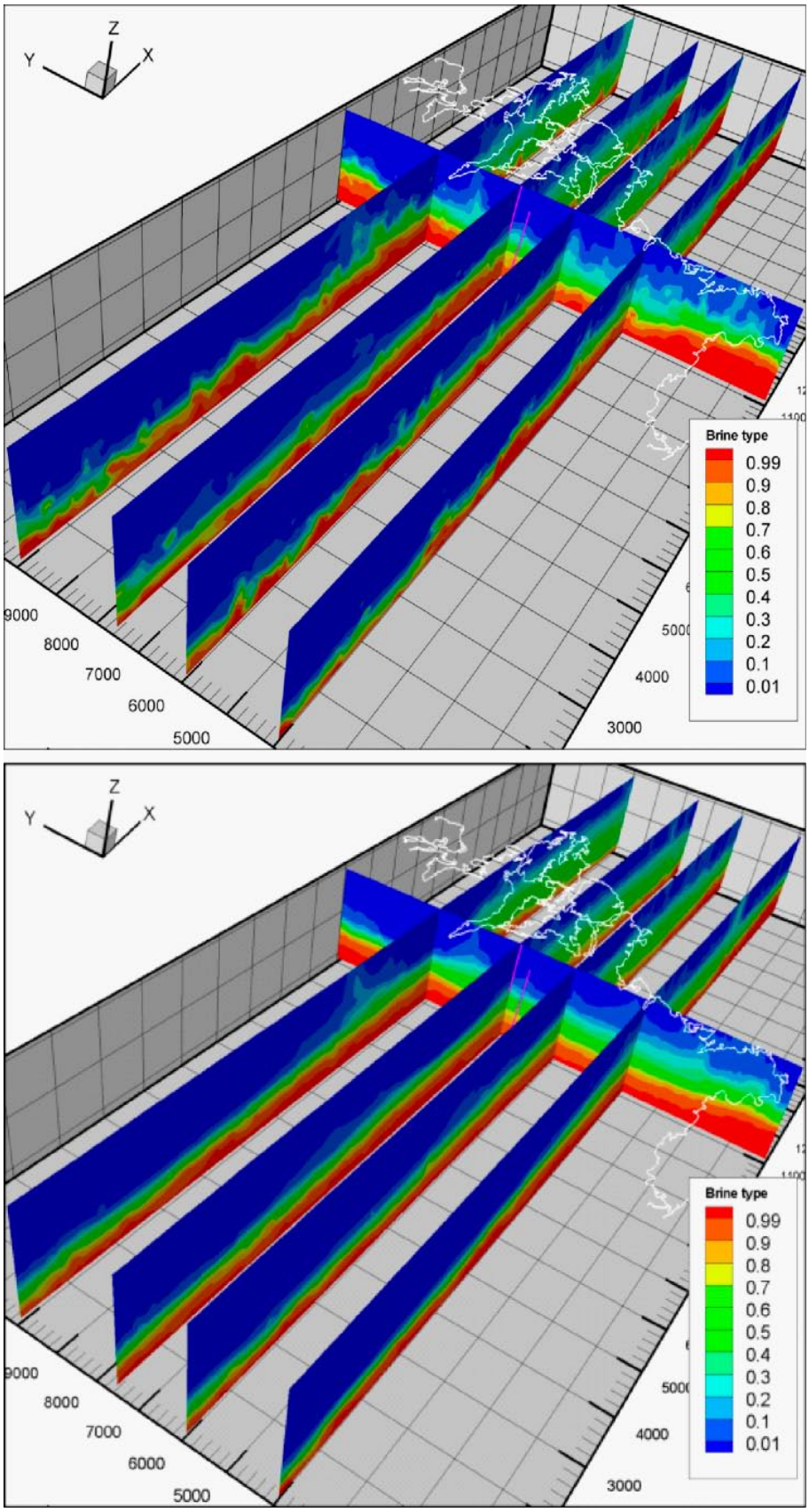

Figure 7-14. *Simulated Brine water type concentrations. Top: Base Case (low DFN intensity). Bottom: High DFN intensity.*

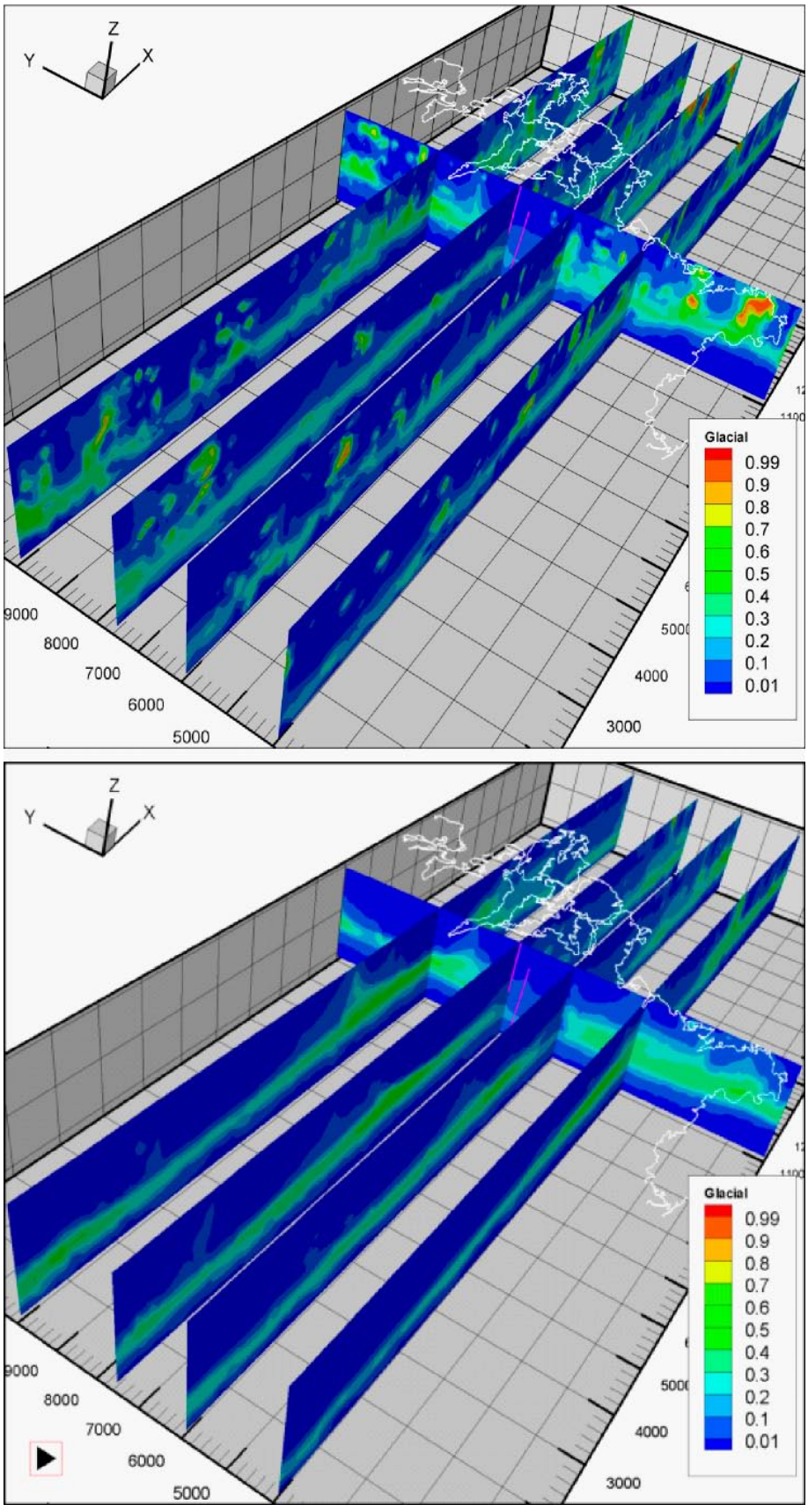

Figure 7-15. *Simulated Glacial water type concentrations. Top: Base Case (low DFN intensity). Bottom: High DFN intensity.*

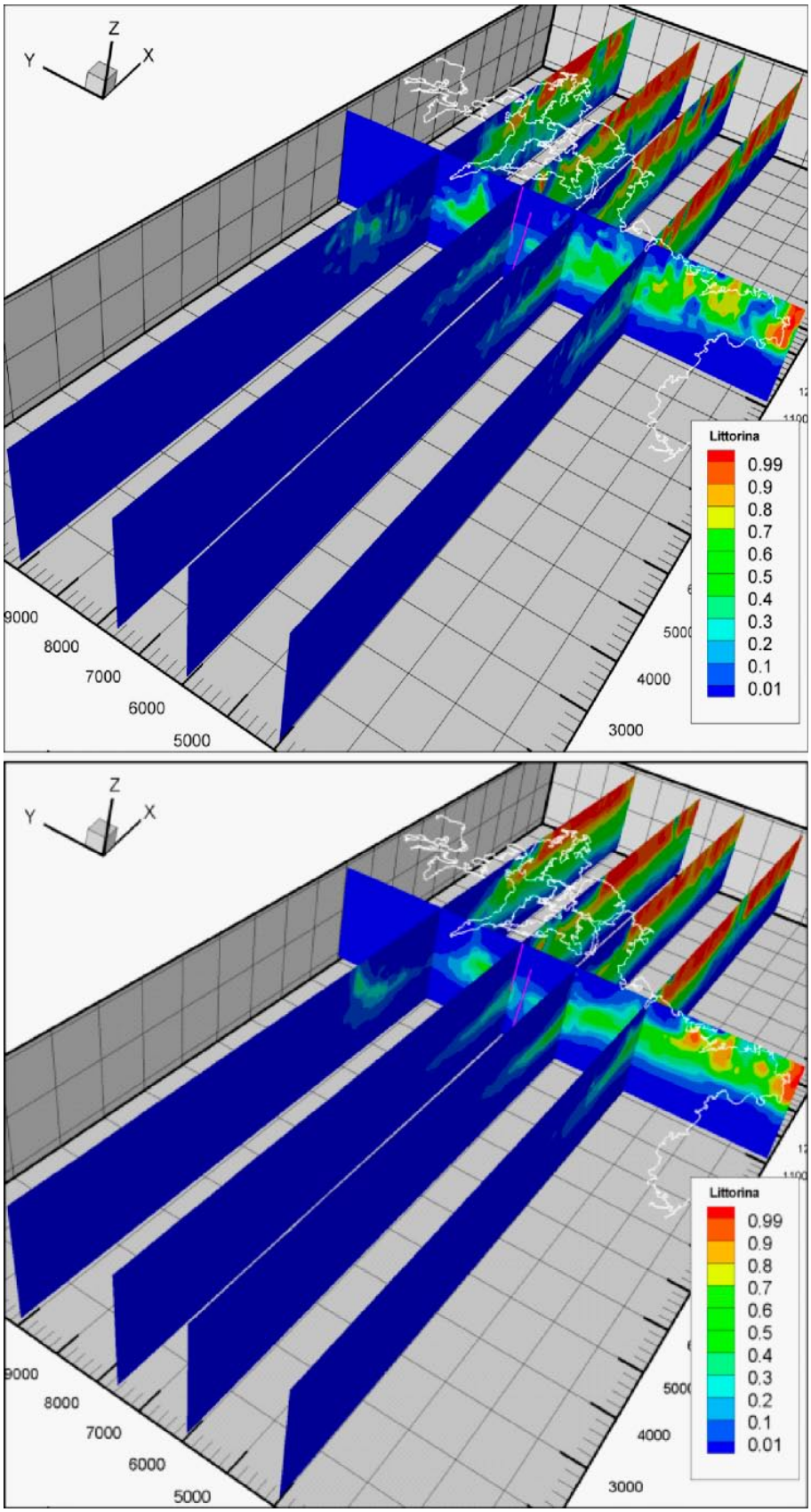

Figure 7-16. *Simulated Littorina water type concentrations. Top: Base Case (low DFN intensity). Bottom: High DFN intensity.*

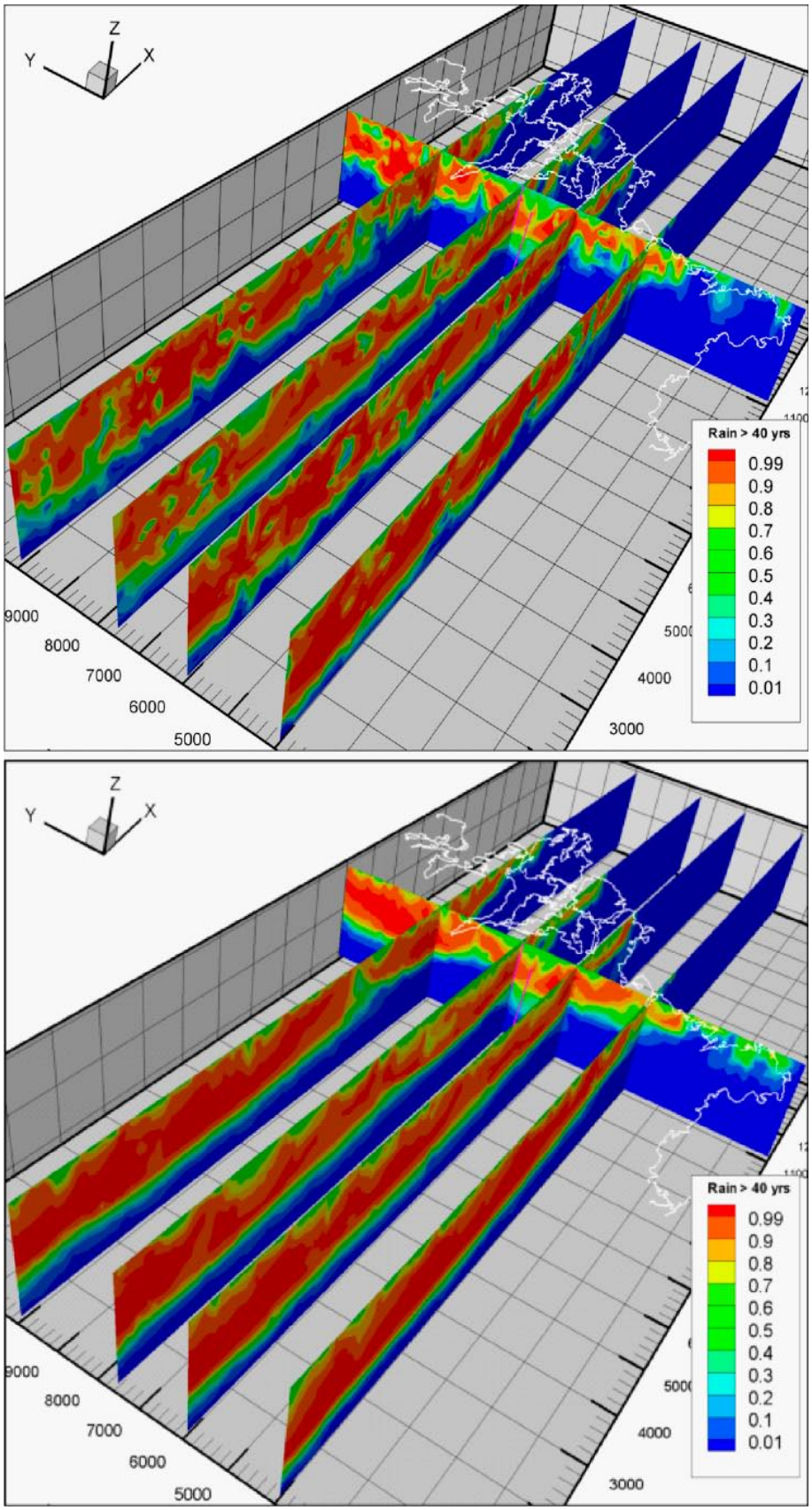

Figure 7-17. *Simulated Meteoric water type concentrations. Top: Base Case (low DFN intensity). Bottom: High DFN intensity.*

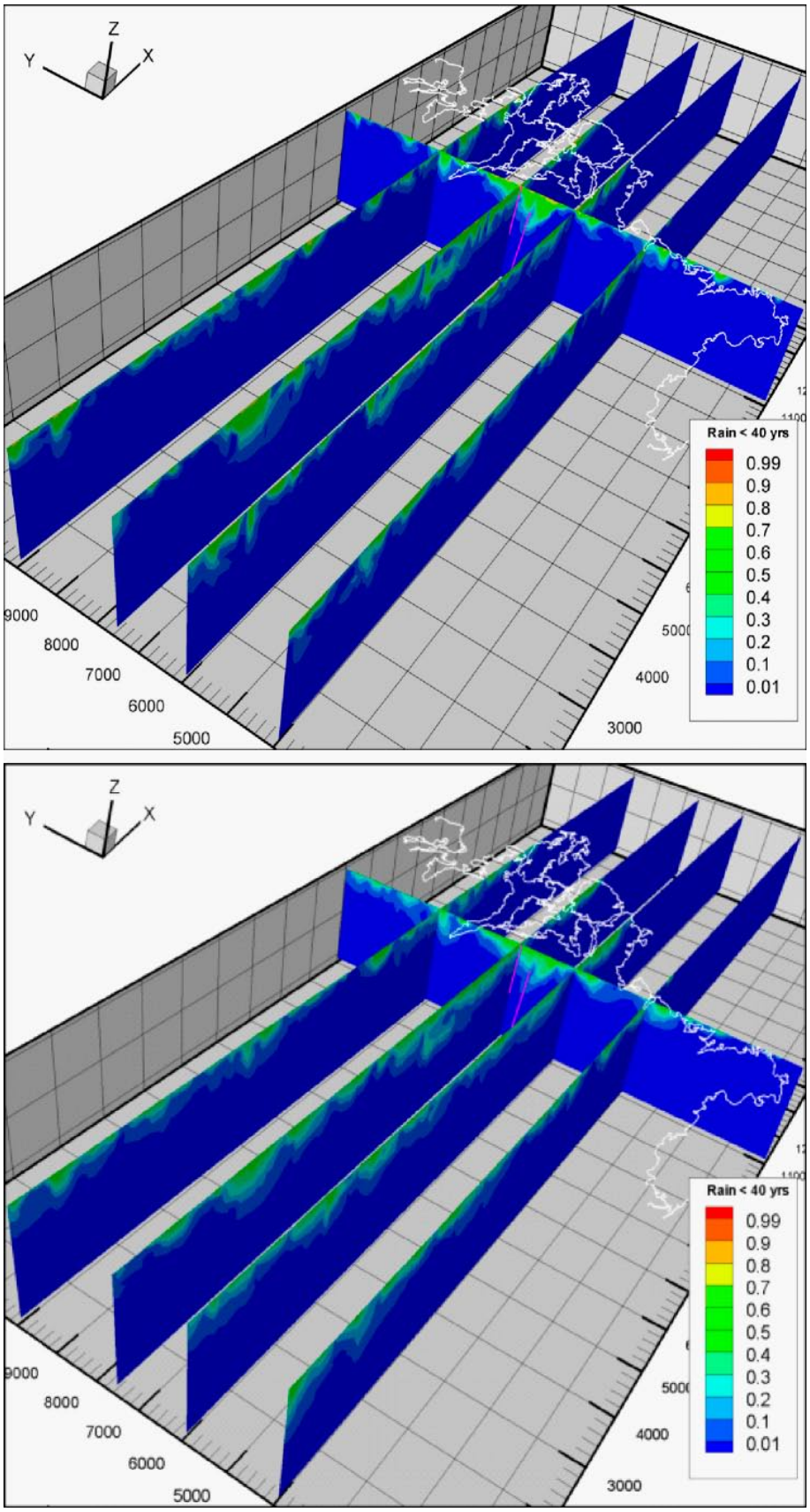

Figure 7-18. *Simulated Rain 1960 water type concentrations. Top: Base Case (low DFN intensity). Bottom: High DFN intensity.*

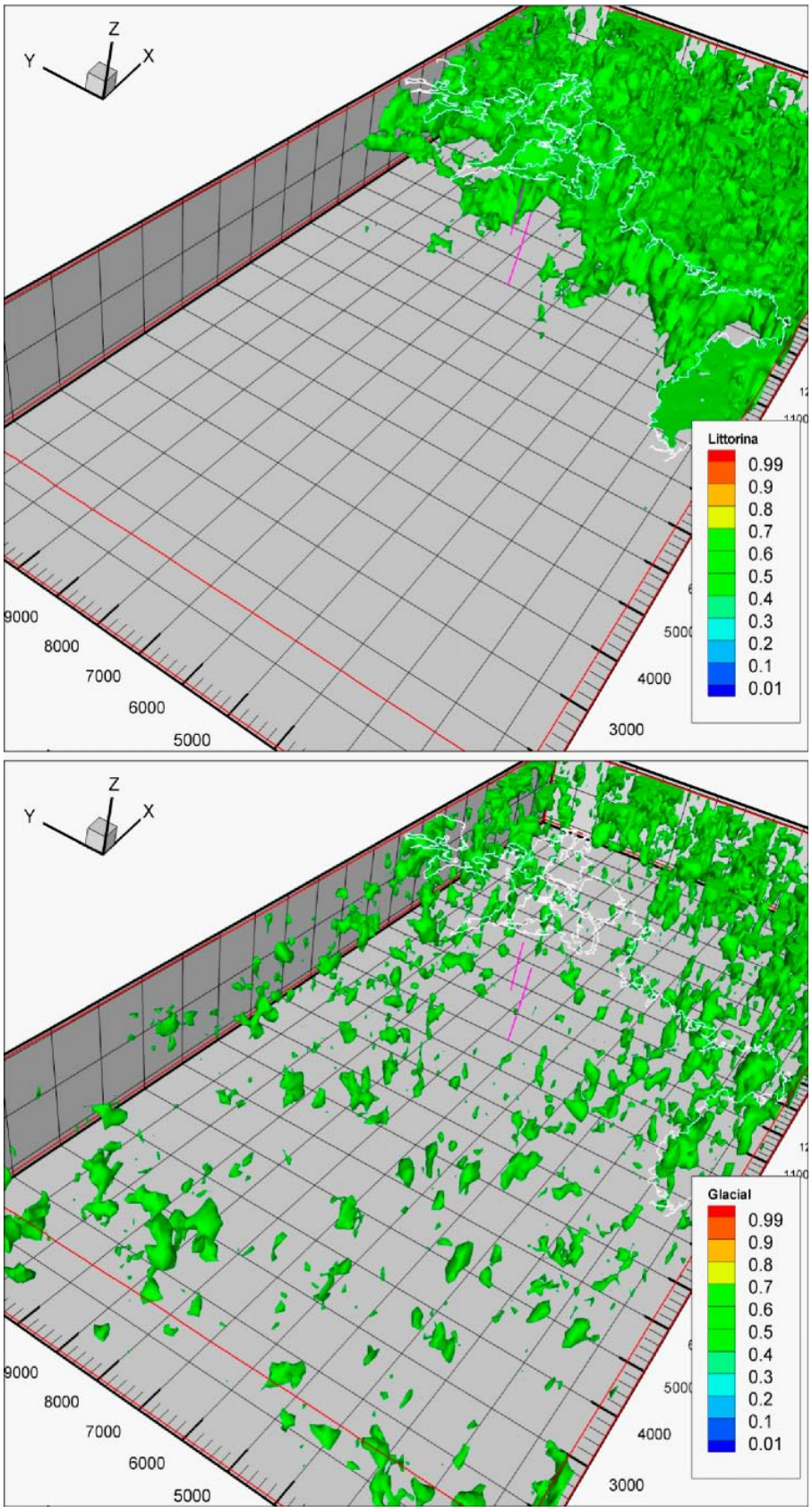

Figure 7-19. *Base Case distribution of volumes with Littorina and Glacial water types, where the residual relative concentrations are greater than 50%, respectively.*

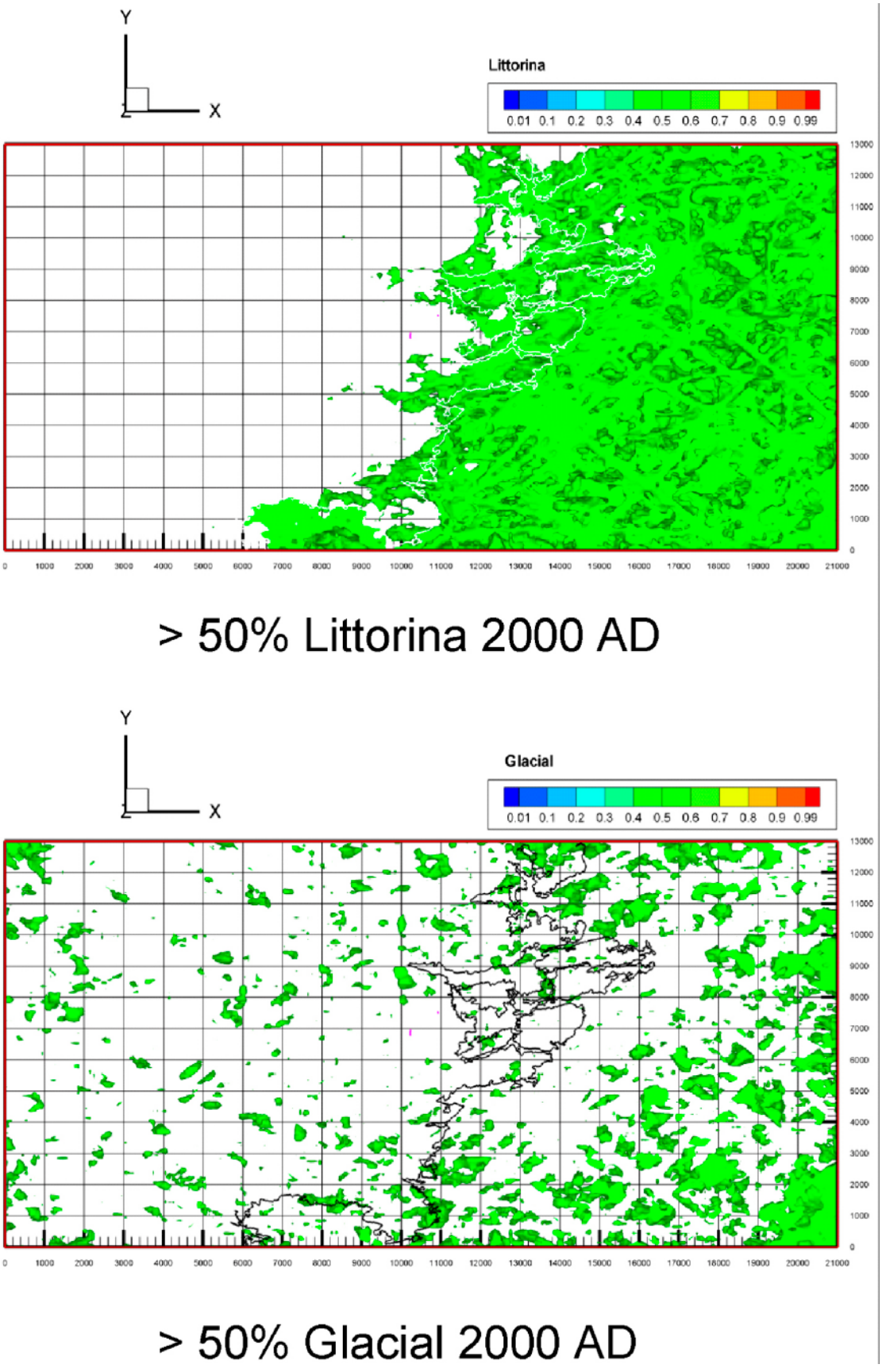

Figure 7-20. *Base Case distribution of volumes with Littorina and Glacial water types, where the residual relative concentrations are greater than 50%, respectively.*

7.5.3 Sensitivity Case B – Size of model domain

/Follin et al. 2004/ concluded in the 1.1 modelling stage that the local topography, the variable fluid density and the regional deformation zones are all important for the flow and discharge pattern in the Simpevarp regional model domain, see Figure 7.2. The results are in accordance with simulation results reported by /Follin and Svensson 2003/, who treated a huge, but hydrogeologically very simplistic, flow domain. Figure 7-21 shows the positions and sizes of the two model domains, respectively.

The position of the western, artificial, no flow boundary in the 1.1 modelling stage was discussed by /Follin et al. 2004/. It was suggested that the position of this boundary is unimportant for the flow and discharge pattern of particles released within the Simpevarp and Laxemar subareas due the closeness to the Baltic Sea of the two subareas, cf Figure 7-3. The hypothesis was tested by means of numerical simulations, see Figure 7-22.

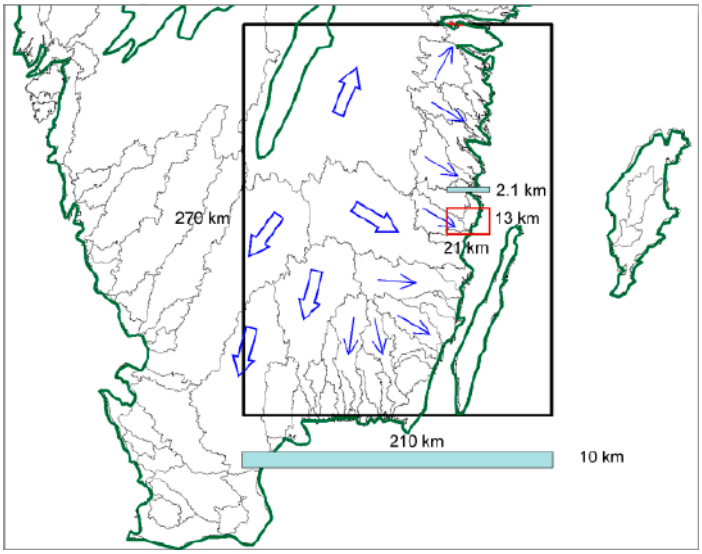

Figure 7-21. *Regional surface water divides and run off directions in south eastern Sweden. The black rectangle shows the position and size of the super regional model domain treated by /Follin and Svensson 2003/. The thickness of this model domain was 10,000 m. The red rectangle shows the position and size of the coastal Simpevarp regional model domain treated in 1.1 modelling stage by /Follin et al. 2004/. The thickness of the latter model domain was 2,100 m.*

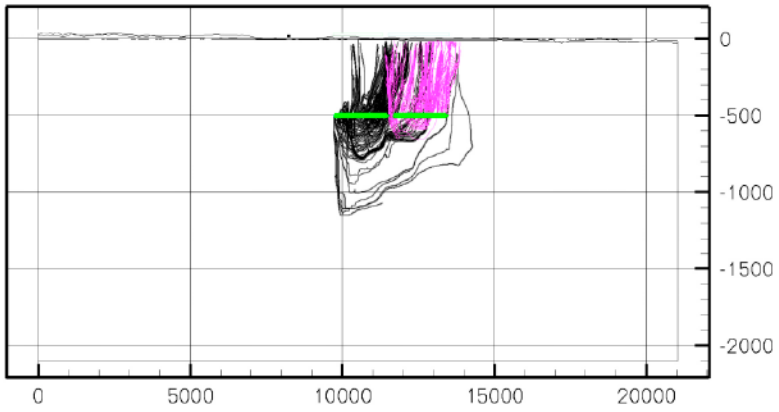

Figure 7-22. *W–E profile in the centre of the 1.1 regional model domain showing flow and discharge pattern of particles released at 500 m depth within the Laxemar (black traces) and Simpevarp (pink traces) subareas /Follin et al. 2004/.*

Figure 7-23 shows the topography, the position of the local model domain and the deformation zone trace lines within the Simpevarp 1.2 regional model domain, which stretches from Easting 1,539,000 to Easting 1,560,000. The model domain is identical to that used in the 1.1 modelling stage. Figure 7-23 also shows two proposals for a lateral extension of the Simpevarp regional model domain towards west. The red trace lines in this part of Figure 7-23 shows the deformation zone traces lines reported /Antal et al.1998/. Figure 7-24 shows the topography in Figure 7-23 for a profile positioned at Northing 6,366,600. The linear topographic gradient seen in the Simpevarp regional model domain ceases west of Easting 1,534,000.

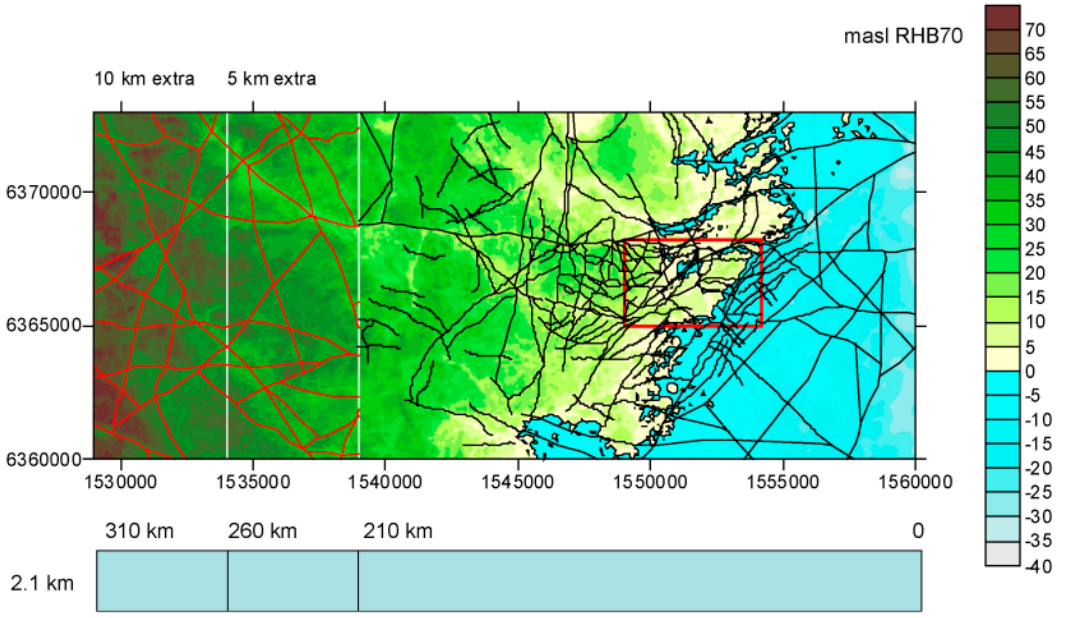

Figure 7-23. *The Simpevarp 1.2 regional model domain stretches from Easting 1,539,000 to Easting 1,560,000, i.e. the same model domain as in the 1.1 modelling stage. Two proposals for a lateral extension of the model domain towards west are indicated. The red trace lines in this part of the picture shows the deformation zone traces lines reported by /Antal et al. 1998/.*

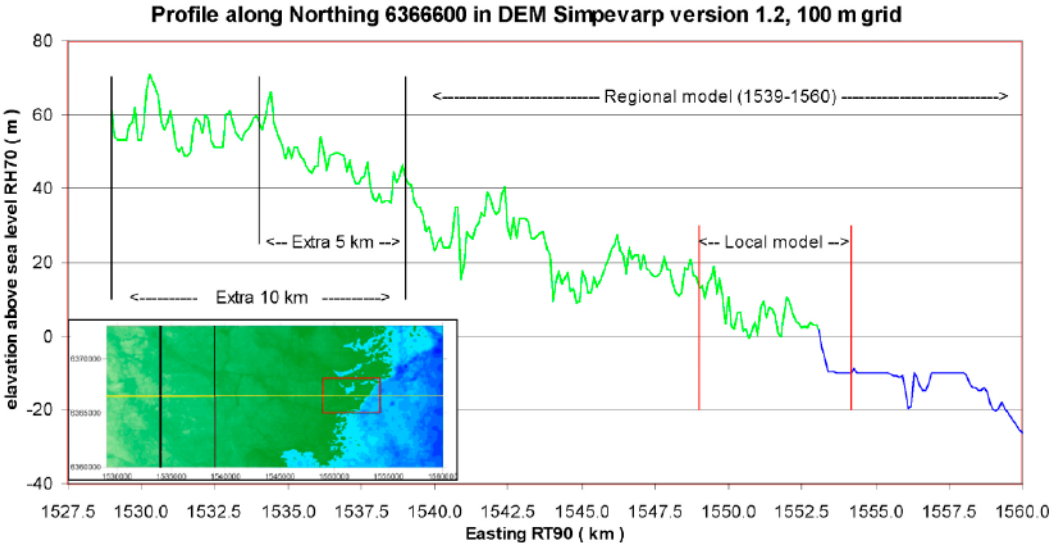

Figure 7-24. *Topography along a profile at Northing 6,366,600. The linear topographic gradient seen in 1.2 regional model domain ceases west of Easting 1,534,000.*

Figure 7-25 shows the model domain setup for Sensitivity Case B. Figure 7-26 shows the 5%, 50% and 95% percentiles of the advective travel time for particles released in the Simpevarp and Laxemar subareas, respectively. Three cases are run for each subarea:

- Easting 1,539,000–Easting 1,560,000, low intensity DFN (Base Case).
- Easting 1,539,000–Easting 1,560,000, high intensity DFN (Sensitivity Case A).
- Easting 1,534,000–Easting 1,560,000, low intensity DFN (Sensitivity Case B).

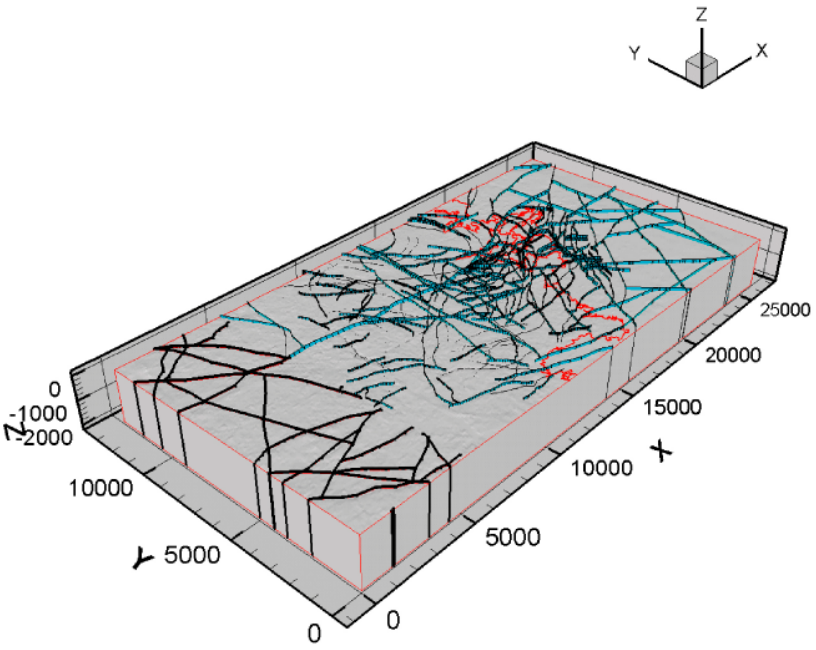

Figure 7-25. *Model domain setup for Sensitivity Case B. The western boundary is positioned at Easting 1,534,000. The deformation zone model incorporates the deformation zones reported by /Antal et al. 1998/.*

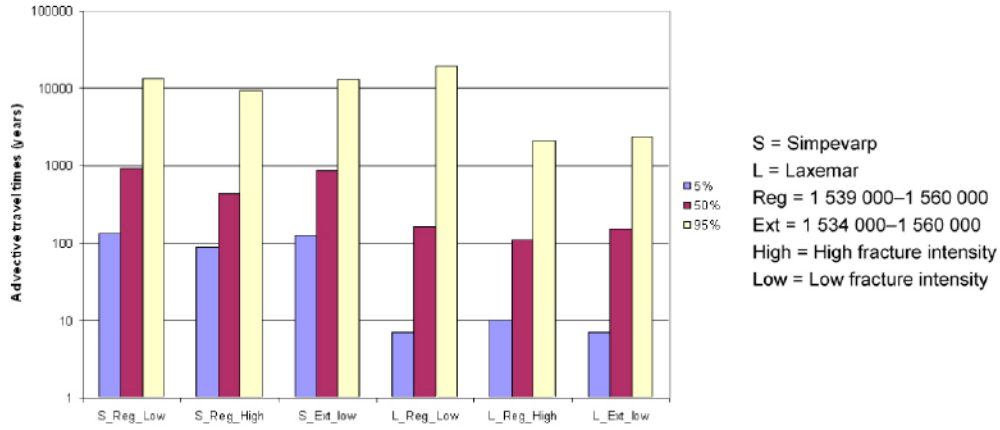

Figure 7-26. *Histogram showing the 5%, 50% and 95% percentiles for the advective arrival time for particles released in the Laxemar and Simpevarp subareas.*

Figure 7-26 suggests that the 5% and the 50% percentiles for the advective travel time are insensitive to the studied positions of the western, artificial, no flow boundary. The 95% percentile for Laxemar appears to be affected by boundary.

Figure 7-22 indicates that the particles released at 500 m depth in the Simpevarp and Laxemar subareas discharge quite nearby. Figure 7-27 shows the simulated discharge positions for the Base Case together with the simulated discharge positions for a reduced defined by the red rectangle. The thickness of the model domain is 2,100 m in both cases. Table 7-3 presents the particle tracking statistics. The reason why the median is larger for the smaller model domain is that the particles goes deeper due to the nearby lateral no flow boundaries, which cut off the regional flow field.

Table 7-3 suggests that the effects of the reduced size of the regional model domain on the advective travel time are fairly marginal.

Table 7-3. Particle tracking statistics for the two model domain shown in Figure 7-27.

Subarea	Base Case 5% t_w	Reduced 5% t_w	Base Case 50% t_w	Reduced 50% t_w	Base Case 95% t_w	Reduced 95% t_w
Simpevarp	70	70	560	650	5,280	7,920
Laxemar	60	50	410	520	2,950	4,310

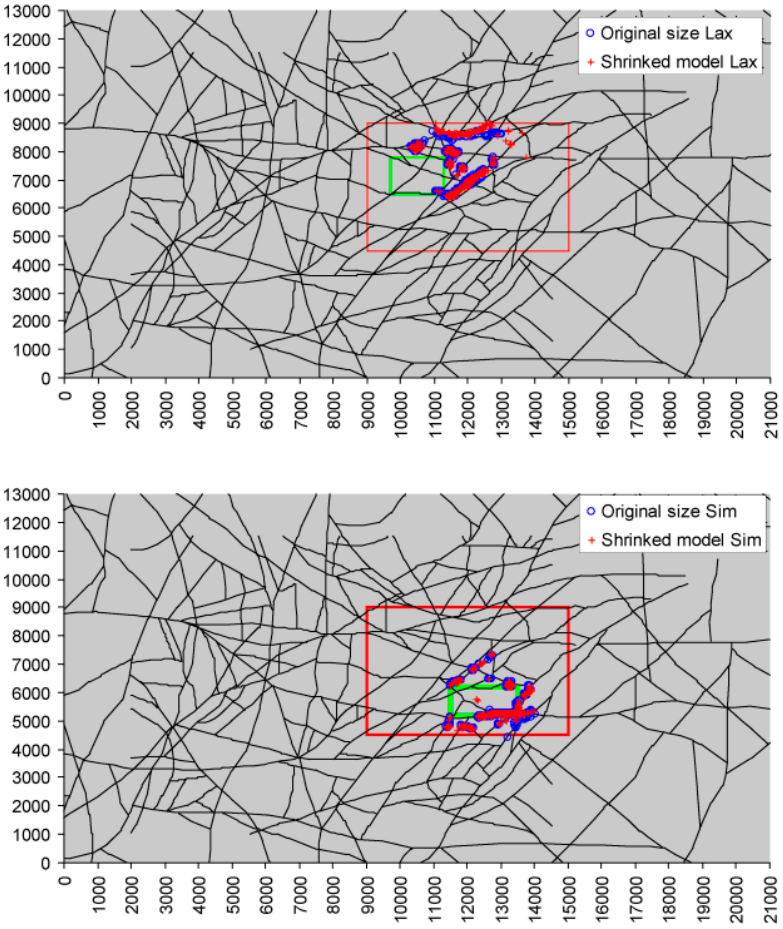

Figure 7-27. *Simulated discharge positions for the Base Case (blue dots) together with the simulated discharge positions for a reduced model domain (red dots) defined by the red rectangle. The thickness of the model domain is 2,100 m in both cases.*

7.5.4 Sensitivity Case C – Depth dependence

In Sensitivity Case C the hydraulic conductivity of the computational grid reduces from the surface by an order of magnate per kilometre, which means that the hydraulic conductivity values at the bottom of the 2,100 m thick model domain are c 100 times less than at surface. Figure 7-28 and Figure 7-29 shows that this condition preserves the initial conditions and makes a better match between simulated and calculated M3 mixing proportions.

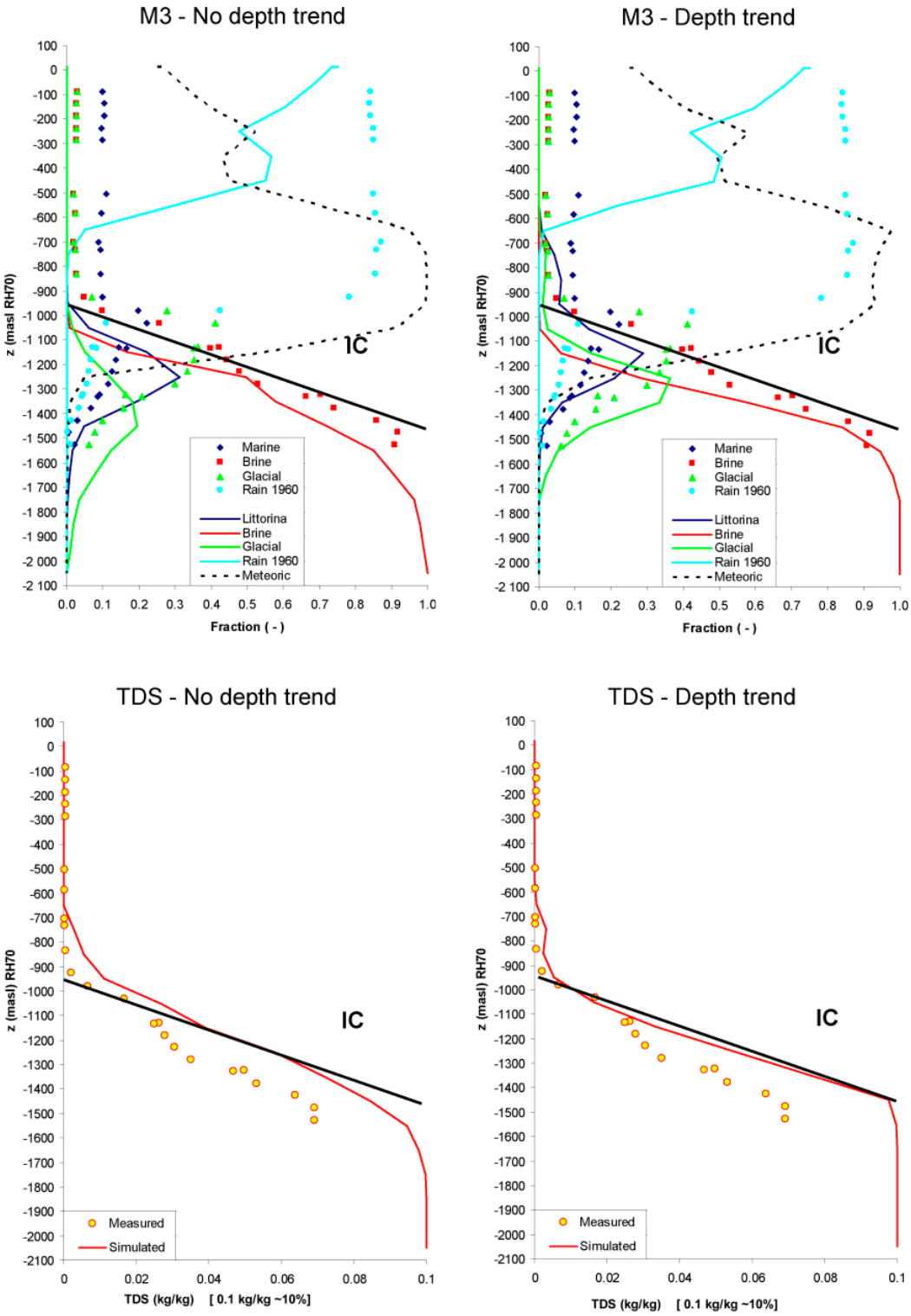

Figure 7-28. *Comparison between the Base Case (left) and Sensitivity Case C (right).*

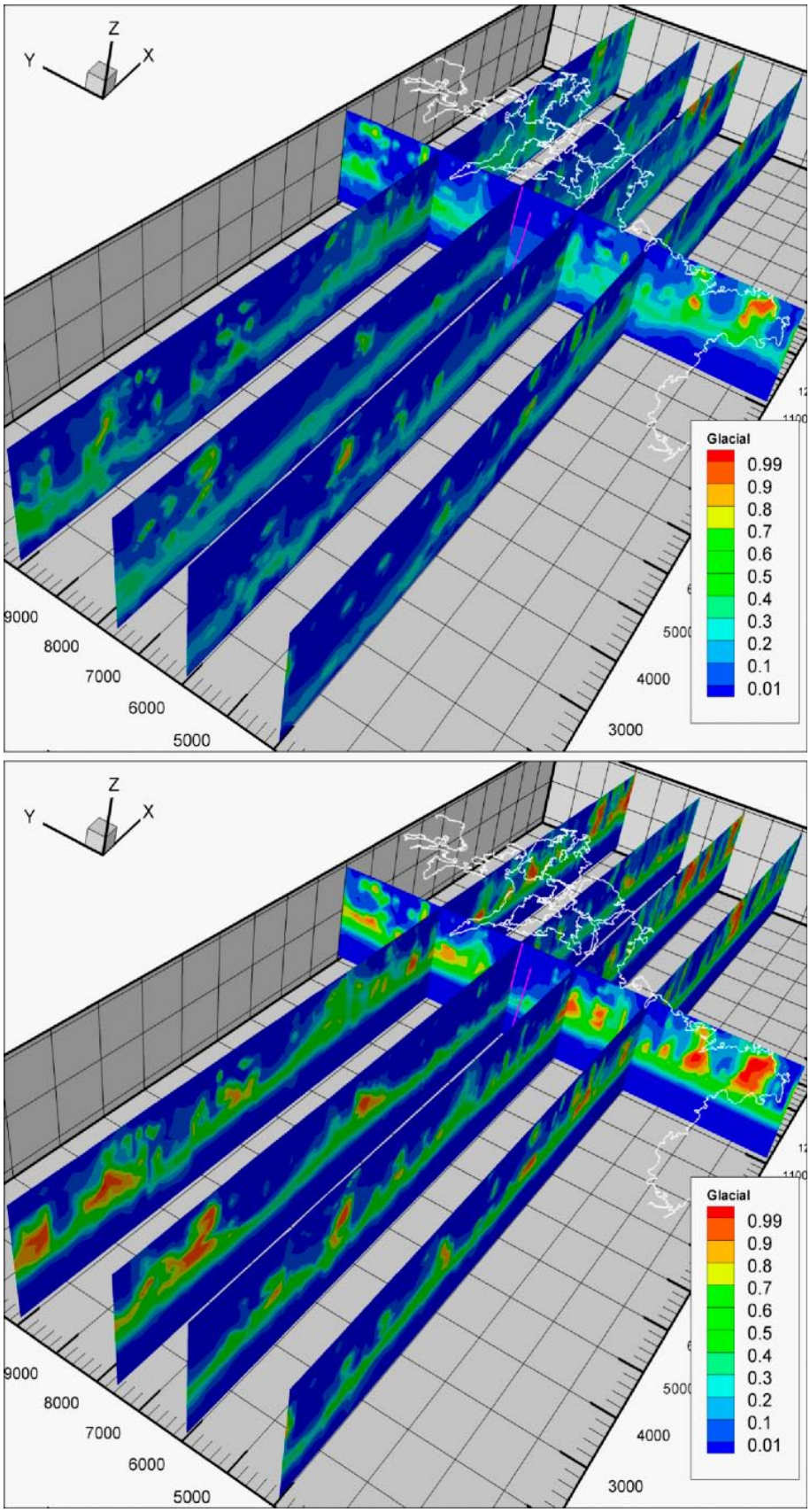

Figure 7-29. *Simulated Glacial water type concentrations. Top: Base Case (no depth trend. Bottom: Sensitivity Case D (depth trend).*

Sensitivity Case C suggests that the sensitivity to a depth trend has important implications for the postulated initial conditions, i.e. the depth to the fresh water – salt water interface at the start of the simulations. Probably, the depth to this interface varied in space at 10,000 BC as opposed to the simplified homogeneous initial condition shown in Figure 7-6.

7.5.5 Sensitivity Case D – Littorina Sea

The exact start and magnitude of the Littorina Sea period is a subject for discussion, see e.g. /Westman et al. 1999/. Sensitivity Case D examines if there any visible effects if the assumed start of the Littorina Sea period is delayed by 750 years, see Figure 7-30. The simulations results show that this order of a delay has no effect on the present-day water type concentrations along the KLX02 borehole, which implies that the subsequent Meteoric flushing is a strong process and governs the hydrogeochemical evolution in the Simpevarp and Laxemar subareas.

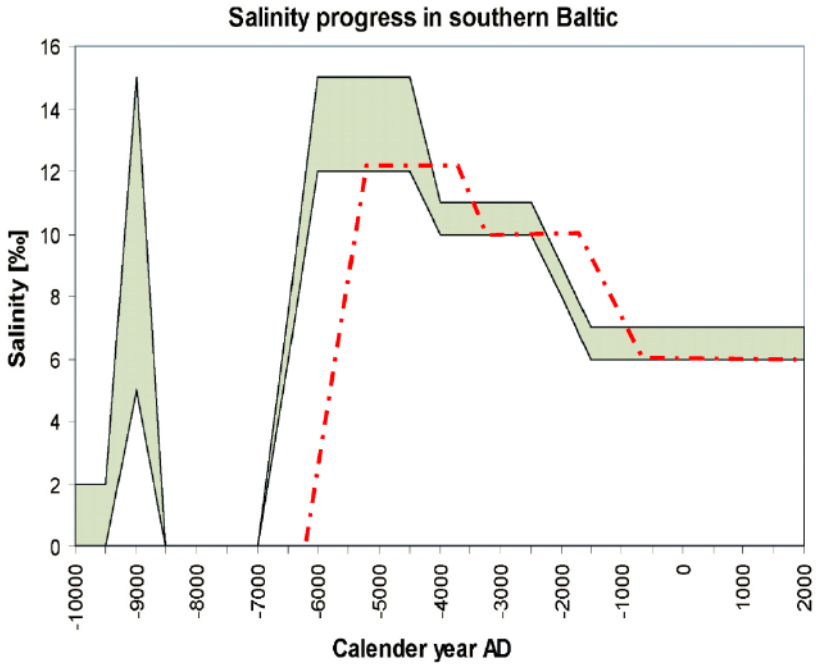

Figure 7-30. *Replicate of Figure 7-6, which shows the Base Case top boundary sea water salinity during Holocene. In Sensitivity Case D, the start of the Littorina Sea period is delayed by 750 years.*

7.5.6 Sensitivity Case E – Immobile volume

One of the key parameters in the multi rate diffusion model is the capacity ratio, β_G, which expresses roughly the volumetric ratio between the immobile (≈ total) and mobile (≈ kinematic) pore volumes, cf Chapter 2. The value of β_G in the Base Case is 2 and in Sensitivity Case E we test two different values, 0.1 and 10.

The simulation results for the different water types are shown in Figure 7-31. The effects on the water types are quite complex. In contrast, the simulation results for the salinity are fairly stable regardless the value of the capacity ratio. For $\beta_G = 0.1$ the penetration of Littorina Sea water is greater than for $\beta_G = 2$ and the Glacial water type is pushed downwards and the Brine water type upwards. Also the Meteoric water goes a bit deeper than in the Base Case. For $\beta_G = 10$ the simulated present-day concentrations of the Glacial water and Littorina Sea water are fairly low and the apparent flushing by Meteroric water is deeper than in the Base Case. Presumable the best results are obtained for $\beta_G = 1$.

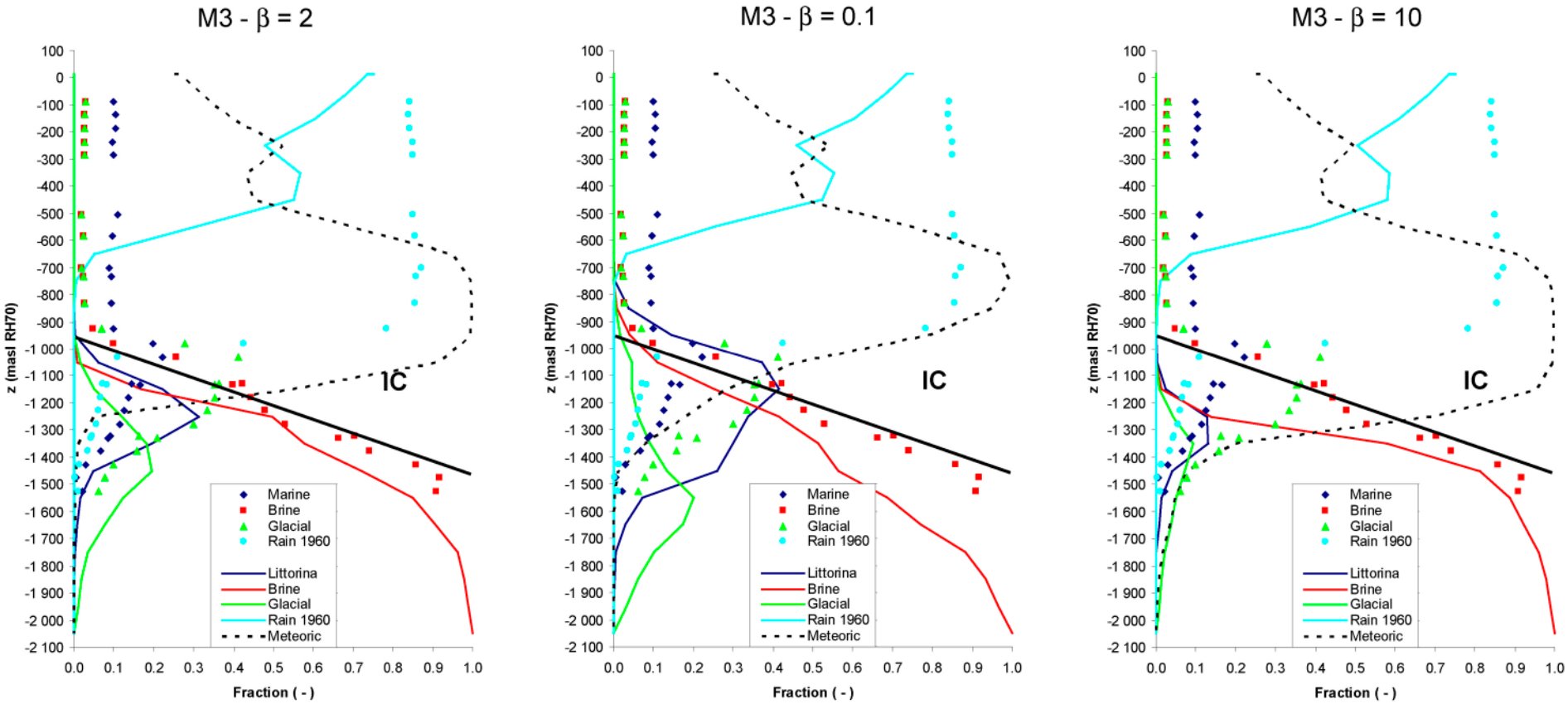

Figure 7-31. *Simulation results for the different water types for three different values of the capacity ratio, β_G. The Base Case results are shown in the left most profile. The simulation results for the salinity (not shown) are fairly stable regardless the value of the capacity ratio. In contrast, the effects on the water types are quite complex. For β_G = 0.1 the penetration of Littorina Sea water is greater than for β_G = 2 and the Glacial water type is pushed downwards and the Brine water type upwards. Also the Meteoric water goes a bit deeper than in the Base Case. Forβ_G = 10 the simulated present-day concentrations of the Glacial water and Littorina Sea water are fairly low and also the Brine water type is more flushed out than in the Base Case. Presumable the best results are obtained for β_G = 1.*

7.5.7 Summary of findings for the Sensitivity Cases A–E

Sensitivity Case A shows that the magnitude of the DFN intensity is crucial for the simulation results, which reinforces the importance of the discussion presented in Section 7.2.4.

Sensitivity Case B shows that the size of the model domain is not a major issue because of the proximity of the Simpevarp and Laxemar subareas to the Baltic Sea.

Sensitivity Case C shows that a depth trend in the hydraulic properties have a fairly large impact on the simulations results. In fact, the match against measured salinities and calculated M3 mixing proportions improve. We note that a decreasing trend is supported by the hydrogeological DFN analysis carried out in Chapter 5.

Sensitivity Case D shows that a delay of the start of the Littorina Sea period by 750 years does not affect the findings for the Base Case.

Sensitivity Case E shows that the magnitude of the capacity ratio alters the grid cell fluxes at depth, which in turn affect the penetration depths of the Littorina Sea water type and the subsequent flushing of the Meteoric water type. The sensitivities observed are complex, however, and demonstrate that the multi rate diffusion model must be subjected to more modelling experiments as a means to better understand how its parameters shall be handled in the site descriptive modelling. The values used in the work reported here, see Table 7-1, are based on the results reported by /Svensson and Follin 2005, Svensson 2004b/.

8 Discussion and conclusions

The 1.1 hydrogeological modelling conducted in the Simpevarp regional model area was fairly uncertain since there was no geological DFN model and no hydraulic test data to take into account, cf /SKB 2004/. Many of the parameter values chosen were based on data from Äspö HRL, TRUE Block Scale and/or the 1.1 site investigations in Forsmark. The main objectives of this study are:

- to develop a hydrogeological DFN model based on the 1.2 geological DFN modelling conducted by /La Pointe and Hermanson 2005/ and the high resolution fracture flow data acquired with the Posiva Flow Log measurements /Rouhiainen and Pöllänen 2003ab/ in deep, core drilled boreholes, and
- to conduct variable density flow simulations on a regional scale with DarcyTools based on an equivalent porous media representation of the hydrogeological DFN model.

Another objective of this study is to assess the assumptions in the geological DFN modelling. The methodology used by /La Pointe and Hermanson 2005/ is based on experiences gained from modelling projects conducted at Äspö HRL primarily, the conditions of which may not be fully compatible with those studied in the Simpevarp and Forsmark areas. An improved understanding of the uncertainties involved is necessary in order to gain credibility for the Site Description in general and the hydrogeological description in particular. The latter will serve as a basis for describing the present-day hydrogeological conditions as well as predictions of future hydrogeological conditions.

As a means to address the third objective we compare the results reported from the geological DFN modelling conducted by /La Pointe and Hermanson 2005/ with those reported from the alternative geological DFN modelling conducted by /Darcel et al. 2004/.

8.1 Analysis of structural and hydraulic data

The body of the geological DFN modelling reported for the 1.2 modelling stage focuses on investigating the scaling properties of steeply dipping fractures in four cleared outcrops in three different rock domains (denoted by A, B and C in the report). Structural and hydraulic data are available for modelling from four deep, core drilled boreholes KSH01A, KSH02, KSH03 and KAV01. The three KSH-holes are all located in the Simpevarp peninsula, which have been assigned a tentative repository layout for the sake of the 1.2 modelling stage.

The work reported here uses a new methodology developed by the DarcyTools modelling team. A cornerstone in this methodology is the high resolution difference fracture flow method (PFL-f; 5 m/0.1 m). The KSH01A and KSH02 boreholes, which penetrate the B and C rock domains, are the only boreholes that are investigated with this method in the Simpevarp peninsula.

8.2 From DFN to block scale properties

The analysis of borehole data and the process by which the DFN properties are transformed to grid cell (block scale) hydraulic properties, e.g. a hydraulic conductivity tensor, is called upscaling. The block scale properties are computed for two purposes:

- to analyse the magnitude of the hydraulic conductivity on a 20 m and a 100 m scale, in particular with regard to hydraulic anisotropy in different rock domains, and
- to model variable density flow on a regional scale (hundreds of square kilometres). Particle tracking from two release areas, Simpevarp and Laxemar, are used to test the sensitivity to different hydrogeological uncertainties and the need for far-field realism.

The first purpose is requested by Repository Engineering, whereas the second purpose addresses issues of importance to Safety Assessment. The upscaling results reported here indicate a fairly homogeneous and isotropic hydraulic conductivity tensor on both scales of interest (20 m and 100 m). The main reasons for this result are the high frequency of Open fractures in all orientations and the flow anomalies reported for the rock mass outside the interpreted deformation zones in the analysed boreholes.

8.3 Regional variable density flow simulations

Many of the assumptions made in the 1.1 modelling stage were made without data support from the site investigations. The work reported here demonstrates that there is considerable overlap between the 1.1 and 1.2 modelling stages in terms of input parameter values. That is, the 1.1 modelling stages have been vindicated by data gathered during the1.2 stage. Hence, the regional variable density flow modelling presented here become on a whole a refinement of the sensitivity study carried out in the 1.1 stage. This inevitable limits the novelty of the work reported here since the overall tasks for the two modelling stages are the same.

Five sensitivity cases are treated in the work reported here:

A. Higher fracture intensity.

B. Larger and smaller size of the model domain.

C. Depth dependence in the transmissivity field.

D. Later start of the Littorina Sea period.

E. Different values of the capacity ratio.

Cases A–D are known to be important for the advective flow, whereas case E controls the effectiveness of rock matrix diffusion as implemented in DarcyTools.

8.3.1 Sensitivity Case A – Fracture intensity

Sensitivity Case A shows that the inferred magnitude of the hydrogeological DFN intensity is crucial for the simulation results. An upscaling of borehole intensity data creates grid cell hydraulic properties on a 100 m scale that resemble a fairly conductive porous medium.

An alternative approach, intensity downscaling, is suggested in the work reported here. The intensity downscaling approach honours the number of large deformation zones. Intensity downscaling renders in this study a DFN intensity on a 100 m scale that is 1/3 of the intensity inferred from the intensity upscaling approach. The effects of this difference are considerable for the simulation of variable density flow.

Figure 8-1 illustrates the concept of intensity upscaling and downscaling, respectively. The top row images in Figure 8-2 illustrate the difference in DFN intensity on a 100 m scale using intensity upscaling and downscaling, respectively. The bottom row images demonstrate the hydrogeological/hydrogeochemical effects. The profiles show the simulated remaining concentrations of initial groundwater of glacial origin for the two approaches of intensity scaling.

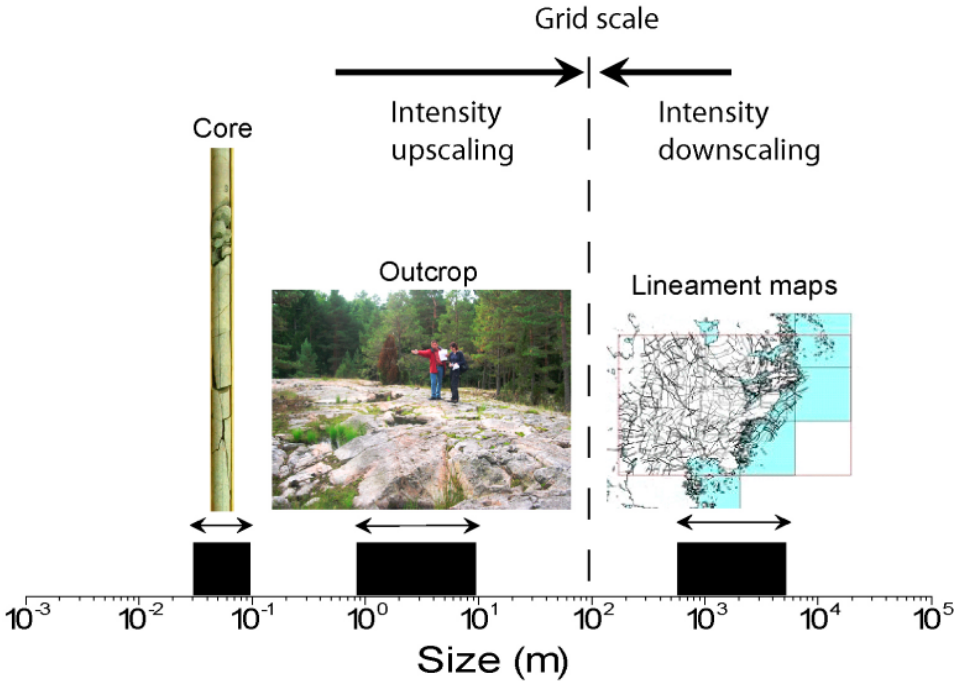

Figure 8-1. *Numerical simulations of groundwater flow in fractured rock are often made with a continuum formulation. The choice of grid scale (resolution) is an important decision as it affects the representation of fracture flow heterogeneity and anisotropy. Usually the size of the smallest fractures in the stochastic fracture network realisations underpinning the computation of grid cell hydraulic properties are on the same order as the chosen grid resolution. The intensity of conductive fractures of different sizes is a vital characteristic of the stochastic network realisations. Simulations based on intensity upscaling (left) and intensity downscaling (right) may lead to quite different results, see Figure 8-2.*

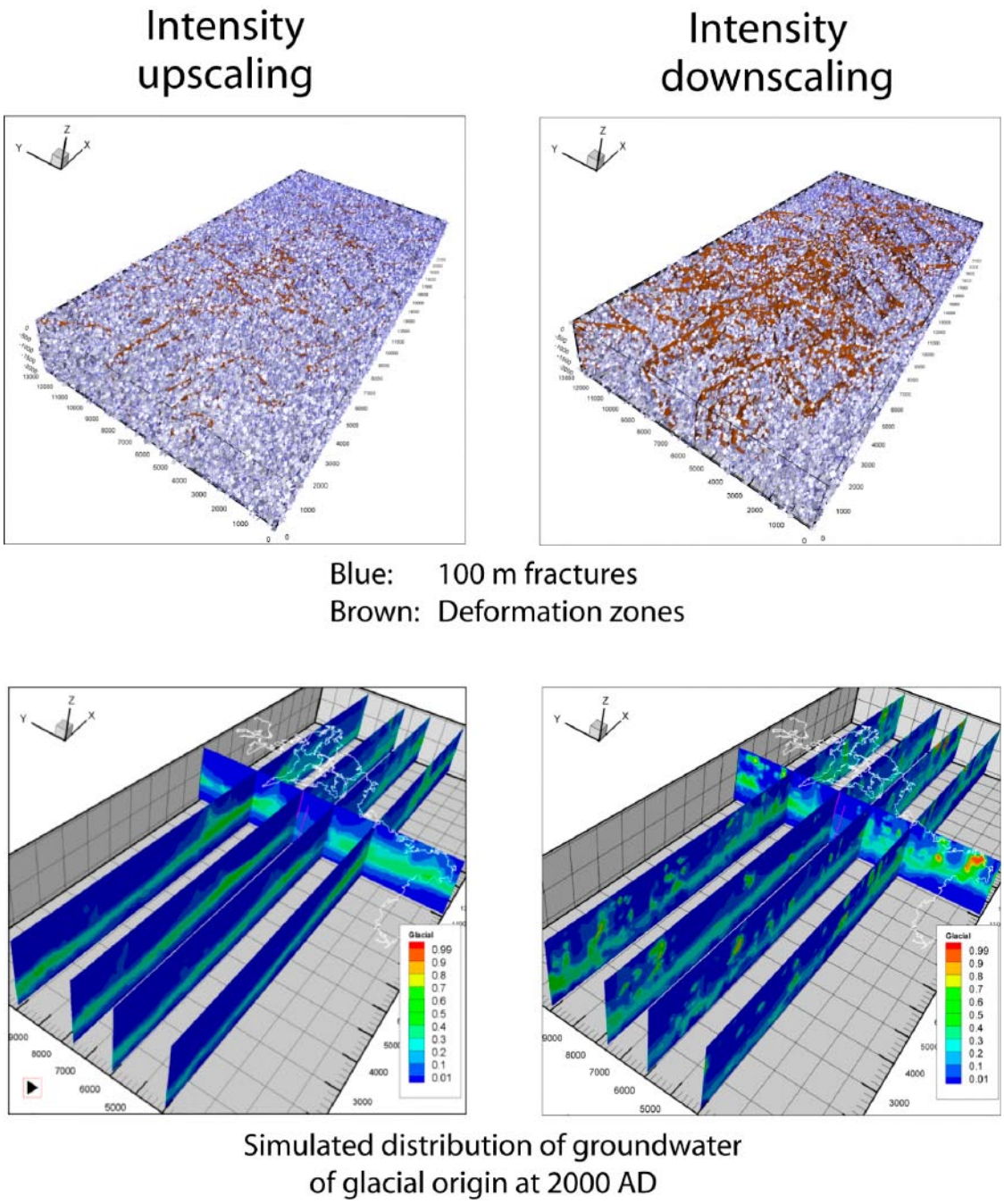

Figure 8-2. *Upscaling of borehole intensity data creates grid cell hydraulic properties on a 100 m scale that resemble a fairly conductive porous medium. An alternative approach, intensity down-scaling, is suggested in the work reported here. Intensity downscaling honours the number of large deformation zones. Intensity downscaling renders in this study a DFN intensity on a 100 m grid scale that is c 1/3 of the intensity inferred from the intensity upscaling approach. The effects of this difference are considerable for the simulation of variable density flow. The top row images illustrate the difference in DFN intensity on a 100 m scale using intensity upscaling and down-scaling, respectively. The bottom row images demonstrate the hydrogeological/hydrogeochemical effects. The profiles show the simulated remaining concentrations of initial groundwater of glacial origin for the two scaling approaches.*

8.3.2 Sensitivity Case B – Size of the model domain

Sensitivity Case B shows that the size of the model domain is not a major issue for the Simpevarp subarea because of its proximity to the Baltic Sea. For the Laxemar subarea more data from this part of the model domain are required. The work presented here assumes that the conditions in Laxemar are the same as in the Simpevarp subarea.

8.3.3 Sensitivity Case C – Depth dependence

Sensitivity Case C shows that a depth trend in the hydraulic properties have a fairly large impact on the simulations results. In fact, the match against measured salinities and calculated M3 mixing proportions improve. We note that a decreasing trend is supported by the hydrogeological DFN analysis carried out in Chapter 5.

8.3.4 Sensitivity Case D – Littorina Sea

Sensitivity Case D suggests that a delay of the start of the Littorina Sea period by 750 years does not alter the simulated present-day concentrations along the KLX02 borehole. The interpretation of this result is not straightforward, however, because the elevation of the Laxemar area may already be above or very close to the highest elevation of the Littorina Sea at the time of interest for the Littorina Sea intrusion.

8.3.5 Sensitivity Case E – Immobile volume

The capacity ratio is a key parameter of the multi-rate diffusion model, which is the diffusion model implemented in DarcyTools. A series of capacity boxes with different mass transfer coefficients are used in the multi-rate model to model the diffusive exchange of matter between the mobile and immobile pore volumes. The classic diffusion model assumes a single-rate.

The capacity ratio is the ratio between immobile and mobile pore volumes. The pore volume in the rock matrix accessible for diffusion is expected to be 10–100 times greater than the pore volume in the water-conducting fractures. The current working hypothesis used in DarcyTools is that the capacity ratio ought to be of the same order of magnitude.

Sensitivity Case E shows that the magnitude of the capacity ratio alters the grid cell fluxes at depth, which in turn affect the penetration depths of the Littorina Sea water type and the subsequent flushing of the Meteoric water type. The sensitivities observed are complex, however, and demonstrate that the multi rate diffusion model must be subjected to more modelling experiments as a means to better understand how its parameters shall be handled in the site descriptive modelling. The values used in the work reported here are based on the results reported by /Svensson and Follin 2005/.

9 References

Andersson J, Elert M, Gylling B, Moreno L, Selroos J-O, 1998a. Derivation and treatment of the flow wetted surface and other geosphere parameters in the transport models FARF31 and COMP23 for use in safety assessment. SKB R-98-60. Svensk Kärnbränslehantering AB.

Andersson P, Ludvigson J-E, Wass E, 1998b. Äspö Hard Rock Laboratory, True Block Scale Project, Preliminary characterisation – Combined interference tests and tracer tests. SKB IPR-01-44. Svensk Kärnbränslehantering AB.

Andersson P, Ludvigsson J-E, Wass E, Holmqvist M, 2000. Äspö Hard Rock Laboratory. True Block Scale Project, Tracer test stage – Interference tests, dilution tests and tracer tests. SKB IPR-00-28. Svensk Kärnbränslehantering AB.

Andersson J, Berglund J, Follin S, Hakami E, Halvarson J, Hermanson J, Laaksoharju M, Rhén I, Wahlgren C-H, 2002. Testing the methodology for site descriptive modelling. Application for the Laxemar area. SKB TR-02-19. Svensk Kärnbränslehantering AB.

Antal I, Bergman T, Gierup J, Rudmark L, Thunholm B, Wahlgren C-H, Stephens M, Johansson R, 1998. Översiktsstudie av Kalmar län – Geologiska förutsättningar. SKB R-98-24. Svensk Kärnbränslehantering AB.

Borg G Ch, Paabo K, 1984. Area description and sediment investigation of the coastal area between karlskrona and Oskarshamn S.E. Sweden. *Striolae*. Uppsala University. 85 pp.

Curtis P, Elfström M, Stanfors R, 2003a. Oskarshamn site investigation. Compilation of structural geological data covering the Simpevarp peninsula, Ävrö and Hålö. SKB P-03-07. Svensk Kärnbränslehantering AB.

Curtis P, Elfström M, Stanfors R, 2003b. Oskarshamn site investigation. Visualization of structural geological data covering the Simpevarp peninsula, Ävrö and Hålö. SKB P-03-86. Svensk Kärnbränslehantering AB.

Darcel C, Davy P, Bour O, De Dreuzy J-R, 2004. Alternative DFN model based on initial site investigations at Simpevarp. SKB R-04-76. Svensk Kärnbränslehantering AB.

Dershowitz W, Winberg A, Hermanson J, Byegård J, Tullborg E-L, Andersson P, Mazurek M, 2003. Äspö Task Force on modelling of groundwater flow and transport of solutes, Task 6C, A semi-synthetic model of block scale conductive structures at the Äspö HRL. SKB IPR-03-13. Svensk Kärnbränslehantering AB.

Elhammer A, Sandqvist Å, 2005. Oskarshamn site investigation. Detailed marine geological survey of the sea bottom outside Simpevarp. SKB P-05-35. Svensk Kärnbränslehantering AB.

Follin S, Årebäck M, Axelsson C-L, Stigsson M, 1996. Förstudie Oskarshamn. Grundvattnets rörelse, kemi och långsiktiga förändringar. SKB R-98-55. Svensk Kärnbränslehantering AB.

Follin S, Svensson U, 2002. Se SKB R-02-29, Svensk Kärnbränslehantering AB.

Follin S, Svensson U, 2003. On the role of mesh discretisation and salinity for the occurrence of local flow cells. Results from a regional-scale groundwater flow model of Östra Götaland. SKB R-03-23 Svensk Kärnbränslehantering AB.

Follin S, Stigsson M, Berglund S, Svensson U, 2004. Variable-density groundwater flow simulations and particle tracking – Numerical modelling using DarcyTools. Preliminary site description Simpevarp area – version 1.1. SKB R-04-65. Svensk Kärnbränslehantering AB.

Forsman, Zetterlund, Forsmark, Rhen, 2005. Se SKB P-05-65, Svensk Kärnbränslehantering AB.

Haggerty R, Gorelick S M, 1995.
Multi-rate mass transfer for modelling diffusion and surface reactions in media with pore-scale heterogeneity. *Water Resources Research*, 31(10), 2383-2400.

Harlow F H, Welch J E, 1965. Numerical Calculation of Time-Dependent Viscous Incompressible Flow of Fluid with Free Surface, *Phys. Fluids*, vol. 8, p. 2182.

Hartley L, Hoch A, Hunter F, Jackson P, Marsic N, 2005. regional hydrogeological simulations – Numerical modelling using ConnectFlow. Preliminary site description. Simpevarp subarea – version 1.2. SKB TR-05-12. Svensk Kärnbränslehantering AB.

Horne R N, 1995. *Modern well test analysis*. 2nd edition. Petroway Inc.

Laaksoharju M, Skårman C, Skårman E, 1999. Multivariate Mixing and Mass-balance (M3) calculations, a new tool for decoding hydrogeochemical information. *Applied Geochemistry,* Vol. 14, #7, 1999, Elsevier Science Ltd. Pp 861-871.

Laaksoharju M, Smellie J, Gimeno M, Auque L, Gómez J, Tullborg E-L, Gurban I, 2004. Hydrogeochemical evaluation of the Simpevarp area, model version 1.1. SKB R-04-16. Svensk Kärnbränslehantering AB.

La Pointe P R, Hermanson J, 2005. Statistical model of fractures and deformation zones. Preliminary site description Simpevarp subarea – version 1.2. SKB R-05-28. Svensk Kärnbränslehantering AB.

Lindborg T (ed.), 2005. Description of the surface systems, Preliminary site description Simpevarp subarea – version 1.2. SKB R-05-01. Svensk Kärnbränslehantering AB.

Moye D G, 1967. Diamond drilling for foundation exploration. *Civ Eng Trans 7th Inst Eng Australia*, 95-100.

Munier R. 2004. Statistical analysis of fracture data, adapted for modelling Discrete Fracture Networks – Version 2. SKB R-04-66. Svensk Kärnbränslehantering AB.

Neretnieks I, 2004. Personal communication, September 2004.

Patankar S V, 1980. *Numerical heat transfer and fluid flow*. Hemisphere Publishing Corporation, McGraw-Hill Book Company.

Rouhiainen P, Pöllänen J, 2003a. Oskarshamn site investigation – Difference flow measurements in borehole KSH01A at Simpevarp. SKB P-03-70. Svensk Kärnbränslehantering AB.

Rouhiainen P, Pöllänen J, 2003b. Oskarshamn site investigation – Difference flow measurements in borehole KSH02 at Simpevarp. SKB P-03-110. Svensk Kärnbränslehantering AB.

Rhen I (ed.), Gustafson G, Stanfors R, Wikberg P, 1997. Äspö HRL - Geoscientific evaluation 1997/5. Models based on site characterization 1986–1995. SKB TR-97-06. Svensk Kärnbränslehantering AB.

Rhén I, Forsmark T, 2001. Äspö Hard Rock Laboratory. Prototype repository, Hydrogeology, Summary report of investigations before the operation phase. SKB IPR-01-65. Svensk Kärnbränslehantering AB.

Rhén I, Follin S, Hermanson, J, 2003. Hydrological Site Descriptive Model - a strategy for its development during Site Investigations. SKB R-03-08. Svensk Kärnbränslehantering AB.

Risberg J, 2002. Holocene sediment accumulation in the Äspö area. SKB R-02-47. Svensk Kärnbränslehantering AB.

Rudmark L, 2000. Beskrivning till jordartskartan 5G Oskarshamn NO. SGU Ae 94. 64 pp.

Rönning H J S, Kihle O, Mogaard J O, Walker P, 2003. Simpevarp site investigation – Helicopter borne geophysics at Simpevarp, Oskarshamn, Sweden. SKB P-03-25. Svensk Kärnbränslehantering AB.

SKB, 2002a. Simpevarp – site descriptive model version 0. SKB R-02-35. Svensk Kärnbränslehantering AB.

SKB, 2002b. Metodbeskrivning för BOREMAP-kartering. SKB MD 143.00. Svensk Kärnbränslehantering AB.

SKB, 2004. Preliminary site description Simpevarp area – version 1.1. SKB R-04-25. Svensk Kärnbränslehantering AB.

SKB, 2005. Preliminary site description Simpevarp subarea – version 1.2. SKB R-05-08. Svensk Kärnbränslehantering AB.

Svantesson S, 1999. Beskrivning till jordartskaratn 7G Västervik SO/7H Loftahammar SV. SGU Ae 124. 109 pp.

Svensson U, 2001a. A continuum representation of fracture networks. Part I: Method and basic test cases. Journal of Hydrology, Volume 250, 170-186.

Svensson U, 2001b. A continuum representation of fracture networks. Part II: Application to the Äspö Hard Rock Laboratory. Journal of Hydrology, Volume 250, 187-205.

Svensson U and Ferry M, 2004. DarcyTools, Version 2.1. User's guide. SKB R-04-20. Svensk Kärnbränslehantering AB.

Svensson U, Kuylenstierna H-O, Ferry M, 2004. DarcyTools, Version 2.1. Concepts, methods, equations and demo simulations. SKB R-04-19. Svensk Kärnbränslehantering AB.

Svensson U, 2004a. DarcyTools, Version 2.1. Verification and validation. SKB R-04-21. Svensk Kärnbränslehantering AB.

Svensson U, 2004b. Modelling flow, transport and retension in a 3D fracture network under a natural head gradient,Äspö Task Force, Task 6E, *in prep.*
Svensk Kärnbränslehantering AB.

Svensson U, Follin S, 2005. Äspö Hard Rock Laboratory, Äspö Task Force – Task 6A, 6B and B2. Simulation of tracer transport considering both experimental and natural time scales. SKB IPR-04-42.Svensk Kärnbränslehantering AB.

Terzaghi R D, 1965. Sources of error in joint surveys, *Geotechnique*, V.15, 287-304.

Thiem G, 1906. *Hydrologische Methoden.* J M Gebhardt, Leipzig.

Triumf C-A, Thunehed H, Kero L, Persson L, 2003. Oskarshamn site investigation. Interpretation of airborne geophysical survey data. Helicopter borne survey data of gamma ray spectrometry, magnetics and EM from 2002 and fixed wing airborne survey data of the VLF-field from 1986. SKB P-03-100. Svensk Kärnbränslehantering AB.

Triumf C-A, 2004. Oskarshamn site investigation. Joint interpretation of lineaments. SKB P-04-49. Svensk Kärnbränslehantering AB.

Westman P, Wastegård S, Schoning K, Gustafsson B, Omstedt A, 1999. Salinity change in the Baltic Sea during the last 8500 years: evidence, causes and models. SKB TR-99-38. Svensk Kärnbränslehantering AB.

Wiklund S, 2002. Digitala ortofoton och höjdmodeller. Redovisning av metodik för platsundersökningsområdena Oskarshamn och Forsmark samt förstudieområdet Tierp Norra. SKB P-02.02. Svensk Kärnbränslehantering AB.

Winberg A, Andersson P, Byegård J, Poteri A, Cvetkovic V, Dershowitz W, Doe T, Hermanson J, Gómez-Hernández J J, Hautojärvi A, Billaux D, Tullborg E-L, Holton D, Meier P, Medina A, 2002. Final report of the TRUE Block Scale project. 4. Synthesis of flow, transport and retention in the block scale, SKB TR-02-16.
Svensk Kärnbränslehantering AB.

Appendix A

Close-ups of the inset images in Figure 7-1, Figure 7-6 and Figure 7-7.

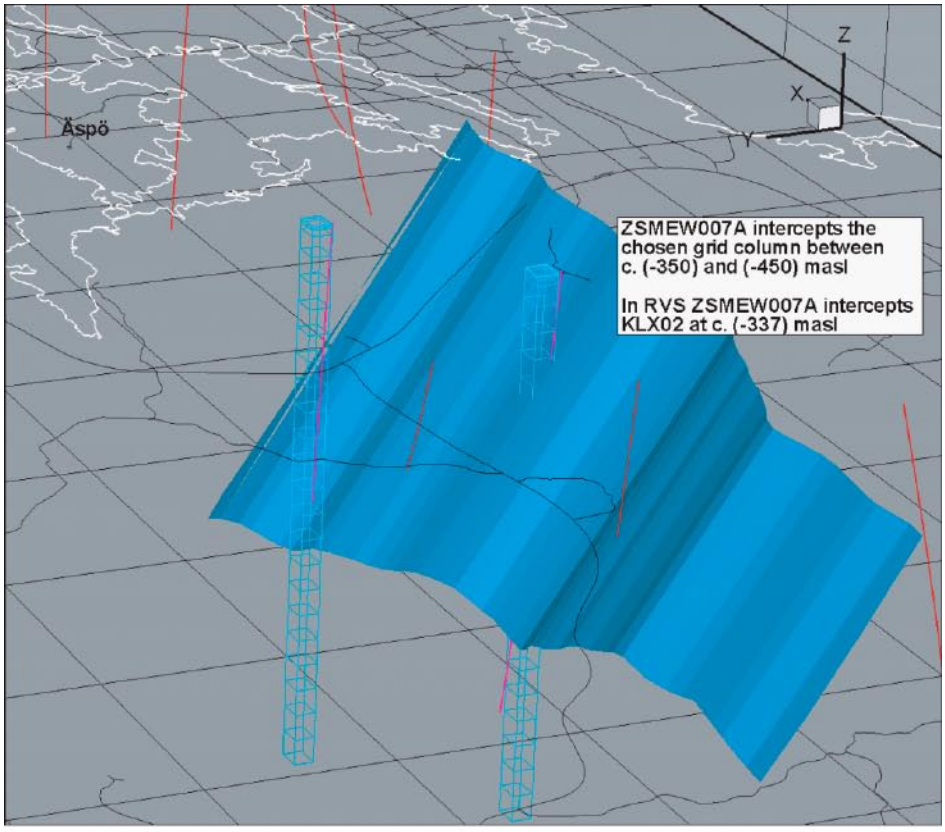

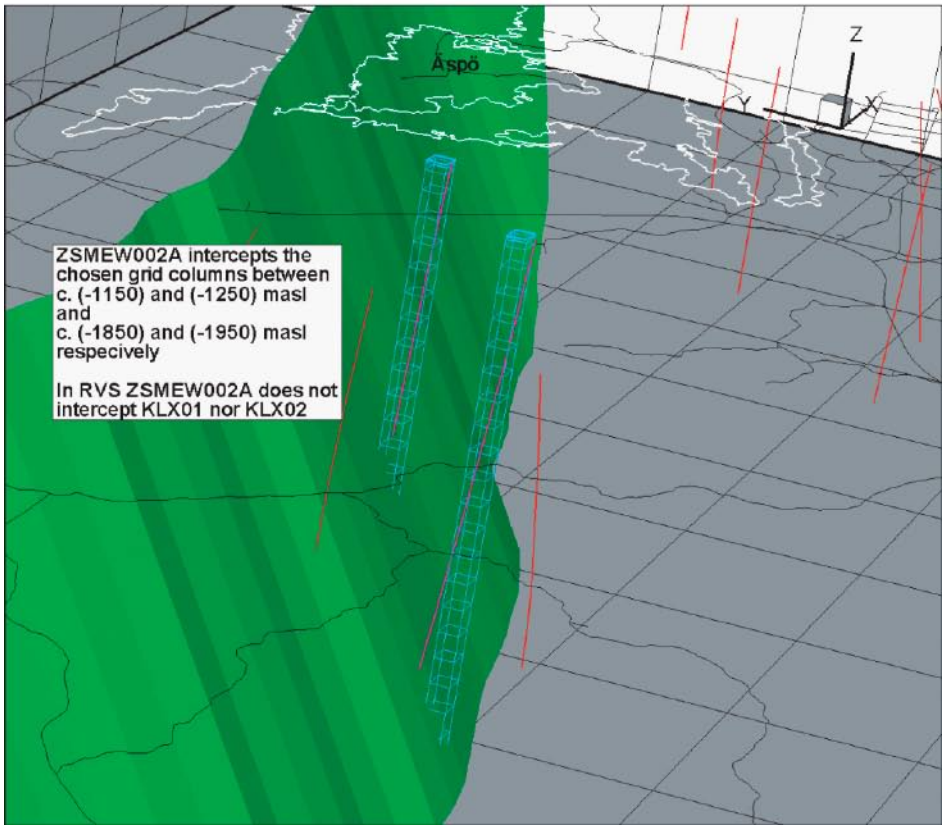

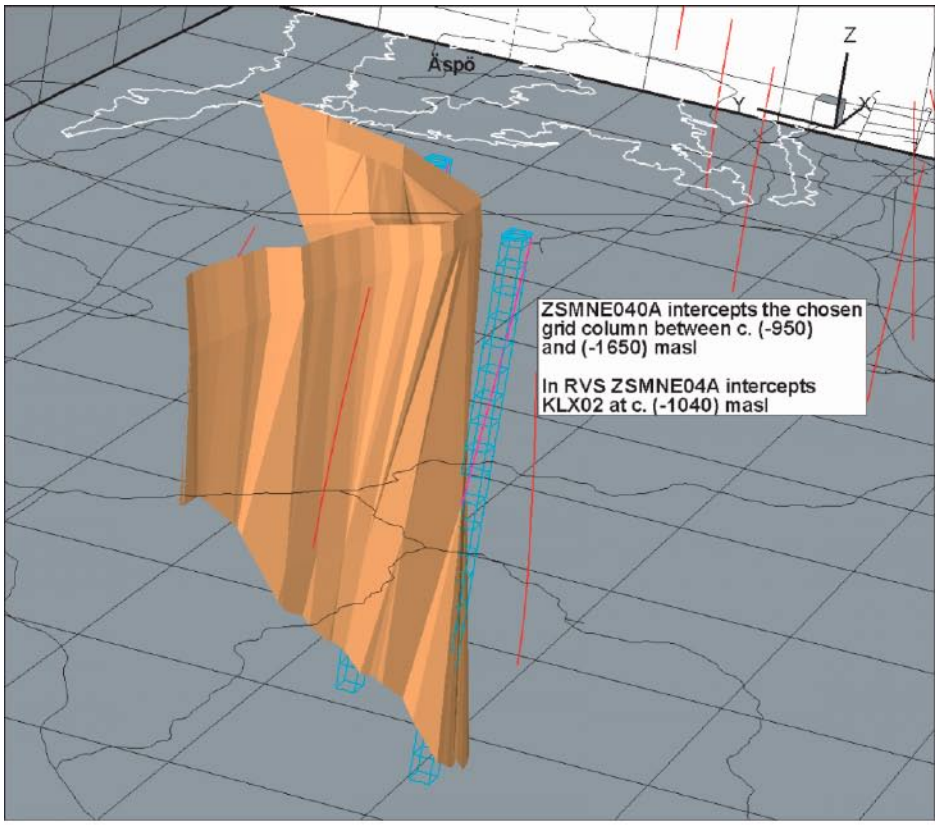
Äspö
Z
Y
X
ZSMNE040A intercepts the chosen grid column between c. (-950) and (-1650) masl
In RVS ZSMNE04A intercepts KLX02 at c. (-1040) masl

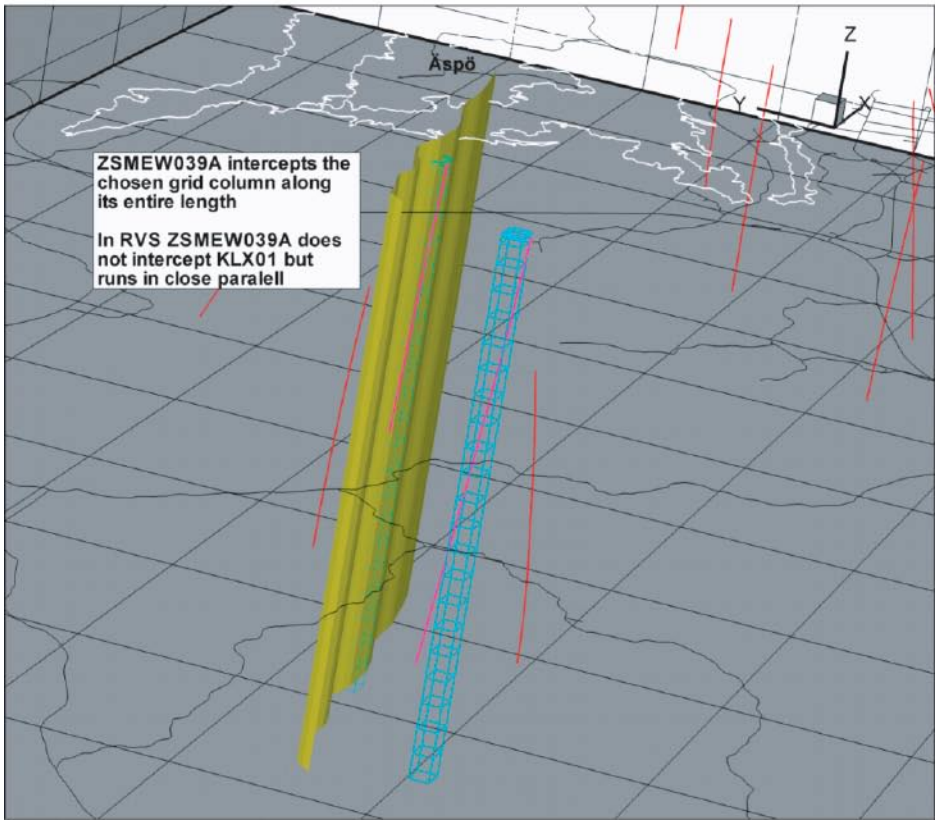
Äspö
Z
Y
X
ZSMEW039A intercepts the chosen grid column along its entire length
In RVS ZSMEW039A does not intercept KLX01 but runs in close paralell

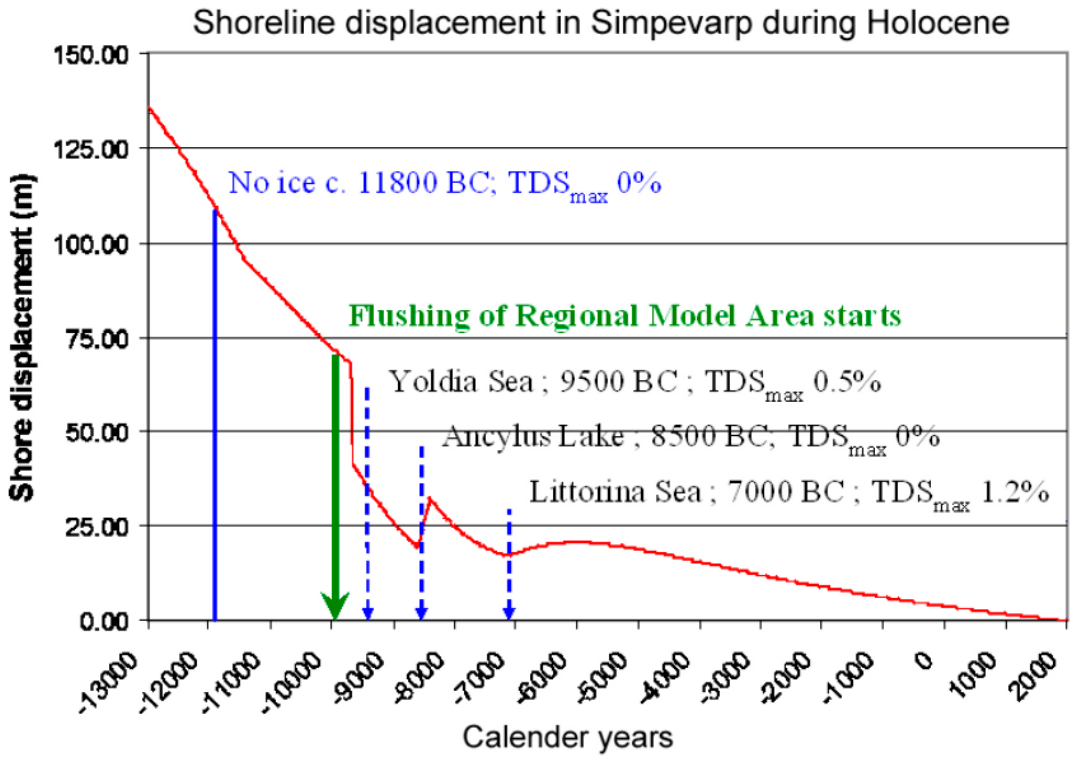
Shoreline displacement in Simpevarp during Holocene
Shore displacement (m)
150.00
125.00
100.00
75.00
50.00
25.00
0.00
No ice c. 11800 BC; TDS$_{max}$ 0%
Flushing of Regional Model Area starts
Yoldia Sea ; 9500 BC ; TDS$_{max}$ 0.5%
Ancylus Lake ; 8500 BC; TDS$_{max}$ 0%
Littorina Sea ; 7000 BC ; TDS$_{max}$ 1.2%
-13000
-12000
-11000
-10000
-9000
-8000
-7000
-6000
-5000
-4000
-3000
-2000
-1000
0
1000
2000
Calender years

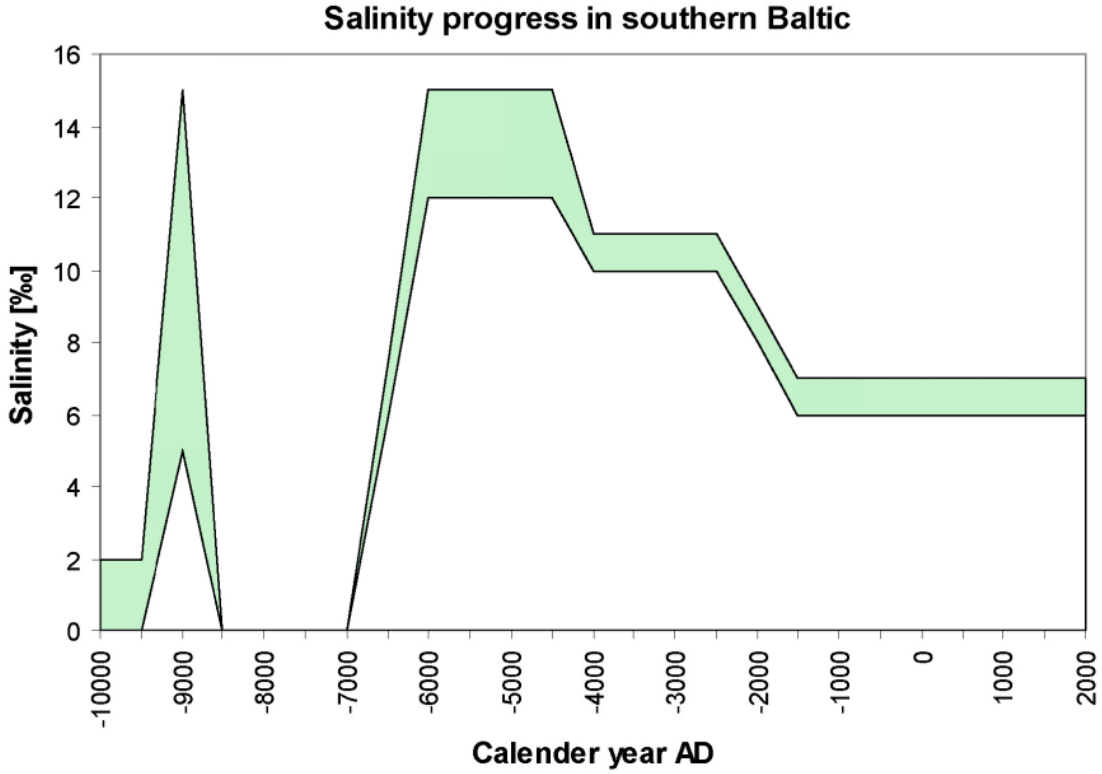
Salinity progress in southern Baltic
Salinity [‰]
16
14
12
10
8
6
4
2
0
-10000
-9000
-8000
-7000
-6000
-5000
-4000
-3000
-2000
-1000
0
1000
2000
Calender year AD

IC: 100% GLACIAL WATER DOWN TO c. - 950 masl

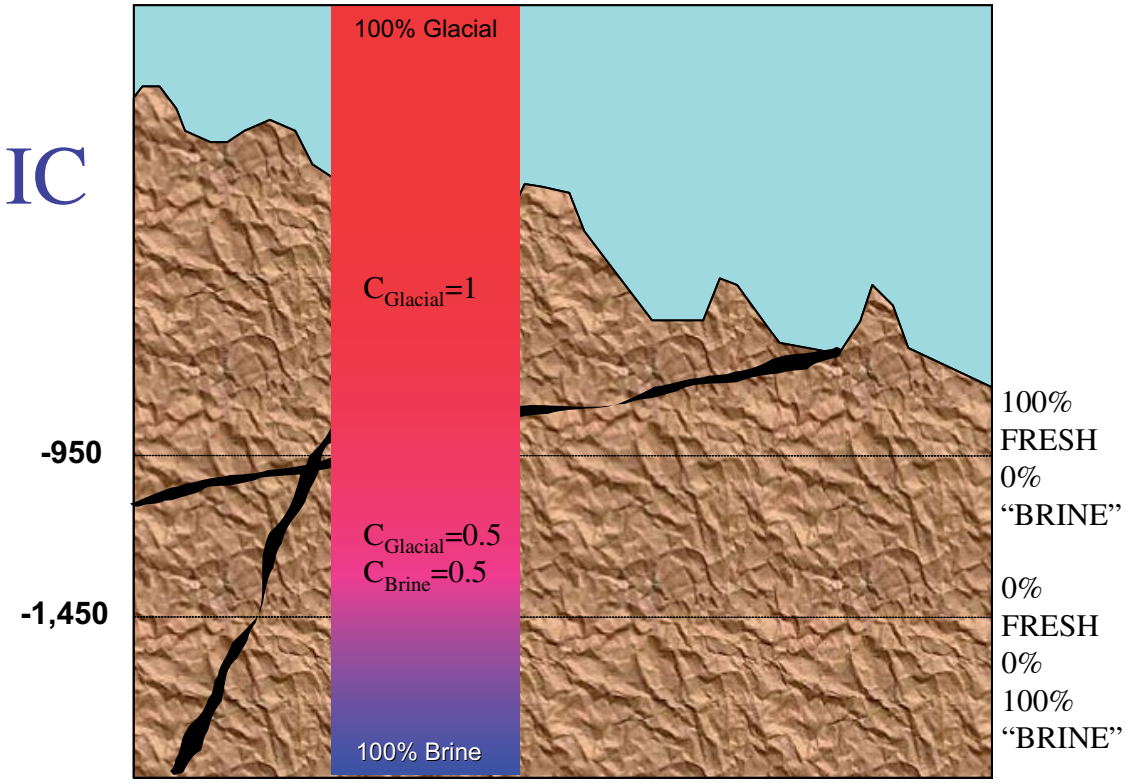

C_{Brine}=1 corresponding to a TDS of 10% by weight

LITTORINA SEA DENSITY TURNOVER

$C_{Littorina}$=1

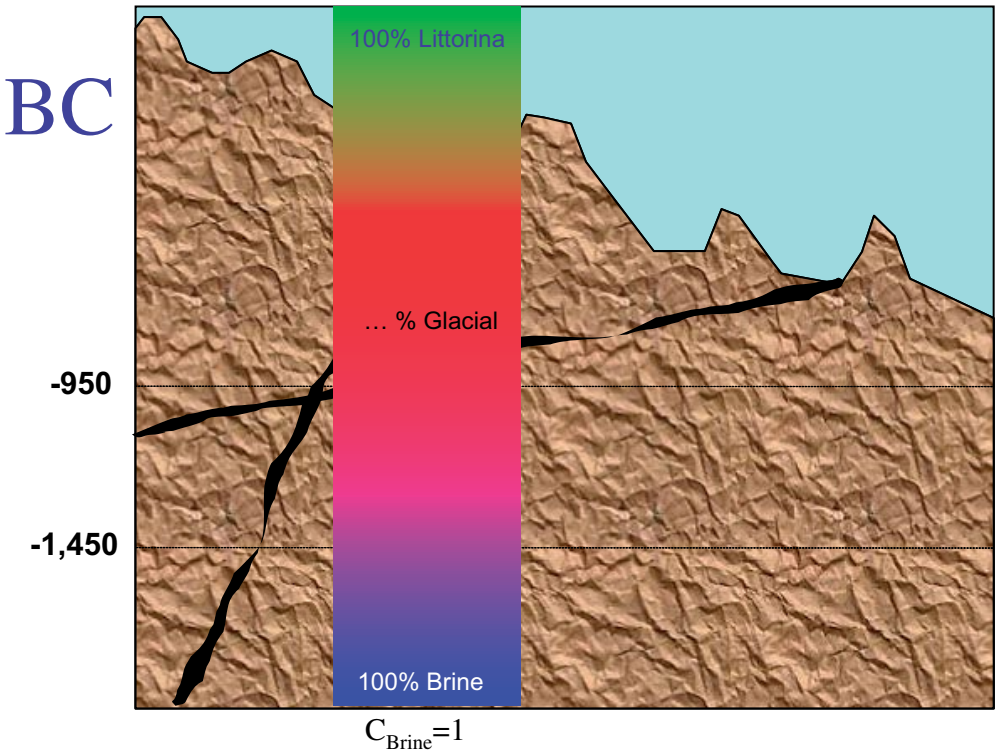

C_{Brine}=1

METEORIC FLUSHING